STUDY ON RUNOFF AND WATER BALANCE IN THE NORTHERN LOESS PLATEAU

January, 2010

Jinbai Huang

Study on Runoff and Water Balance in the Northern Loess Plateau

Jinbai Huang

A dissertation submitted in fulfillment of the requirements for the degree of doctoral of engineering

Graduate School of Engineering
Tottori University·Japan

Major in
Social Infrastructure Engineering of Social Development Engineering

Supervisor: Prof. Osamu. Hinokidani

January, 2010

ABSTRACT

Chinese Loess Plateau is well known for its severe loss of soil and water and such a condition has caused unceasingly regressive ecological environment. As a vast area in semi-arid environment, the risk of desertification on Loess Plateau is increasing gradually and impactful measures thereupon ought to be adopted without delay. Especially for the water-wind erosion crisscross region at the northern Loess Plateau, due to the reasons of even more atrocious weather, over-cropping and etc, the environment in this region has become more severe than other areas in Loess Plateau.

Vegetation cover is expected as an effective means to resist land desertification. However, re-vegetation is difficult to be extensively implemented in Loess Plateau because available water resources are relatively deficient. Consequently, clarification of the runoff characteristics, establishment of index of annual water balance and estimation of annual available water resources are significant to implement the landscape engineering in Loess Plateau region.

The research activities of this study have been conducted as a part of the Core University Program on combating desertification and development in inland of China supported by Japanese Sciences Promotion Society (JSPS). The project has been performed as the cooperation between JSPS and Chinese Academy of Science (CAS). The main objectives of this study mainly focused on the following aspects:

1. To clarify the characteristics of the surface runoff in the northern Loess Plateau region.
2. To establish index of annual water balance and index of monthly water income and expenditure of the study location, further, to evaluate the annual available water resources in the northern Loess Plateau region.
3. To clarify the effects of the check dam system from the view of the runoff redistribution.

With the aims to achieve these research objectives, we carried out the field survey and the field observation on a basin named Liudaogou which was located at the northern Loess Plateau. This basin was chosen as the study location of the No. 1 research group of CAS-JSPS Core University Program. It has representative topographic and hydrologic characteristics of the northern Loess Plateau.

To clarify the characteristics of the surface runoff, we analyzed runoff events corresponding to two types of rainfall events: low intensity with long duration, and high intensity with short duration.

The analyzed results showed the relationship between the rainfall type and the generation of the surface runoff. The essential condition of the surface flow generation is the rainfall intensity $\geqq$ 2.6 mm/5min for unsaturated topsoil condition and the rainfall intensity $\geqq$ 0.6

mm/5min for saturated topsoil condition. Contemporaneously, some physical properties of the topsoil such as the thickness and the infiltration velocity were also evaluated. Analysis of rainfall-runoff indicated that the average rainfall intensity is the key factor for the runoff rate. By analyzing the variation of the soil water content during the rainfall time combined with the rainfall intensity and the surface flow generation in the river channel, mechanism of the surface flow generation was clarified for the topsoil attained saturated situation and was in unsaturated situation respectively.

Based on the investigated results of the topography and ground condition, we developed a runoff calculation model based on the kinematic wave theory combined with the hypothetical channel networks. The applicability of this model was validated by numerical simulation of the observed results of the surface flow. Differences between the simulated results and the observed data were less than 3 %, so the runoff calculation model was considered to be applied to the actual conditions of the study location. The surface runoff calculation in 2005, 2006, 2007 and 2008 were performed respectively. According to the calculated results, the surface runoff rate in the normal year was approximately estimated to be 10 % - 15%. Some main characteristics of the surface runoff have been evaluated through analysis of the numerical results and the observed results.

To establish index of annual water balance, further to estimate the annual available water in the study location, we estimated components of the annual water budget. Water consumption including the irrigation water and domestic water was estimated basing on the results of the target investigation. Annual surface runoff was estimated through analysis of the numerical calculation results of the surface runoff in recent years. Annual groundwater outflow, annual groundwater change and annual variation of the soil water content were estimated by analyzing the observed results. Evapotranspiration was roughly estimated by subtracting the amount of the surface runoff, the groundwater runoff and the water consumption from the annual precipitation because annual groundwater change and annual variation of the soil water content were both approximately 0. Based on the results of each component of annual water budget, index of the annual water balance in the study location was established approximately. Moreover, the annual available water resources were approximately evaluated. Using the same method of data analysis, index of the monthly water income and expenditure was also approximately established.

Field observation of the shallow groundwater was conducted to evaluate fluctuation of the groundwater. Through the analysis, the short-dated fluctuant characteristics and annual fluctuant characteristics of the groundwater were clarified.

In Loess Plateau, an effective engineering control measure for mitigating the soil erosion is the construction of the check dam (earth-filled dam) at downstream in a gully. In several gullies of Liudaogou Basin, the check dams were constructed at different times in the past recent 20-30 years. The check dam system (a check dam system combined with sediment filled area in front of the check dam) significantly impacts on the runoff redistribution in the basin. To clarify the effects of the check dam system on the runoff redistribution, based on actual conditions of a sediment filled area in the study location, a numerical calculation model was developed. The model was validated by fit to the observed data of the groundwater level. Because the simulated results reproduced the observed results well, so the calculation model is considered to be applied to the runoff calculation of the sediment filled area in Liudaogou Basin.

In given year of 2006, a comparison of the numerical results between the current condition with the check dam system and a control case of the original condition without a check dam was presented to evaluate effects of the check dam system on runoff redistribution. The results showed that the effects of the check dam system were reduction of the surface runoff, increase of the evapotranspiration and contribution to the infiltration. The annual water inflow of the present condition was redistributed at the sediment filled area with the results as follows:

(1) About 60 % of the surface runoff was reduced.

(2) Evaportranspation and infiltration accounted for 49.3 % and 11.6 % of the total annual water inflow respectively.

Based on the analysis of the check dam in this study and the related studies on reduction of soil erosion by check dam system, the effects of the check dam system mainly manifest in the followings.

(1) Increase the available water resources in basins and increase rainfall probability within the range of Loess Plateau.

(2) Create the farmland and promote agricultural production

(3) Reduce soil erosion and sediment transportation

Because the study location has representativeness of the topography and the hydrology of the wind-water erosion crisscross region at the northern Loess Plateau, the research results in the current study such as the surface runoff characteristics, index of the annual water balance and index of monthly water income and expenditure in addition to the effects of the check dam system can be approximately considered as the general research conclusions in the water-wind erosion crisscross region at the northern Loess Plateau.

The results of this study indicates that shallow groundwater (phreatic water) combined with its outflow is the most important available water in the study basin and in the northern Loess Plateau.

The research findings in this study are expected to support and to promote the studies on hydraulics and hydrology in the northern Loess Plateau and to provide basis for sustainable utilization of water resources in the northern Loess Plateau.

ACKNOWLEDGEMENTS

I am deeply gratitude to my academic supervisor Dr. Osamu Hinokidani, Professor in the Faculty of Engineering, Tottori University and the member of JSCE (Japan Society of Civil engineering), for his unreserved, kind guidance, understanding and support during the course of this study.

I wish to express my deep gratitude to Prof. Dr. Yuhei Matubara, Prof. Dr. Yoshiharu Matsumi, and Associate Prof. Dr. Hiroshi Yajima in Faculty of Engineering, Tottori University, for their understanding, support and encouragement throughout my doctoral study time.

Special thanks for Assistant Prof. Dr. Yuki Kajikawa in Hydraulic Laboratory of Department of Engineering, for the enthusiastic assistance and cooperation in ordinary days.

I deeply grateful to Associate Prof. Dr. Hiroshi Yasuda and Associate Prof. Dr. Kimura in Arid Land Research Center, Tottori University; and Associate Prof. Dr. Nobuhiro Matsuoka, in Chiba University; Prof. Shiqing Li and Associate Prof. Jiyong Zheng in Institute of Soil and Water Conversation, Academy of Science, China; for their kind help and beneficial suggestion on my study in different time of my doctoral study phase. Specially, Associate Prof. Dr. Hiroshi Yasuda provided the necessary groundwater data, rainfall data and the data of soil water content, Associate Prof. Dr. Kimura provided the essential meteorological data which profitably guaranteed the integrity of this study.

Appreciations are also extended to my colleagues in Hydraulic Laboratory, Department of Engineering, Tottori University, for their cooperation during this study.

Also, I gratefully acknowledge the JSPS Core University Program, and the COE Program of the Ministry of Education, Culture, Sports, Science and Technology, Japan, for the financial support.

In addition, my sincere gratitude to those people whom had help me in one way or another in China or in Japan to get this opportunity to complete my doctoral study.

TABLE OF CONTENTS

Chapter 1

Introduction

1.1 Motivation

At present, government and people in many countries show their unprecedented anxiety on environment since mankind has already perceived cacoethic aftermaths directly from the gradual environmental deterioration. The global warming, the land desertification and the air pollution and etc affect human life and activities of production severely, even survival in some regions in the world.

China is the world's most populous country and the fourth largest in area. Its economy, already huge, is growing at the fastest rate of any major nation. Its environmental problems are among the most severe of any major country, and are mostly getting worse[1)]. Land degradation in the drylands, also called desertification, has affected the world for centuries[2)]. China has a severe environmental problem of land desertification. It is estimated that desert area and the area affected by desertification cover one third of the territory of China[3)]. Although China has made a great effort to combat land desertification, it seem not very successful and land desertification is still expanding at an increasing and alarming rate[4)]. For instance, the rate was 1560 km^2 per year in 1950-1975, while it increased to 2100 km^2 per year in 1975-1987, and to 3600 km^2 per year in 1988-2000. On average, deserts eat up 2460 km^2 of land every year[5), 6), 7)]. Nowadays, environmental protection and improvement has already become a significant problem which all humanity must confront collectively.

1.2 Background

Chinese Loess Plateau, as a vast semiarid-land region and high risk region of desertification has widely being concerned not only in China but also in the world. Severe desertification, especially critical soil erosion, has occurred on Loess Plateau since the 17th century from improper land use, including over-cultivation, over-grazing and over-deforestation[8)]. Environmental degradation and ecological destruction caused severe land erosion and intensified desertification. Yang and Shao, (2000) divided soil erosion into three types: water erosion, wind erosion and water-wind crisscross erosion[9)]. The long-term water erosion caused the serious water and soil loss in Loess Plateau, and the amount of earth and sand pouring into Yellow River is still particularly large[10)]. Due to the long-term wind erosion, the surface soil has become very loose and the sandstorm occurs readily and frequently in the spring with an average frequency of thirteen per year in recent years. Since the 1980's, the climate of Loess Plateau has shown a dramatic warming and drying trend and the human activities have continually strengthened which causes the desertification tendency aggravates continuously. Currently, desertification around Chinese Loess plateau is focused on more attention than before and the practical countermeasures must be urgently adopted to prevent this region from being desertification[11),12),13),14)].

Many large-scale projects have been implemented and many detailed techniques have been used to combat desertification[15), 16)]. Wang, X.H., (et al., 2007), Feng, Z.M., (et al., 2005), and Ginsberg, P.,(2000) pointed out the grain-for-green project is the most renowned activity, which is usually explained as "returning steep cropland into forest". Tree planting has played a pivotal role in renewing the battered landscape of many of the world's arid areas[4),17),18)]. Afforestation can conserve soil on degraded land by reducing soil erosion[19)], increasing soil organic matter, improving the soil structure[20), 21)], assisting in nutrient cycling[22)], providing wildlife habit[23)], improving the landscape and the climate[24), 25)], and promoting the livelihood of farmers by permitting agro-forestry that can reduce the pressure on forested lands[23), 26)].

Now that increase of the vegetation coverage is respected as an effective mean to resist land desertification and to realize ecological restoration, incontrovertibly, the available water resources is essential for guaranteeing the landscape engineering into practice. However, re-vegetation of arid regions is primary water-limited[18)].

Loess Plateau of China (area: 62.68×10^4 km^2; latitude: 34° -40° N and longitude: 110° -115° E) is located in the upper and middle reaches of the Yellow River, at an elevation ranging from 1000 to 1500 m above the sea level, and has a loess cover with thickness largely ranging from 30 m to 80 m. The water deficit index (WDI) and the aridity index indicate that Loess Plateau is Located at a semi-arid region[27), 28)]. In Loess Plateau region, annual average precipitation is only 350-550 mm, which gradually decreases from the southeast to the northwest, and with fairly different-seasonal distribution, more than 60 % of the total is centralized in rainy season from July to September generally in the form of rainstorms. Except the rainy season, the dry conditions combined with the fine texture of the soil make the area very susceptible to the outbreak of dust storms especially during the spring. The annual potential evapotranspiration exceeds 1000 mm which is in much more predominant status than the annual precipitation[29),30),31),32)]. These climatological characteristics results in the relative deficiency of the annual available water resources in Loess Plateau region.

In the past, especially in recent years, how to use the limited water resources to guarantee the people's normal agricultural production, to improve ecological environment, as well as to realize the sustainable survival and development becomes a key research problem in Loess Plateau. Many researchers conducted their studies involving the meteorological characteristics, the soil erosion, basin hydrology and etc on Loess Plateau. The researches on hydrology and water resources were conducted relatively late, but it has achieved the quick progress in recent years. The related studies mainly focused on the rainfall characteristics, the soil water movement, the groundwater, the evapotranspiration, the hydrological circle of the water in a basin and runoff characteristics. The main research technique is to carry out field survey and observation on a chosen basin which has representativeness of a certain area in Loess Plateau. However, research on characteristics of the surface runoff and the groundwater runoff in a basin is still at a primary phase. Apparently, studies on surface runoff and groundwater outflow are essential to clarify the basin hydrologic circle, moreover are necessary to provide the scientific basis for the reasonable development and utilization of the water resources in Loess Plateau.

1.3 Objectives

In the current study, the main research objectives mainly focused on clarification of the runoff characteristics and effects of the check dam system on runoff redistribution, and establishment of index of annual water balance and monthly water income and expenditure in the northern Loess Plateau. The study purposes specifically concentrated on the following aspects.

(1) To clarify the main characteristics of the surface runoff in the study location.

(2) To establish index of the annual water balance of the study location.

(3) To establish index of the monthly water income and expenditure of the study location.

(4) To evaluate annual available water resources.

(5) To clarify the effects of the check dam system on runoff redistribution.

1.4 Methodology

With the aims to achieve the research objectives, we carried out the field survey and field observation on a basin named Liudaogou which is located at wind-water erosion crisscross region on the northern Loess Plateau. The reason of the study location was chosen because the formidable natural environment especially the atrocious climate which causes the more serious land degradation and higher risk of desertification than other areas in Loess Plateau. Contemporaneously this basin has representative hydrological, topographic and the meteorological feathers of the northern Loess Plateau[33), 34), 35)].

The study purposes were mainly achieved through the following approaches.

(1) Analysis of various kinds of data obtained from the field survey and observation.

(2) Development of the numerical calculation models respectively for calculation of the surface runoff and runoff of the sediment filled area (the check dam system).

(3) Validation of the developed models through numerical simulation of the corresponding observed data.

(4) Analysis of the numerical results achieved by the numerical calculation.

The concrete research activities corresponding with the anticipant research objective are as follows:

(1) Carried out the observation of the rainfall and the surface flow. Through analyzing the observed results of the typical rainy events with the corresponding surface runoff, the relationship between the rainfall intensity and the surface runoff generation was clarified. Furthermore, some physical properties of the topsoil such as the thickness and the infiltration velocity were also evaluated.

(2) Carried out the observation of the soil water content on the slope on both sides of the surface flow observed section. Through analyzing the rainfall intensity combined with analyzing the variation of the soil water content during the rainfall time and the surface runoff generation, mechanism of the surface runoff generation for saturated topsoil situation and unsaturated situation were clarified respectively.

(3) Conducted the field survey of the topography and ground condition. Based on the actual conditions of the study area, a numerical calculation model for the surface runoff calculation was developed according to kinematic wave theory combined with hypothetical channel networks. Applicability of the model was validated through numerical simulation of the observed discharge of the surface flow.

(4) Through analysis of the observed results combined with the numerical calculation results of the surface runoff, some characteristics of the surface runoff were evaluated.

(5) Through analyzing the observed results of the fluctuation of the water level in a large reservoir, combined with considering relational results of the purposive investigation of the water utilization in the study basin, the annual domestic water and the irrigation water was approximately estimated.

(6) Based on the analyzed results of the observed data and numerical calculation results of the surface runoff, index of the annual water balance, and index of the monthly water income and expenditure were established respectively. Moreover the annual available water resources were also approximately estimated.

(7) Conducted the observation of the shallow groundwater. Through the data analysis, the short-dated fluctuant characteristics and annual fluctuant characteristics of the groundwater were clarified.

(8) Based on the actual topographic and ground conditions of the sediment filled area in front of a check dam in Liudaogou Basin, a numerical calculation model for the runoff calculation of the sediment filled area was developed. Validation of this model was verified by numerical simulation of the observed groundwater level. Further, the effects of the check dam system were evaluated through comparison of the numerical calculation results between the original condition without a check dam and the present condition with a check dam system from the view of runoff redistribution.

1.5 Brief procedure

The brief procedure of this study is shown in Figure 1.1.

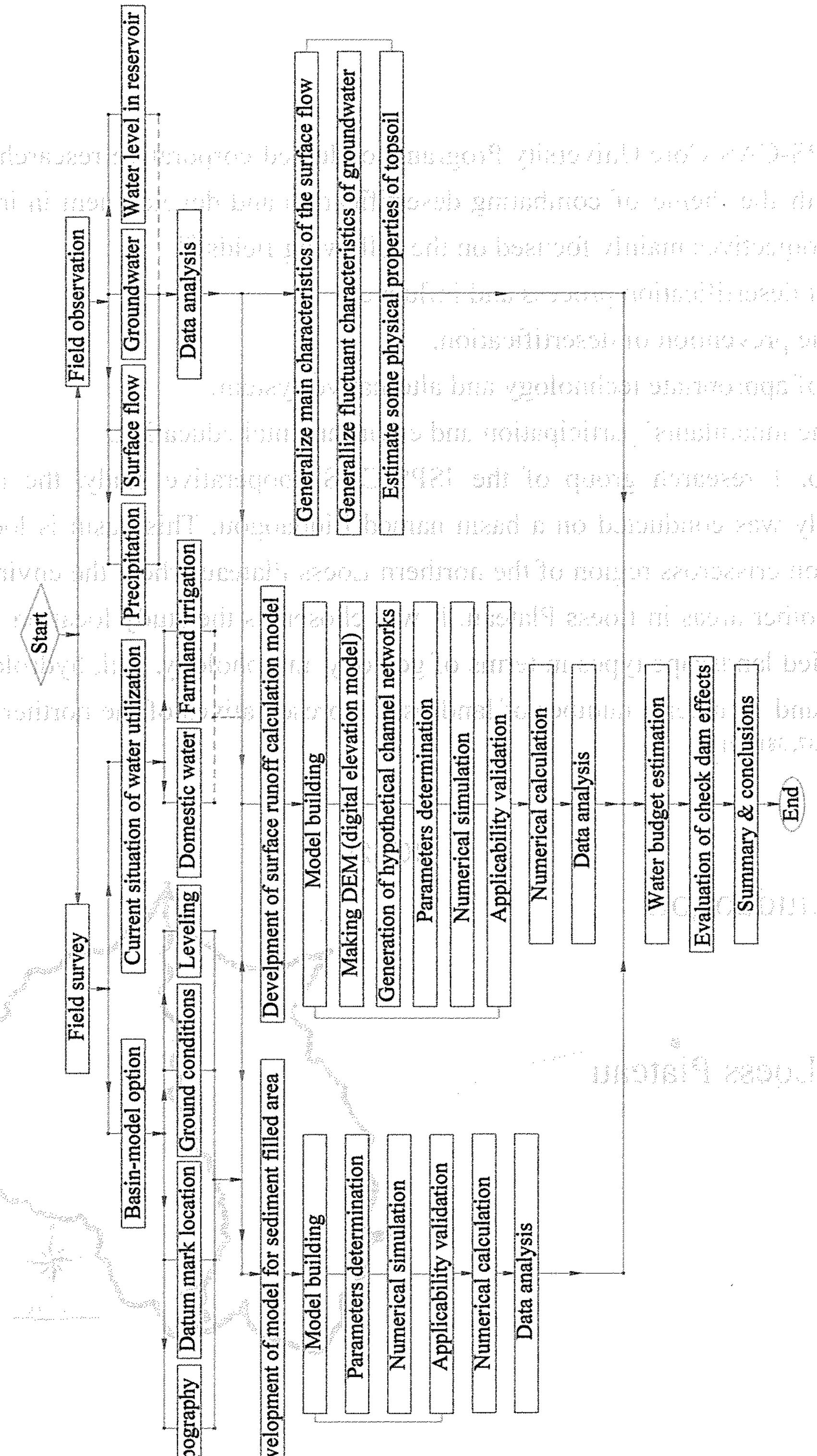

Fig 1.1 Research procedure

Chapter 2

General Situation of the Study Area

2.1 Introduction

Since 2001, JSPS-CAS Core University Program conducted corporative research project on Loess Plateau with the theme of combating desertification and development in inland of China. The research objectives mainly focused on the following fields[36].

1) Clarification of desertification process and influence.
2) Planning for the prevention of desertification.
3) Development of appropriate technology and alternative system.
4) Planning for the inhabitants' participation and environmental education.

As a part of No. 1 research group of the JSPS-CAS cooperative study, the research activities of this study was conducted on a basin named Liudaogou. This basin is located at the water-wind erosion crisscross region of the northern Loess Plateau where the environment is much severe than other areas in Loess Plateau. It was chosen as the study location because it represents diversified landscape types in terms of geology, morphology, soil, hydrology and climatic conditions, and is under a number of land-uses representatives of the northern Loess Plateau environment[37, 38), 39)].

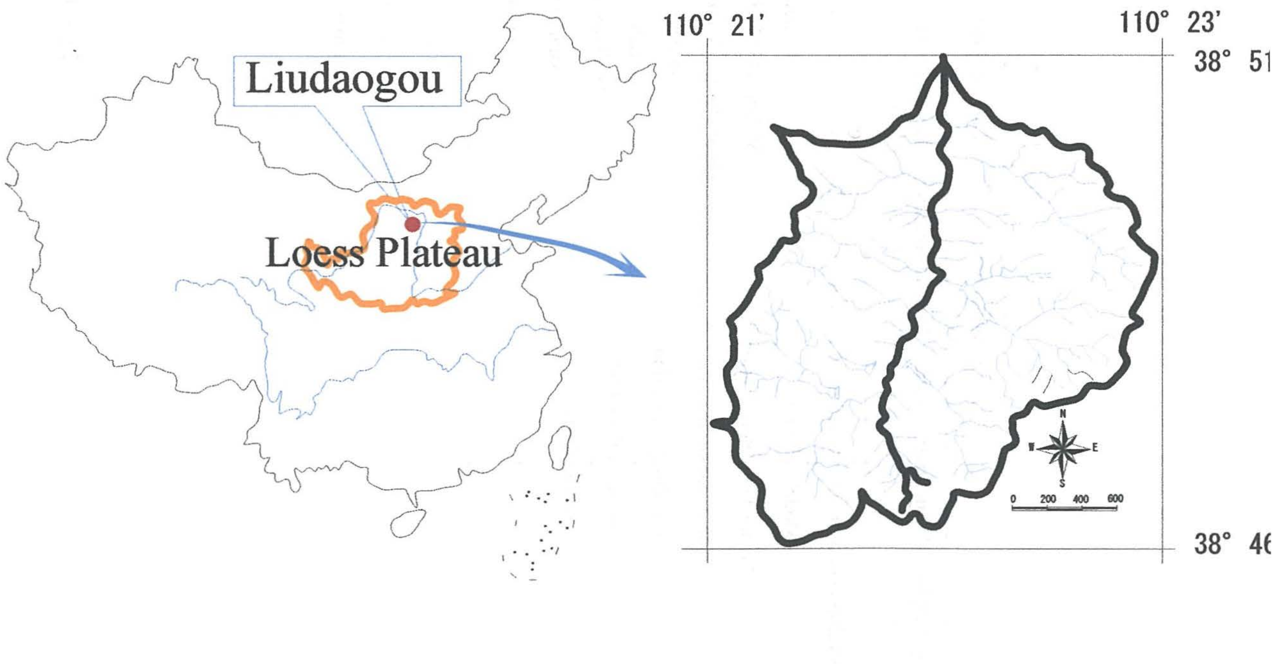

Fig 2.1 Position of Loess Plateau in China & Liudaogou in Loess Plateau

2.2 General situation of the study location

2.2.1 Position & Area

Liudaogou (Position: 110°21'-110°23' E longitude and 38°46'-38°51' N latitude) belongs to Shenmu County, Shaanxi Province. This basin situated at the transitional area between the edge of the Maowusu desert and loess hill zone, simultaneously, belongs to water-wind erosion crisscross region at the northern Loess Plateau[35), 37)]. Liudaogou is one of a second-rate tributary of Kuye River. Area of Liudaogou Basin is 6.89 km^2, the length of the main river channel is 4.21 km in direction from south to north (Fig. 2.1).

2.2.2 Climate

Temperate continental-monsoon climate is remarkable. The monsoon is prevalent and the annual mean wind speed is 2.5-2.7 m/s. Annual average number of days which the wind speed exceeds 17.2 m/s is 13.5 days. The annual average temperature is 8.4 °C and the frost-free period is 169 days.

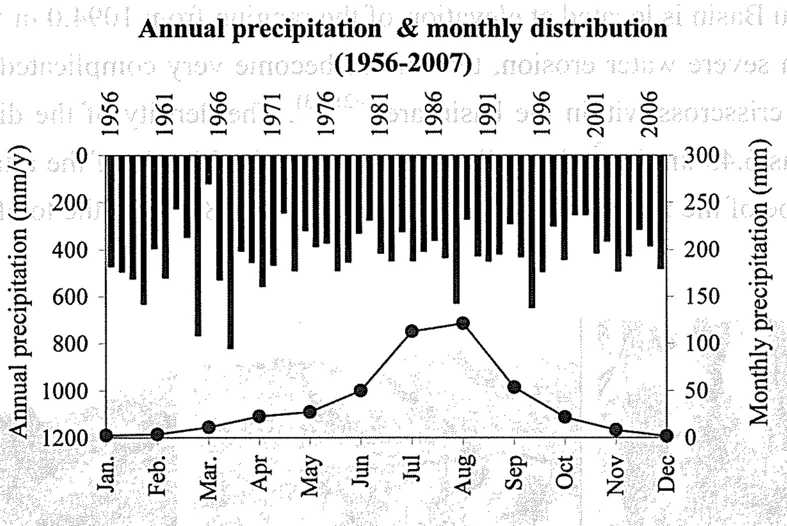

Fig 2.2 Annual precipitation & Monthly rainfall distribution

The mean annual precipitation is 437.4 mm, however distribution of the annual precipitation is considerably non-uniform, 77.4 % of the total is received in the rainy season from June to September generally with several heavy rains. The yearly precipitation and monthly distribution of the rainfall is shown in Figure 2.2. The different-seasonal rainfall distribution results in the dry climate except the rainy period. Especially in spring and winter the climate is extremely dry with frequent gale which causes the sandstorm occurring readily with an average frequency of thirteen per year in recent years. The annual potential evapotranspiration surpasses 1000 mm which is about 2.5 times of the yearly rainfall. The diurnal evaporation capacity possibly attains or surpasses 5.0 mm/d on some days in July and

August[38), 40), 41),42)].

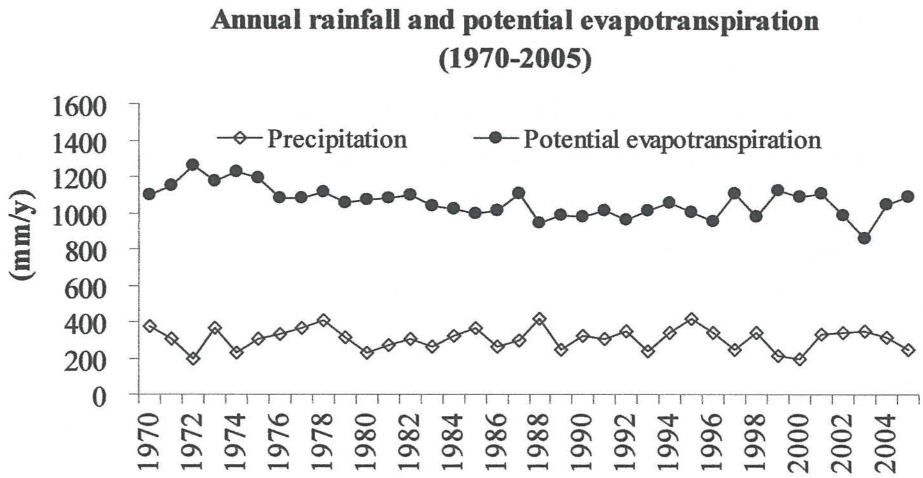

Fig 2.3 Annual rainfall & Annual potential evapotranspiration

2.2.3 Topography & Ground conditions

Liudaogou Basin is located at elevation of the ranging from 1094.0 m to 1273.9 m. Due to the long-term severe water erosion, terrain has become very complicated, many gullies in different scales crisscross within the basin area [42), 43)]. The density of the ditch which length ≧ 100 m attains 6.45 km/km^2, the gully area accounts for 32.6 % of the total basin area, and the gradient slope of the most loess hill < 15° accounts for 98.4 % of the total of the slope area [43), 44), 45)].

Fig 2.4 Complicated landform

Cotemporaneously, the long-term grisliness wind erosion caused the serious land deterioration and high risk of the land desertification. The topsoil becomes very loose with the thickness of 10 cm- 20 cm. The particle size ≦ 0.01 mm only accounts for 9.4 %-36.1 %. The increase of the grains of sand content in the topsoil results in the mean particle density reaches 2.71 g/cm^3 which is higher than the range of the normal value[35),38), 44)].

The main earthbased material is the thick deposited loess which formed in Quaternary period. Subsequent to the loose topsoil is the hard yellow ocher with thickness over 20 m, and the bottom is sandstone which was formed in Jurassic period of Mesozoic[35),45),46)]. The schematic diagram of the common vertical ground profile is extracted as Figure 2.5.

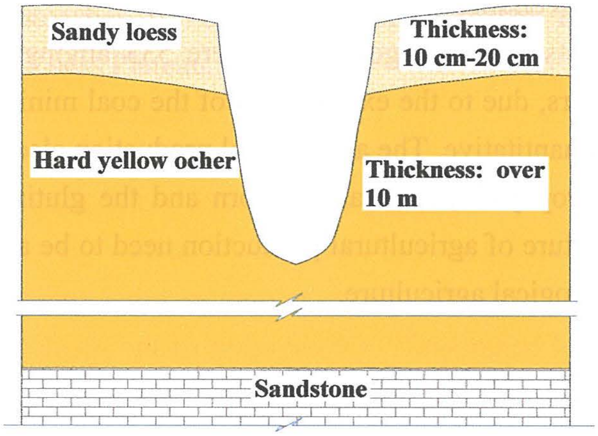

Fig 2.5 Schematic diagram of the common vertical profile of ground

2.2.4 Land use & Vegetation cover

Vegetation in Liudaogou Basin belongs to brush-grassland type. Due to the excessive pasturage and serious land erosion, the natural bush was severely destroyed and there is nearly no large-area distribution. The artificial vegetation was arduously developed in recent 20-30 years, but for the rigorous vegetal environment, the vegetation is in miserable condition. The ecological condition has become terribly frail[47), 48), 49)]. The general land use patterns and typical vegetation distribution is shown in Figure 2.6.

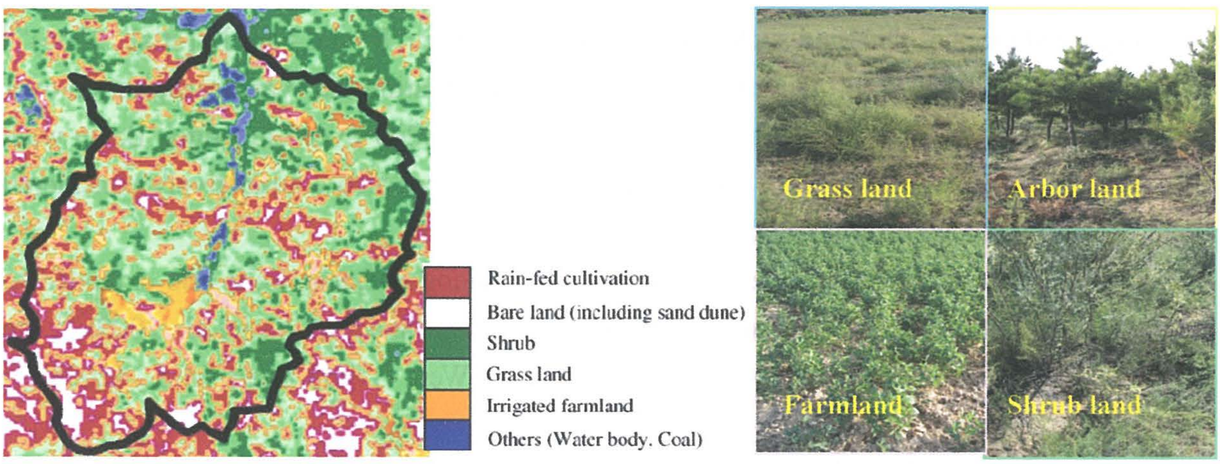

Fig 2.6 Land use pattern & Vegetation distribution[49)]

According to actual investigation in the year of 2007, area of rain-fed terrace and mesa terrace was 28 ha. Total area of the farmland was 49.2 ha among which the irrigated area is 20.6 ha. Towards decreasing the land erosion and sediment transportation, six check-dams (earth-filled dam) were built in each gully at different time in the past 30 years by which the loss of soil and water from Liudaogou Basin has been considerably mitigated.

2.2.5 Population & Miscellanea

In 2007, inhabitants in Liudaogou Basin were 533 among which resident population were 410. In recent years, due to the exploitation of the coal mining, the transient population increased in a certain quantitative. The agricultural production also got the quick development in recent years. The crop yield, such as the corn and the glutinous millet, achieved rapid growth. However, structure of agricultural production need to be adjusted towards developing the highly efficient ecological agriculture.

2.3 Related studies

In the same study location, various studies were carried out which involves the wide fields.

Studies on mechanism of soil erosion and gully erosion and its combating countermeasures was prior carried out and has got rapid progress, the recent typical studies such as conducted by Li, M. and Li, Z.B., (et al., 2005)[50)], and Wen, B. and Shao, M.A., (2006)[51)].

Studies on soil properties involve several aspects such as the soil properties affected by landforms for an example conducted by Wei, X.R. and Shao, M.A, (2007)[52)]; Soil water moisture, for instances of the variability and pattern of the surface moisture carried out by Zhu, Y.J. and Shao, M.A., (2008)[53)], and impact of gully on soil moisture conducted by Zhu, H. and Shao M.A., (et al., 2008)[54)]; Hydraulic properties such as conducted by Zheng, J.Y. and Shao, M.A., (et. al., 2004)[55)], Hu, W. and Shao, M.A., (et al., 2009)[56)].

Some researches which have close relationships with this study are the studies on hydrology, instances of this kind such as conducted by Kimura, R. and Fan, J., (et al., 2006)[10)], and Kimura, R., (2007)[57)]. In their studies, methods for estimating the evapotranspiration over the grassland field and the estimation of the moisture availability over Liudaogou Basin were proposed. The meteorological data and properties of soil were also conjunctively considered when executing the algorithmic method for evapotranspiration.

In addition, scientific researches conducted on Lioudaogou Basin were also extended to the vegetation restoration such as carried out by Fu, X.L. and Shao, M.A., (et al., 2009)[58)], the GIS model on hydrological cycle such as conducted by Wen, B. and Shao, M.A., (2005)[59)], and also else research fields.

In spite of the study and research fields as above mentioned, the study on the surface runoff and groundwater, especially the study on numerical calculation of the surface runoff and groundwater were carried out relatively late due to some limiting conditions on observation of the surface runoff and the groundwater. Further, modeling of the complicated landform is also very difficult. The current study mainly focuses on clarifying the surface runoff characteristics, evaluating annual water balance and clarifying the effects of the check dam system on runoff redistribution. Thus, in a certain sense, this study is not only an essential supplementation of the researches carried out on Liudaogou Basin, but also advances the related studies on hydrology and water resources in the northern Loess Plateau, especially advances the research approaches on numerical calculation of the surface runoff and groundwater in the northern Loess Plateau.

Chapter 3

Relationships between the Rainfall and the Surface Runoff

3.1 Introduction

Because the natural condition is similar within the scope of the Liudaogou Basin, observation of the rainfall, the surface flow and the shallow groundwater were carried out on the upstream of Liudaogou Basin due to seldom external interferences such as caused by human factors or animal behaviors[60]. Observation of the precipitation and the surface flow were conducted as early as started in 2004. Due to some limiting factors such as the limited opportunities of the field survey, the lack of the electric battery of the observational apparatus and influence by the external uncertain factors, the data of various kinds has partial deficiency in different period of time of whole observational span.

Items of the field survey mainly included the topographic survey, cross sectioning of the river channel, longitudinal leveling survey of the river channel, GPS survey of the main datum marks and etc.

3.2 Arrangement of field observation

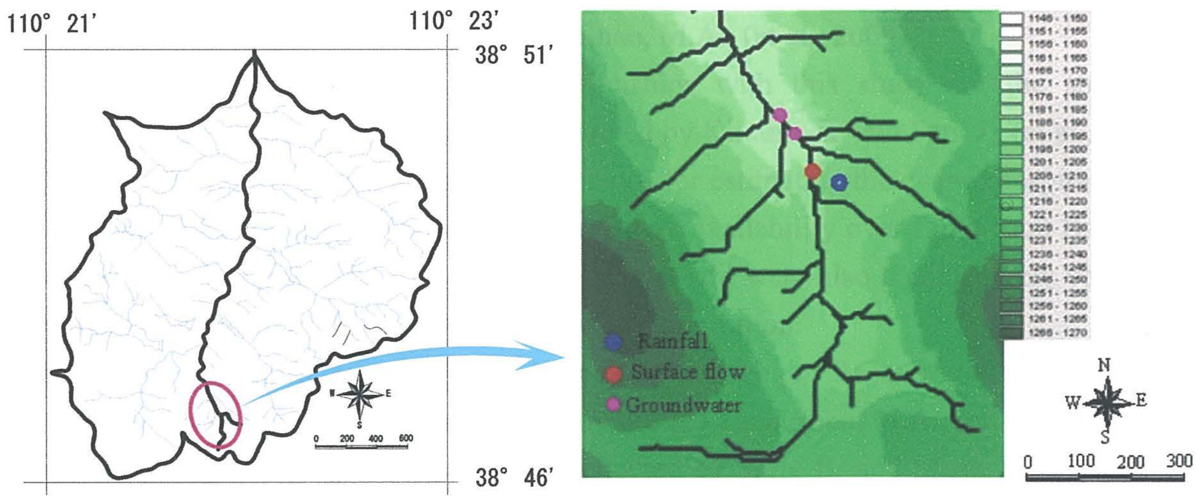

Fig 3.1 Sketch-map of the observation arrangement

The rainfall intensity was observed by an automatic rain gauge which records the data once by every 0.2 mm rainfall occurred. The installed point of the rain gauge is near the surface flow observed site. Simultaneously, a water level recorder automatically recorded the depth of water in the river channel (gully) at a selected cross-section in a branch of upstream.

The time interval for the surface flow observation was set to be 5 minutes in consideration of the scale of the surface flow is significantly impacted by the rainfall intensity. Because the shallow groundwater level (phreatic water) is relatively stable and there is no direct impact of the rainfall, the groundwater level was observed by the water level recorders on 2 points with time interval of 1 hour. The observational accuracy of the water level recorder is 1 millimeter. Arrangement of field observation is shown in Figure 3.1.

3.3 Distribution characteristics of the rainy events

3.3.1 Rainfall in 2007

3.3.1.1 Rainfall process in 2007

With the purpose of evaluating the distribution characteristics of annual rainy events such as distribution of the rainfall amount and distribution of the rainfall duration, the observed rainfall data in 2007 was selected for analysis. The rainfall amount in 2007 (481 mm) was approximate to the mean annual rainfall (437 mm) and rainfall temporal distribution was similar to the annual rainfall process in the normal year. In 2007, during the period of the main rainy season from June to September, the rainfall amount was 271 mm which accounted for 56.3 % of the total. This result is obviously lower than the long-time average annual value in the corresponding period (77.0 %). However, during the time from 21 May to 6 October, which covered the entire rainy season in the study location, the rainfall amount attained 84.7 % of the total. The rainfall process in 2007 is shown in Figure 3.2.

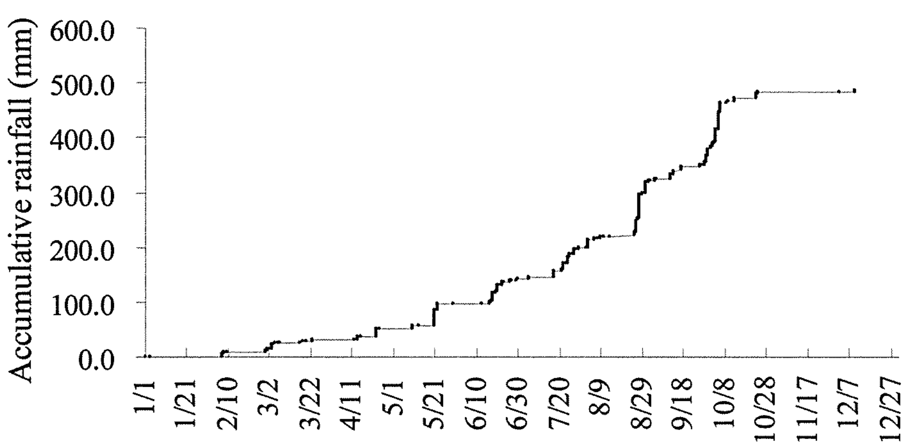

Fig 3.2 Rainfall process in 2007

Figure 3.3 is a rainfall distribution graph which was achieved by discretizing the rainfall data (As shown in Figure 3.2) on the time axis and 5 minutes is defined as the time unit. Figure 3.3 also represents the most rainfall was centralized in the period of time from the third of May to the first of October in 2007.

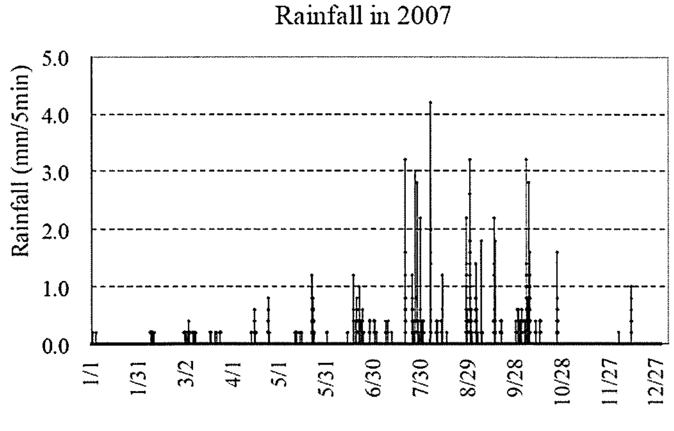

Fig 3.3 Rainfall distribution graph for the time unit of 5 minutes

3.3.1.2 Statistics of the rainfall intensity

Different time series were used to discretize the rainfall data on the time axis. The used time units for discretization are 5 minutes, 10 minutes, 30 minutes, 1 hour, 6 hours, 12 hours and 24 hours (1 day) respectively. The maximum rainfall intensity, the minimum rainfall intensity, and the average rainfall intensity of all the rainy events for the different time series are shown in Table 3.1.

Table 3.1 Statistics of the rainfall intensity

Time unit	5 min	10 min	30 min	1 hr.	6 hr.	12 hr.	24 hr.
Maximum (mm)	4.2	5.6	9.2	11.0	36.6	39.8	44.0
Minimum (mm)	0.2	0.2	0.2	0.2	0.2	0.2	0.2
Average of all rainy events (mm)	0.4	0.5	0.8	1.2	2.8	3.9	5.5

In view of the maximum rainfall intensity for the different time series, the maximum rainfall for the time unit of 6 hours, 12 hours and 24 hours has no distinct difference, and the similar situation also exists between the time unit of 30 minutes and 1 hour, also for the time unit of 5 minutes and 10 minutes. However, there is a large difference between the maximum hourly rainfall and the maximum value of the time unit of 6 hours. For the time series are no more than 1 hour, a relatively large difference exists between the maximum rainfall intensity for the time unit of 5 minutes and the time units of 30 minutes. The maximum hourly rainfall intensity is only about two times of that of 5 minutes, and the maximum rainfall for the time unit of 10 minutes is only slightly more than that of 5 minutes (about 1.3 times)

In regard to the average rainfall intensity of all the rainy events, the average of 10 minutes is only 1.2 times, and the hourly average is only 3 times of the average of 5 minutes.

For all the time series, the minimum rainfall intensity is the same, only 0.2 mm.

3.3.2 Distribution of the rainy events

3.3.2.1 Separation of the rainy events

The numbers of the rainy events were determined by analyzing the discretized results for the time unit of 5 minutes as shown in Figure 3.3. The main separation methods of the rainy event are as follows.

(1) When the intensive rainfall occurred without interruption (interval of the unit time: 5 min), and there was no rainfall occurred within an hour before and after the time of the intensive rainfall, such intensive rainfall was considered as a single rainy event separately.

(2) Towards the scattered short-duration rainfall whose duration was less than 1 hour, as there was no rainfall occurred within a few hours before and after such rainfall, the rainfall of this kind was regarded as a single rainy event respectively in spite of the number of interruptions.

(3) For the rainfall whose duration was more than 6 hours with a few interruptions, if the longest break time is less than 1 hour, and the rainfall continued after each interruption, such rainfall was regarded as a single rainfall event respectively.

Additionally, except the methods for the rainy event separation as above mentioned, some rainy events were properly determined by considering the actual rainfall process.

As the results, the number of the observed rainy events is 80 in 2007. Distributions of the rainfall amount and distribution of the rainfall duration of all the rainy events are shown in Table 3.2.

Table 3.2 Distribution of the rainy events in 2007

Items		Distribution of rainfall amount (mm)							Distribution of rainfall duration (hr.)					
		< 1	1-5	5-10	10-20	20-30	30-40	>40	<0.5	0.5-1	1-6	6-12	12-24	>24
Month	Number of the rainy events													
Jan	2	2	…	…	…	…	…	…	2	…	…	…	…	…
Feb	4	1	3	…	…	…	…	…	1	…	2	1	…	…
Mar	11	8	2	1	…	…	…	…	5	5	…	…	1	…
Apr	5	3	1	…	1	…	…	…	3	…	1	1	…	…
May	6	4	…	1	…	…	1	…	4	…	…	1	…	1
Jun	12	2	8	1	1	…	…	…	-	3	8	1	…	…
Jul	14	5	4	3	2	…	…	…	6	…	7	…	1	…
Aug	8	2	3	…	1	1	…	1	2	1	3	…	1	1
Sep	9	…	5	1	2	1	…	…	…	1	5	2	1	…
Oct	7	…	2	1	2	1	…	1	…	3	3	…	1	…
Nov	…	…	…	…	…	…	…	…	…	…	…	…	…	…
Dec	2	1	1	…	…	…	…	…	1	…	1	…	…	…
Σ	80	28	29	8	9	3	1	2	24	13	30	6	5	2

3.3.2.2 Analysis of the results

According to the analyzed results as shown in Table 3.2, there were 43 rainfall events occurred from June to September in 2007 which accounted for more than 50 % of the total number.

There were 18 rainy events whose rainfall amount was more than 10 mm occurred in the period of time from the last third of May to the first third of October (rainy season in 2007). The surface runoff may be generated by some of such rainy events in the study area. Additionally, the rainy events whose duration was longer than 30 minutes mainly occurred before the rainy season (from January to May).

There were 57 rainy events (more than 70 % of the total) whose rainfall was less than 5 mm and such rainy events could not cause the runoff generation.

Although there were 11 rainy events occurred in March, but the rainfall amount of the most was less than 5 mm and the rainfall duration was less than 1 hour. In November, there was no rainy event observed. And in winter (January, February and December) there was only a small amount of precipitation in the form of snow.

3.3.3 Rainfall distribution graphs

Towards evaluating the rainfall distribution characteristics for a single event which were discretized by the different time units on the time axis, a rainy event which happened on 17 July, 2007 was chosen as an example for analysis. The rainfall occurred in period of time from 21:20 to 23:30 with a relatively long break, and the rainfall mainly concentrated in the period from 21:20 to 22:30 as shown in Figure 3.4. The total rainfall is 12.4 mm.

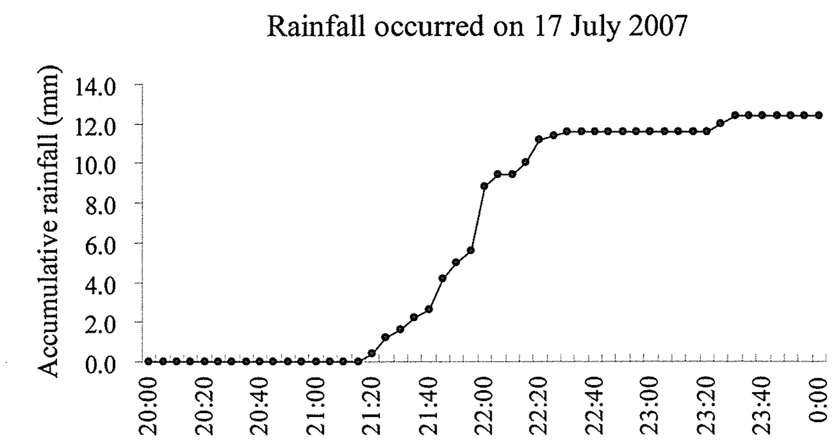

Fig 3.4 A rainy event on 17 July, 2007

The rainfall distribution which was discretized by the time unit of 5 minutes, 10 minutes, 30 minutes and 1hour are shown in Figure 3.5.a Figure 3.5.d respectively.

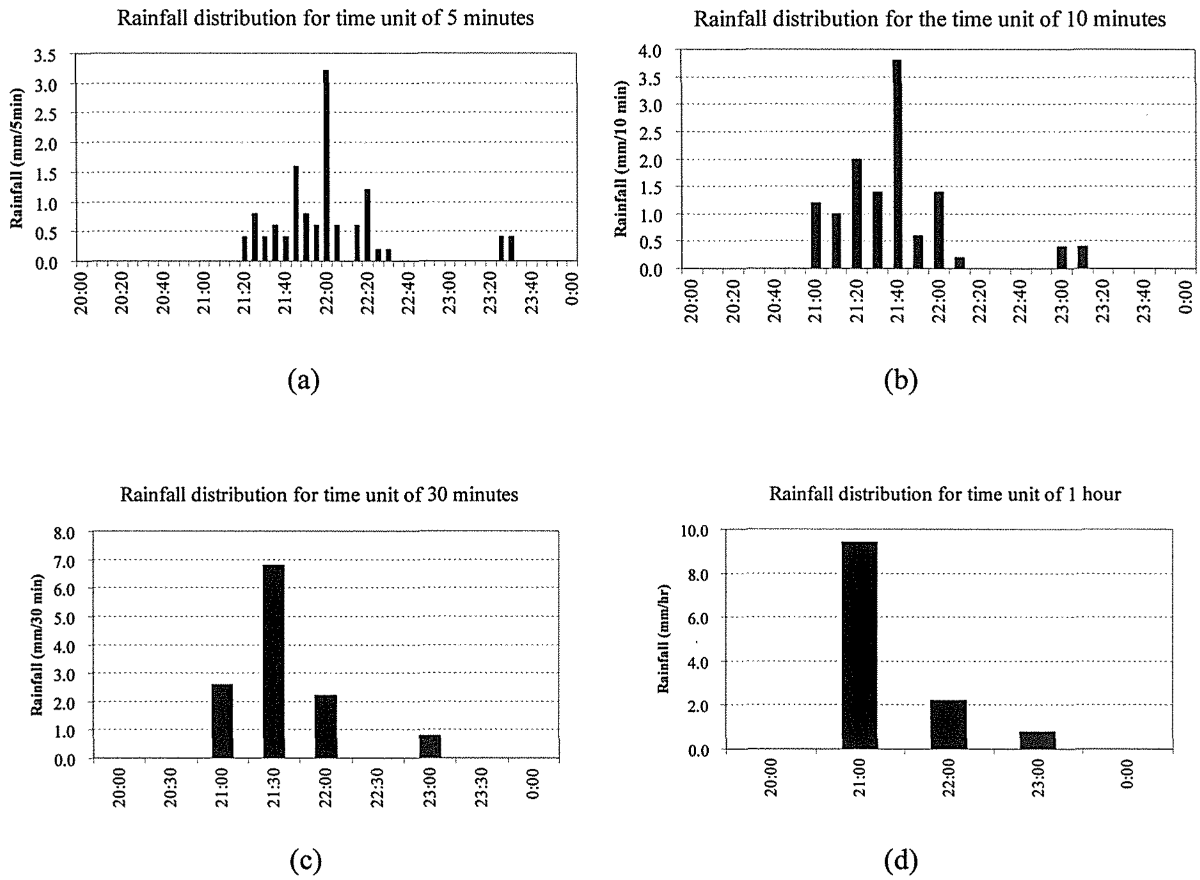

Fig 3.5 Rainfall distribution graphs for the different time series
(Example: A rainy event occurred on 17 July, 2007)

Figure 3.5 represents that the increase of the time unit for discretization causes the reduction of the number of the discretized points, thereby, the rainfall distribution becomes more concentrated on the time axis. On the other hand, the expression of the rainfall distribution and the rainfall process becomes more and more rough. Compared with Figure 3.5.d, obviously, the rainfall distribution and process can be expressed better by Figure 3.5.a which was discretized by the time unit of 5 minutes. Consequently, with regard to the rainfall distribution graph, using the smaller time unit for discretization (such as 5 min) can reflect the actual rainfall process and the rainfall distribution better than using the larger time unit (such as 1 hour).

As a reality in the study location, the short-duration rainfall accounts for the most of the annual rainy events. Such as in 2007, there are 67 rainy events whose duration is less than 6 hours which accounts for more than 80 % of the total number of the rainy events. Therefore, the time interval of 5 minutes, which is corresponding to the time unit of the surface flow observation, was selected as the time unit to discretize the rainfall data on the time axis in this study.

3.4 Computational method on flow-discharge

3.4.1 Surface flow observed section

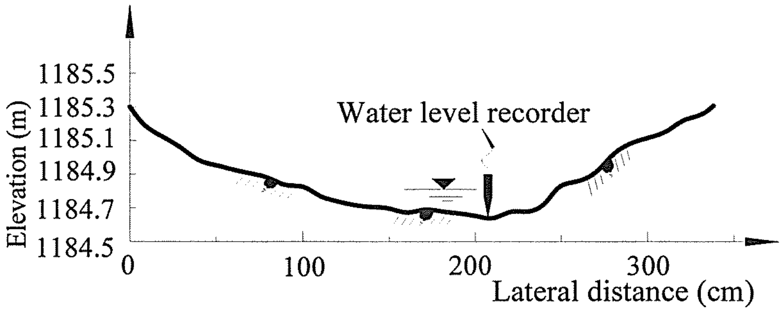

Fig 3.6 Surface-flow observed cross-section

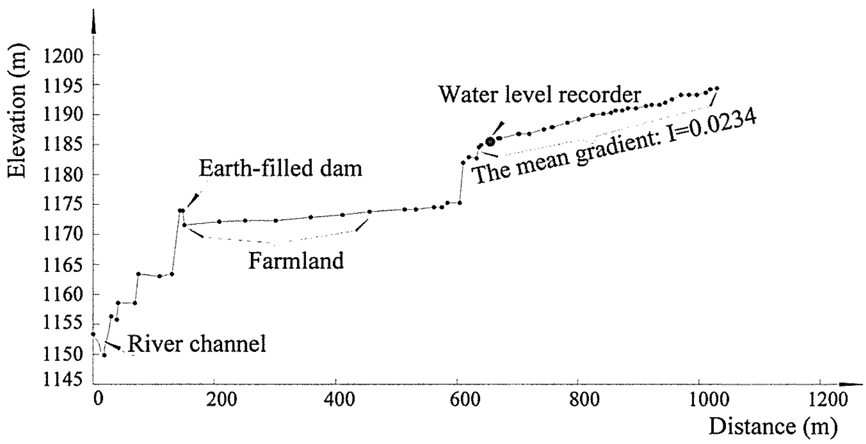

Fig 3.7 Longitudinal profile of the river channel

The lateral profile of the river channel at the surface flow observed site was determined by cross-leveling as shown in Figure 3.6. The data which directly recorded by water level recorder is the depth of the surface flow (water level). A usable method for data transformation from the depth of water to the data form of discharge on this irregular cross-section was developed as expounded in Chapter section 3.4.2 and Chapter section 3.4.3.

3.4.2 Computing formula

A conventional computational method of the flow-discharge calculation is using Manning's mean velocity formula (Equation 3.1) which is equivalent to the resistance law of the uniform flow of the river channel[61)].

$$v = \frac{1}{n} R^{\frac{2}{3}} I^{\frac{1}{2}} \qquad 3.1$$

$$Q = vA(h) \tag{3.2}$$

where, v-flow velocity ($m\cdot s^{-1}$), n-Manning's coefficient of roughness ($s\cdot m^{-1/3}$), R-hydraulic radius (m), I-gradient of river channel, Q-flow discharge ($m^3\cdot s^{-1}$), A-sectional area of flow (m^2) varies with different depth of water h (m) on this irregular cross-section (Fig.3.6).

3.4.3 Related parameters

The mean gradient of the channel I of the reach in which the water level recorder was installed was ascertained by longitudinal leveling of the river channel (Fig 3.7).

Coefficient of roughness was determined by Bathurst's equation (Equation 3.3) which has already been verified that applies to the river channel in the mountain field[62].

$$\frac{v}{v_*} = 10.57\left[\frac{R}{d_{84}}\right]^{2.34}\left[\frac{b}{h}\right]^{7(\lambda-0.08)} \tag{3.3}$$

$$v = Q/(bh) \tag{3.4}$$

$$v_* = \sqrt{ghI} \tag{3.5}$$

$$\lambda = 0.139\log_{10}\left[1.91\frac{d_{84}}{R}\right] \tag{3.6}$$

where, b-width of the river channel (m), d_{84}-particle size of 84 % (m), v_*-friction velocity ($m\cdot s^{-1}$), g-gravitational acceleration (9.81 $m\cdot s^{-2}$), λ-a coefficient which can be determined by Equation 3.6. Other factors are same as the above mentioned.

Table 3.3 d_{84} & n

d_{84} (m)	h (m)	n
0.4	0.515	0.0705
0.5	0.548	0.0781
0.6	0.579	0.0855
0.7	0.608	0.0926
0.8	0.635	0.0994
0.9	0.660	0.1059
1.0	0.684	0.1123

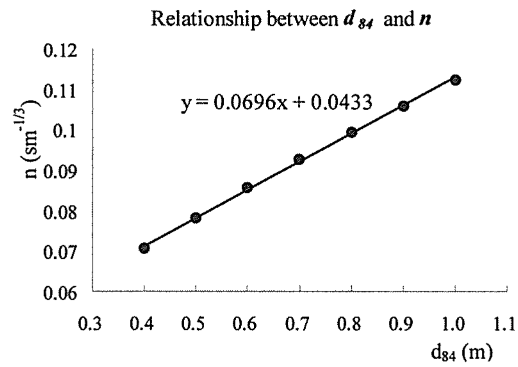

Fig 3.8 Relationship between d_{84} and n

Towards determining the relationship between the various d_{84} and the coefficient of roughness, the lateral section of the river channel was assumed to be wide rectangular form (R=h). With a certain d_{84}, the calculation was carried out by using Equation 3.3, Equation 3.4 and Equation 3.5 with different discharge repeatedly. Various depth of water h under the different discharge Q could be obtained. Then, various depth of water h combined with velocity v were substituted into Equation 3.1 respectively, thereby, different coefficient of roughness could be obtained. The referenced results are listed in Table 3.3 and shown in Figure 3.8.

Moreover, the determined method for n was suggested by Bray's equation (Equation 3.7). If the flood occurs with the condition of $R/d_{84}>1.5$, the coefficient of roughness can be expressed by the following equation.

$$n = 0.104 I_w^{\ 0.177} \qquad 3.7$$

Here, I_w-gradient of the water surface within the reach of the uniform flow.

The calculated results of n by Equation 3.1 and Equation 3.7 with the different discharge were shown in Figure 3.9. Figure 3.9 shows that the value of n attains a constant value when the discharge exceeds 60 m^3.

As the discharge exceeding 5 m^3/s did not occur on the flow observed cross-section in recent 5 years, the value of n was determined by Bathurst's method.

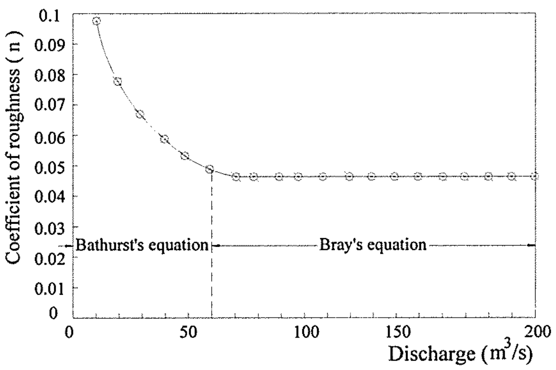

Fig 3.9 Relationship between discharge and roughness coefficient

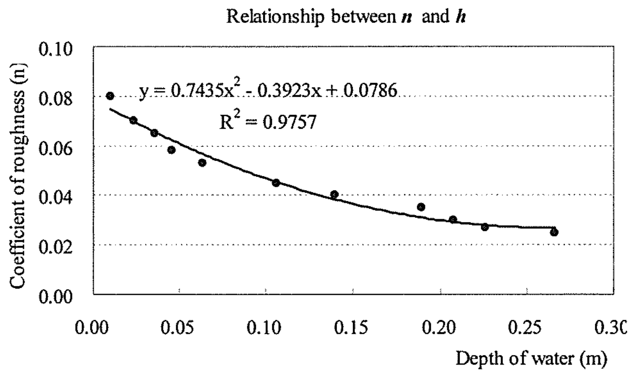

Fig 3.10 Relationship between n and h

Because the actual condition of the river channel such as the particle size of the solid in the river channel, and the vegetation type on both sides of the slope impacts on the roughness coefficient significantly, so the value of n must vary with the depth of water. Based on consideration of the actual condition of the river channel in the surface flow observed gully, each value of n at different depth of water was adopted as shown in Figure 3.10. As the roughness coefficient changes with in a range of 0.02-0.10, its mean value was approximately confirmed to be 0.06.

3.4.4 Relationship between discharge and depth of water

With regard to the flow observed lateral section, the investigated result of the maximum stage revealed the depth of water was almost no more than 0.5 m thereby the value of the water depth was randomly set to be no more than 0.5 m. The discharges corresponding with the different depth of water were calculated by using Equation 3.1. The relationship between the discharge and depth of water on the flow-observed section was shown in Figure 3.11.

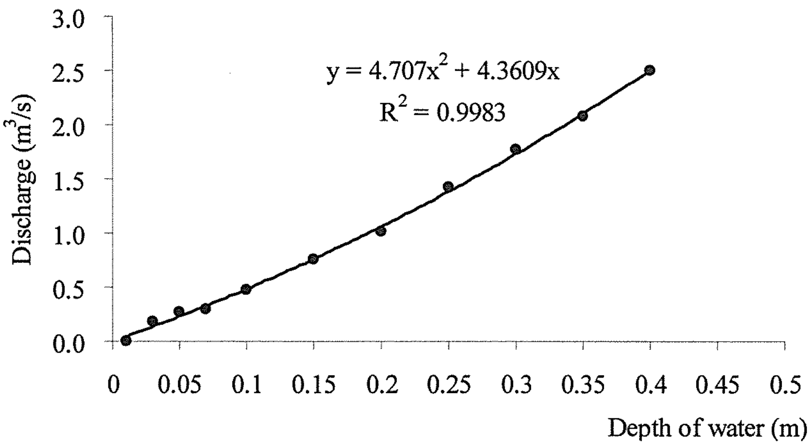

Fig 3.11 Relationship between discharge and depth of water on the flow-observed section

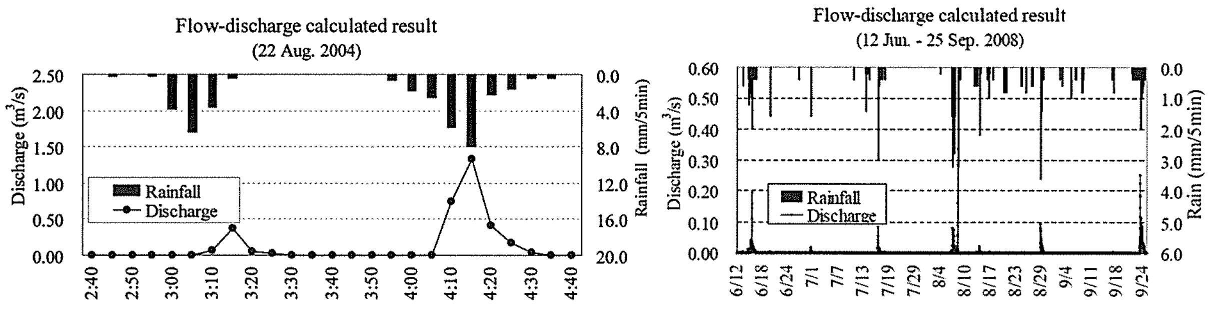

(a) (b)

Fig 3.12 Examples of flow-discharge calculation

The equation of the relation curve which is depicted in Figure 3.11 is extracted as below.

$$Q = 4.707h^2 + 4.3609h \quad 3.8$$

Every factor in Equation 3.8 is same as the above mentioned.

For instances of the flow-discharge calculation by using Equation 3.8, the calculated results on 22 August, 2004 and in a certain period from 12 June, 2008 to 25 September, 2008 are shown in Figure 3.12.a and Figure 3.12.b respectively.

3.5 Relationship between rainfall intensity and the surface flow generation

3.5.1 Surface flow generation for saturated topsoil condition

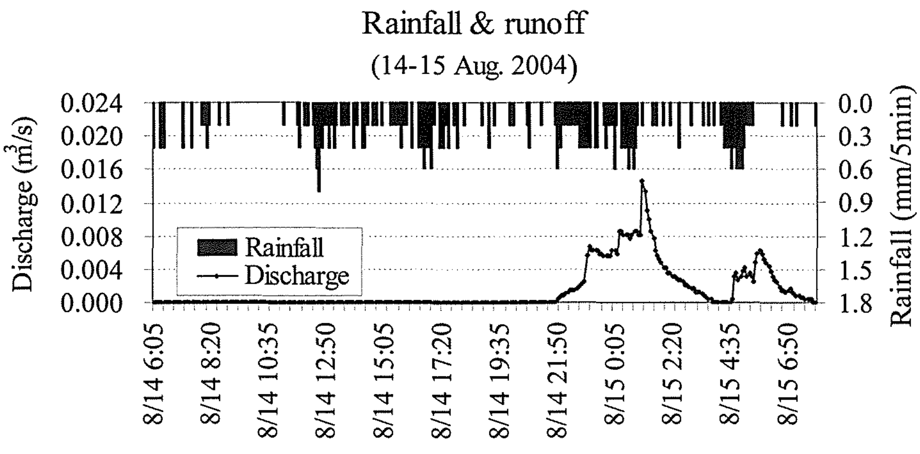

Fig 3.13 Rainfall-runoff hydrograph (14-15 Aug. 2004)

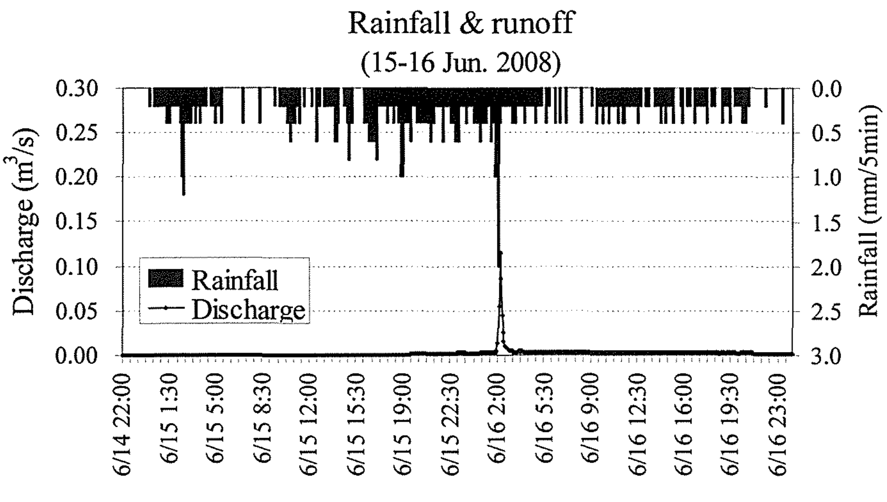

Fig 3.14 Rainfall-runoff hydrograph (15-16 Jun. 2008)

With an aim to evaluate the relationship between generation of the surface flow for saturated topsoil condition, further to estimate the thickness and the mean infiltration velocity of the topsoil, two paradigms of the low intensity with long duration rainfall with the corresponding surface runoff were chosen for analysis. The selected rainy events happened on 14-15 August, 2004 and on 15-16 June, 2008 respectively as shown in Figure 3.13 and Figure 3.14. The results which are related to the surface flow generation of each rainy event are listed in Table 3.4.

According to the results in Table 3.4, the surface runoff was generated by the rainfall intensity of 0.6 mm/5min in the both rainy events. Because the rainfall intensity which was higher than 0.6 mm/5min occurred before the surface flow generation and the lag time from the start of rainfall to runoff generation was long enough which exceeded 10 hours in the both rainy events, therefore, the topsoil could be affirmed to attain the saturated condition.

Table 3.4 Results of rainfall analysis (1)

Rain event	Rainfall duration (min)	Max. intensity (mm/5min)	Total rainfall (mm)	Intensity when runoff occurred (mm/5min)	Before runoff occurrence	
					Max. intensity (mm/5min)	Rainfall infiltrated (mm)
14-15 Aug. 2004	1550	0.8	44.2	0.6	0.8	22.6
15-16 Jun. 2008	2700	2.0	86.2	0.6	1.2	27

With regard to the porosity of the topsoil within the range of the study basin, the porosity of the sand loess is mostly more than 0.35, and the soil porosity of the grassland on the slope is around 0.25-0.30 which could be roughly estimated by analyzing the variation of the saturated soil water content at different sites[38), 63)]. By considering the soil condition of the surface flow observed area, average porosity of the topsoil was approximately estimated to be 0.30. Consequently, in the case of the first rainy event (14-15 Aug. 2004), thickness of the topsoil could be approximately estimated to be about 8.0 cm by considering the infiltrated rainfall before the surface flow generated (22.6 mm) and the mean porosity of the topsoil. Using the same method, the thickness of the topsoil could be estimated to be about 9.0 cm due to the infiltrated rainfall was 27 mm before the surface flow generated in the second instance.

Naturally, the ground condition varies with the weather condition in different season and the soil water content changes dynamically. In the rainy season, the soil water content in the topsoil generally keeps higher level than other seasons which consequentially impacts on the natural state of the topsoil. Therefore, the exact thickness of the topsoil is difficult to be ascertained. Actually, there is no obviously boundary between the topsoil and the subsequent soil layer. Based on the analyzed results as mentioned above, the thickness of the topsoil is roughly estimated to be 10 cm and this result is necessary for the development of the surface runoff calculation model (the relational content was expounded in Chapter 4).

Simultaneously, as generation of the surface flow was caused by the rainfall intensity of 0.6 mm/5min when the topsoil attained saturation, the mean saturated infiltration velocity of the topsoil (thickness about 10 cm) could be confirmed to approximately 0.6 mm/5min. Meanwhile, the mean infiltration velocity of the subsequent soil-layer is less than 0.6 mm/5min, which could be ascertained.

Consequently, it can be concluded that the necessary condition of the surface flow generation is the rainfall intensity attains 0.6 mm/5min for saturated topsoil condition.

Additionally, Figure 3.13 and Figure 3.14 depict that the surface flow was unstable after generating and its scale was significantly influenced by the rainfall intensity, as well as the surface runoff would quickly disappear after the rain stopped.

3.5.2 Surface flow generation for unsaturated topsoil condition

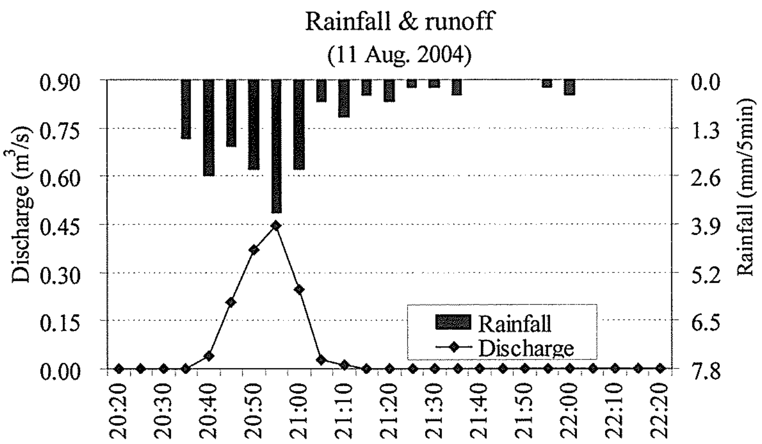

(a)

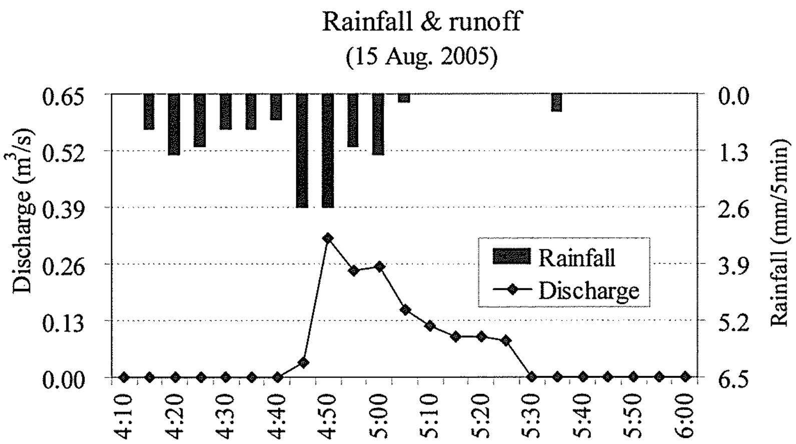

(b)

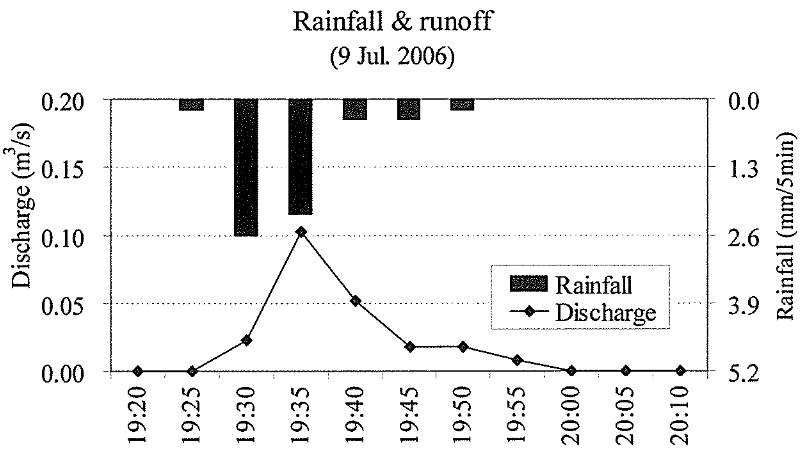

(c)

Fig 3.15 Rainfall-runoff hydrographs

Three paradigms of the high intensity with short duration rainfall which separately happened on 11 August, 2004, 15 August, 2005 and 9 July, 2006 (Fig 3.15.a-Fig 3.15.c) were adopted with an aim to evaluate the critical condition of the surface flow generation under the condition of the unsaturated topsoil. The analyzed results related to the surface flow generation of the three rainy events were listed in Table 3.5.

Table 3.5 Results of rainfall analysis (2)

Rain event	Rain last (min)	Max. intensity (mm/5min)	Total rainfall (mm)	Intensity when runoff occurs (mm/5min)	The time from rain start to the runoff generated (min)
11 Aug. 2004	80	3.6	18.4	2.6	5
15 Aug. 2005	80	2.6	13.6	2.6	30
9 Jul. 2006	30	2.6	6.0	2.6	5

For all the three rainy events, the surface flow was immediately generated by the rainfall intensity of 2.6 mm/5min. Because the lag time from the start of rainfall to the surface flow generation were all less than 30 minutes, the topsoil could be affirmed still in unsaturated condition when surface runoff generated. Furthermore, the analyzed results of other several rainy events indicated that the surface flow could not be generated when the rainfall intensity was less than 2.6 mm/5min, whereas the surface flow was generated by all rainy events whose intensity attained or more than 2.6 mm/5min for unsaturated topsoil (Fig 3.19). Therefore, the critical condition of the surface flow generation for unsaturated topsoil condition is the rainfall intensity attaining 2.6 mm/5min, which can be ascertained. Furthermore, the average unsaturated infiltration velocity of the topsoil can be estimated to be slightly less than 2.6 mm/5min.

3.6 Mechanism of the surface flow generation

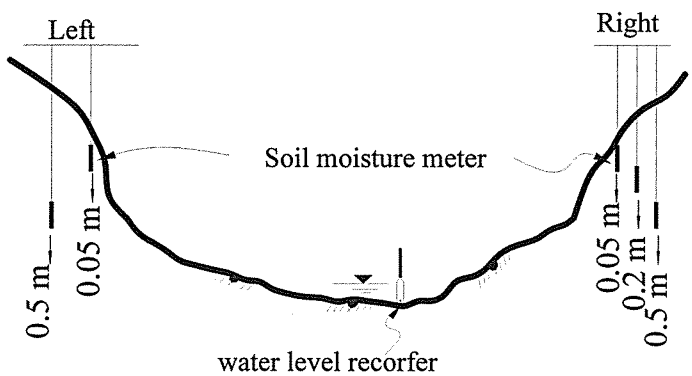

Fig 3.16 Schematic diagram of the soil moisture meters installed section
(Due to uncertain reason a soil moisture meter installed at the depth of 20 cm on the left side was destroyed)

With an aim to clarify the mechanism of the surface flow generation in the river channel, the observation of the soil water content was conducted on the surface flow observed section. The soil moisture meters were installed at the depths of 5 cm, 20 cm and 50 cm respectively in both sides of the slope (Fig 3.16).

3.6.1 Mechanism for Case 1

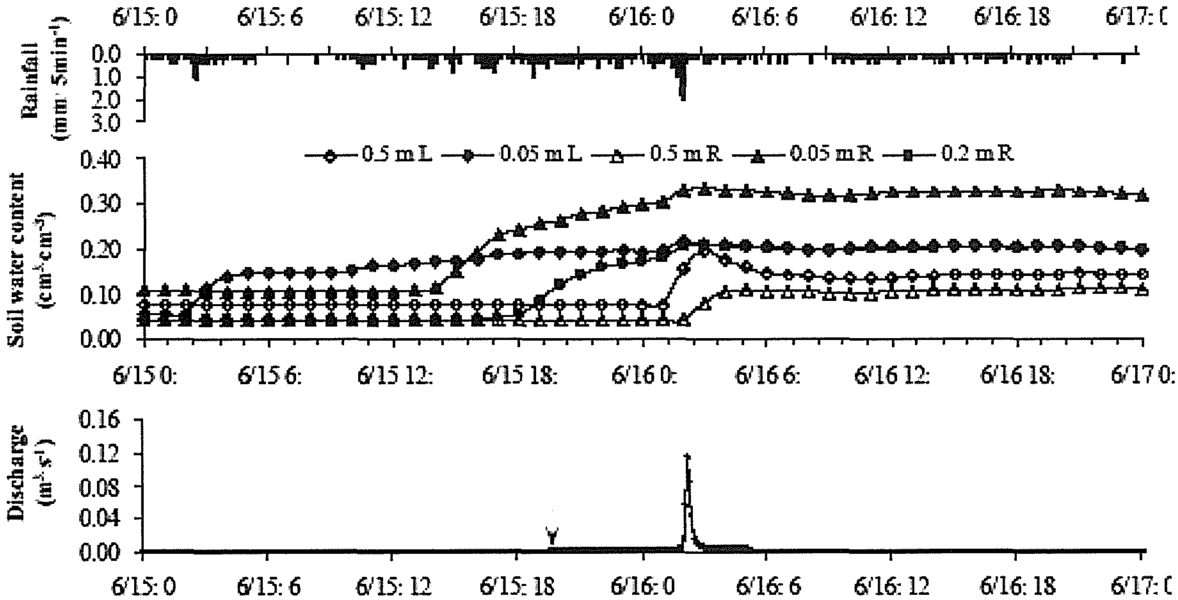

Fig 3.17 Process of rainfall, variation of the soil water content and surface runoff

(Case 1: a low intensity with long duration rainfall event happened on 15-16 Aug., 2008. Arrow indicates the time of surface flow generated)

Figure 3.17 depicts the temporal process of the rainfall, variation of the soil water content at different depth in the slope and the surface runoff which happened on 15-16 August, 2008. Rainfall of this time can be regarded as a case of the low intensity with long duration rainy events (Case 1).

During the time after the rain started and before the runoff generated, because the rainfall intensity was less than 2.6 mm/5min which has been confirmed as the necessary condition of the surface runoff generation for unsaturated topsoil, the surface runoff could not be generated. However, the soil water content at the depth of 5 cm in both sides of the slope began to increase at different time point respectively, and increased gradually. The water content at the depth of 5 cm in both sides reached to different level till the same time point, this situation was considered to be caused by the different porosity of the topsoil on the both sides. The soil water content at the depth of 20 cm also increased from a time point which legged the start time of the soil water content increase at the depth of 5 cm. However, the soil water content at the depth of 50 cm kept stable state and without increasing before the runoff generated.

The surface runoff was generated by the rainfall intensity of 0.6 mm/5min when the soil thickness of the depth of 5 cm on both sides of the slope attained saturation. At the time when the runoff generating, the soil water content at the depth of 20 cm was also obviously increased. However the water content at the depth of 50 cm had no visible increase.

Based on the analyzed results herein, mechanism of the surface runoff generation caused by the low intensity with long duration rainfall is summarized as below.

The surface flow can be generated when the topsoil attains saturation and the rainfall intensity reaches or surpasses 0.6 mm/5min.

3.6.2 Mechanism for Case 2

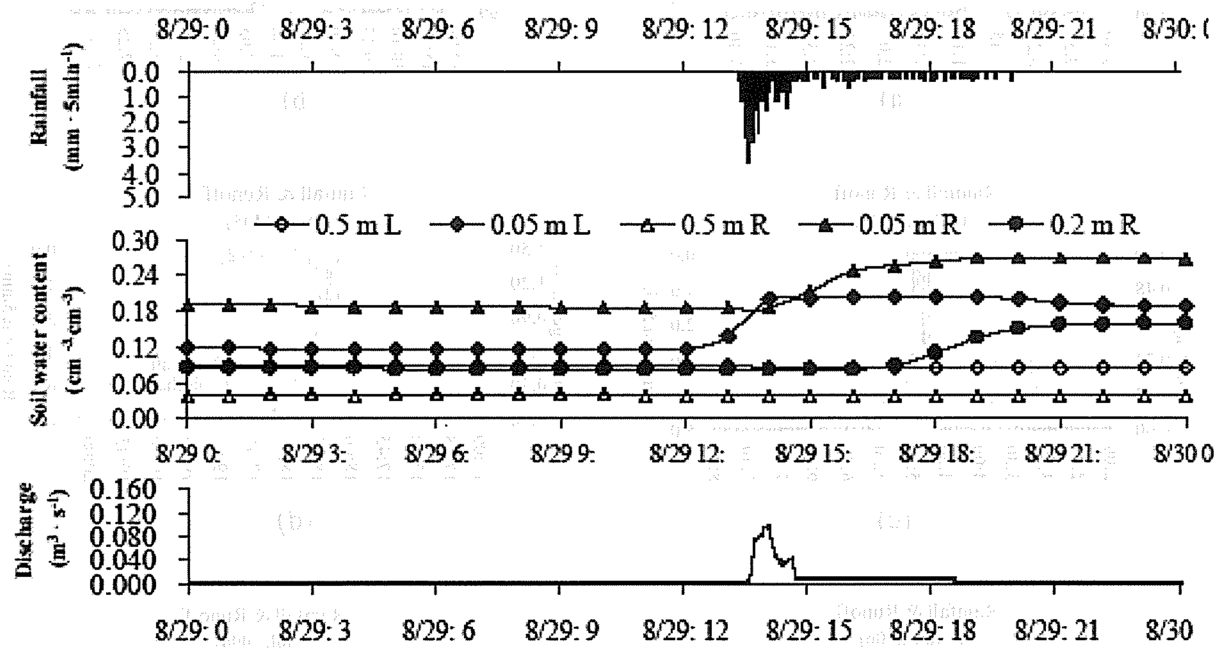

Fig 3.18 Process of rainfall, variation of the soil water content and surface runoff

(Case 2: a relatively high intensity rainfall event happened on 29 Aug., 2008)

Figure 3.18 shows the temporal process of the rainfall, the surface runoff and variation of the soil water content, which occurred on 29 August, 2008. The rainfall of this time can be considered as a case of the high intensity rainy events (Case 2). The rainfall was mainly centralized in the period of time of 13:30 -14:30 in the post meridian with the mean intensity of 1.67 mm/5min, then the rainfall intensity became very low, only about 0.22 mm/5min.

The surface flow immediately generated by the rainfall intensity of 2.6 mm/5min after the start of the rainfall. The soil water content at various depths kept relatively stable level at the time point when the runoff generated. The soil water content at depth of 5 cm began to increase from a time point after the runoff generated. Therefore, mechanism of the surface runoff generation caused by the high intensity rainfall is tersely generalized as below.

The surface flow can be generated when the rainfall intensity attains or exceeds 2.6 mm/5min in spite of the condition of the topsoil.

3.7 Correlation between mean rainfall intensity and runoff rate

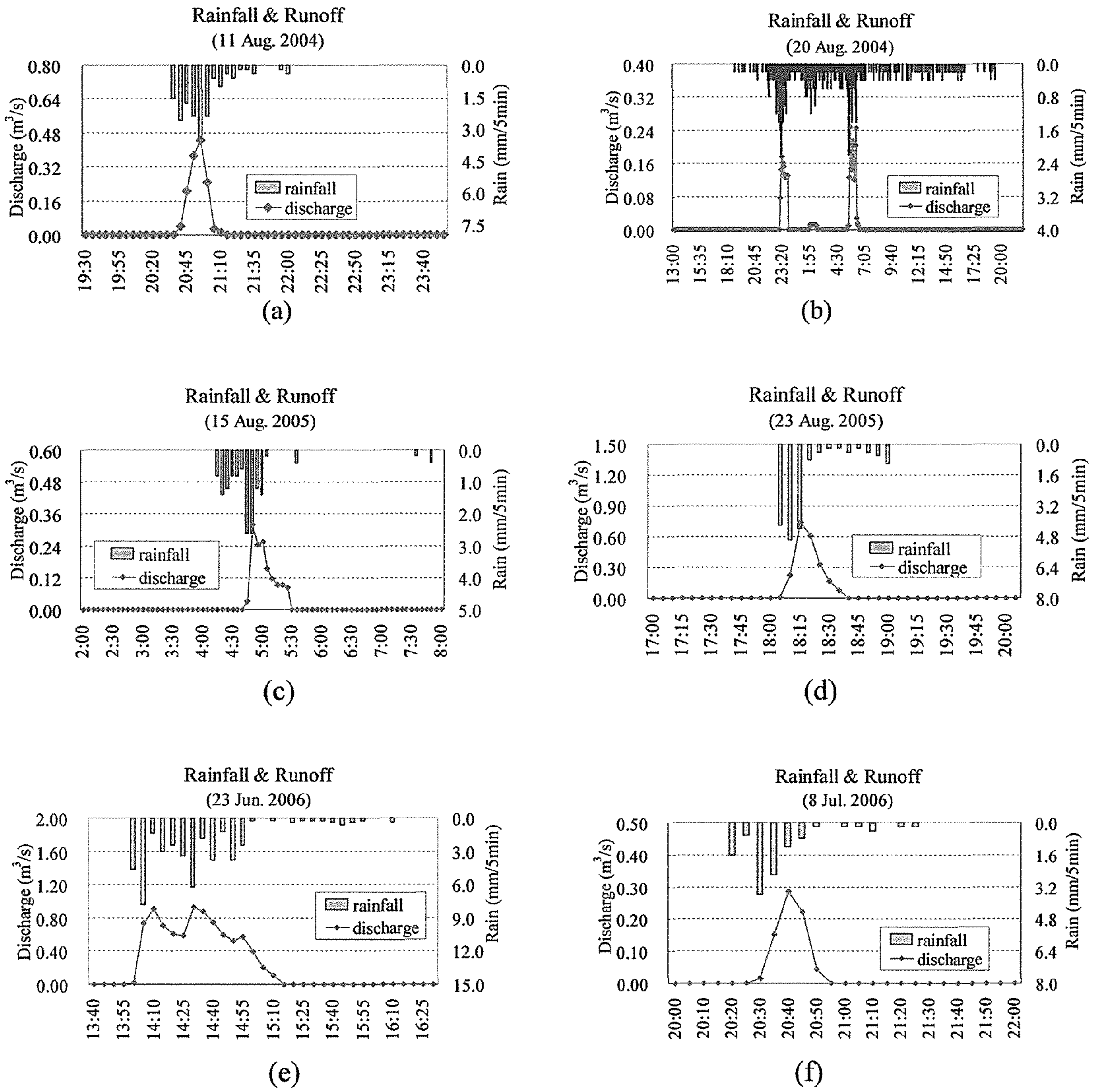

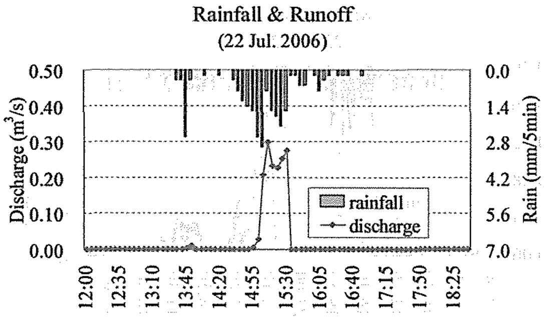
Rainfall & Runoff
(22 Jul. 2006)
Discharge (m³/s)
Rain (mm/5min)
rainfall
discharge

(g)

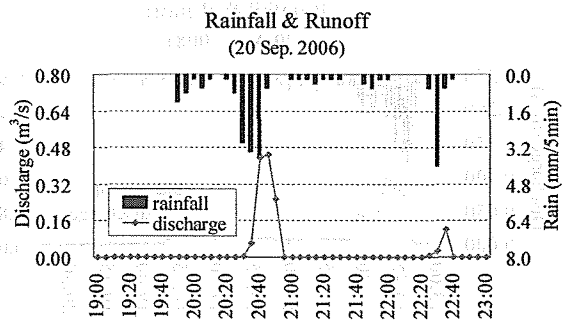
Rainfall & Runoff
(20 Sep. 2006)
Discharge (m³/s)
Rain (mm/5min)
rainfall
discharge

(h)

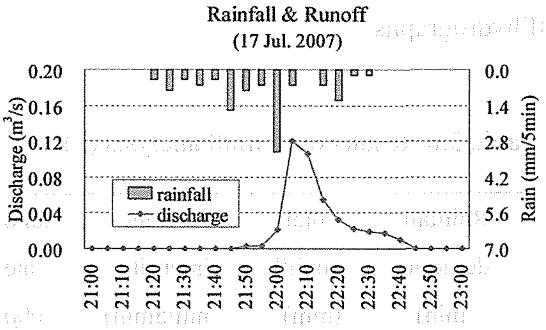
Rainfall & Runoff
(17 Jul. 2007)
Discharge (m³/s)
Rain (mm/5min)
rainfall
discharge

(i)

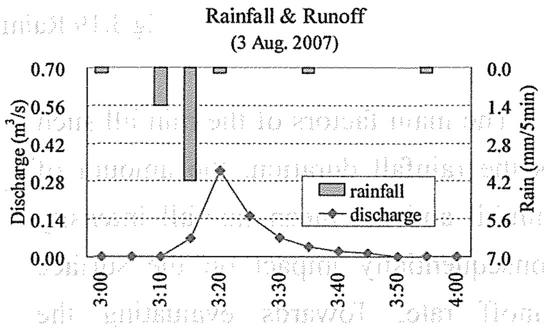
Rainfall & Runoff
(3 Aug. 2007)
Discharge (m³/s)
Rain (mm/5min)
rainfall
discharge

(j)

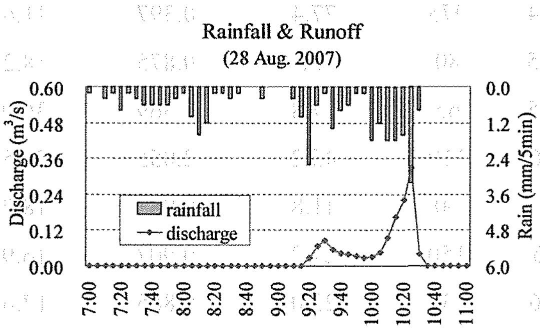
Rainfall & Runoff
(28 Aug. 2007)
Discharge (m³/s)
Rain (mm/5min)
rainfall
discharge

(k)

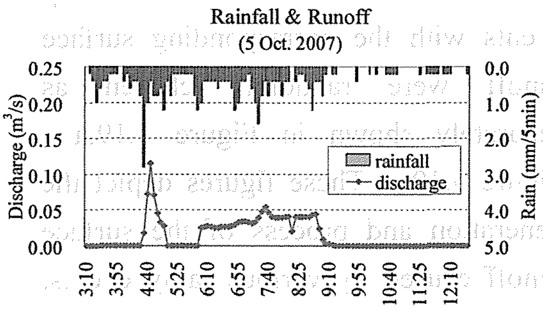
Rainfall & Runoff
(5 Oct. 2007)
Discharge (m³/s)
Rain (mm/5min)
rainfall
discharge

(l)

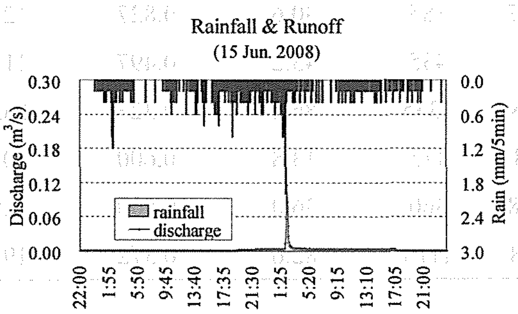
Rainfall & Runoff
(15 Jun. 2008)
Discharge (m³/s)
Rain (mm/5min)
rainfall
discharge

(m)

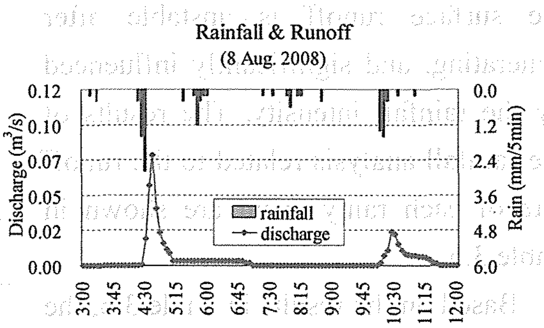
Rainfall & Runoff
(8 Aug. 2008)
Discharge (m³/s)
Rain (mm/5min)
rainfall
discharge

(n)

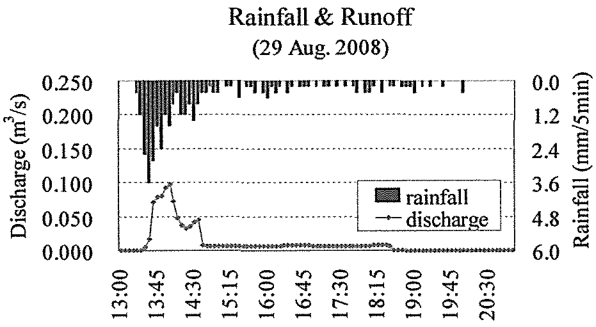

(o)

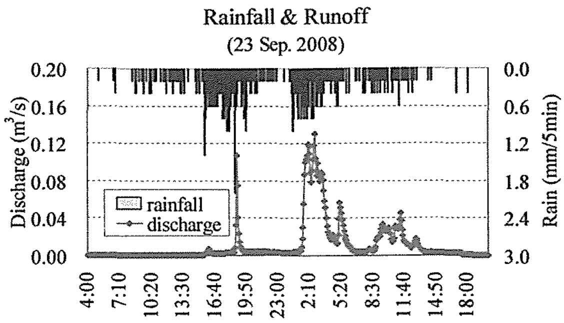

(p)

Fig 3.19 Rainfall-runoff hydrographs

The main factors of the rainfall such as the rainfall duration, the amount of rainfall and the mean rainfall intensity consequentially impact on the surface runoff rate. Towards evaluating the relationships between these factors and the runoff rate, a certain number of rainy events with the corresponding surface runoff were randomly chosen as separately shown in Figure 3.19.a - Figure 3.19.p. These figures depict the generation and process of the surface runoff caused by various rainy events. All the instances indicate a common characteristic of the surface runoff that the surface runoff is unstable after generating, and significantly influenced by the rainfall intensity. The results of the rainfall analysis related to the runoff rate of each rainy event are shown in Table 3.6.

Table 3.6 Results of rainfall analysis (3)

Date	Rainfall duration (min)	Total rainfall (mm)	Average intensity (mm/5min)	Runoff rate (%)
11 Aug.04	80	18.4	1.150	22.1
20 Aug.04	975	77.4	0.397	11.6
15 Aug 05	80	14	0.875	18.2
23 Aug 05	65	17.8	1.369	36.0
23 Jun.06	110	45.2	2.055	56.5
8 Jul.06	60	11.8	0.983	18.2
22 Jul.06	150	27.2	0.907	16.9
20 Sep.06	130	23.0	0.885	17.6
17 Jul.07	70	11.6	0.829	12.2
3 Aug.07	30	6.4	1.067	31.2
28 Aug.07	185	30.6	0.827	12.8
5 Oct.07	435	43.2	0.497	11.2
15 Jun.08	1335	86.2	0.323	8.05
8 Aug.08	115	13.8	0.600	10.0
29 Aug.08	360	36.0	0.500	8.9
23 Sep.08	1110	82.6	0.372	19.5

Based on the results in Table 3.6, the relational curve of the mean rainfall intensity and the runoff rate was obtained as shown in Figure 3.20. This curve indicates that the relatively high correlation exists between the mean rainfall intensity and the runoff rate. That is, with increasing of the mean rainfall intensity, the runoff rate generally increases. In other words, the mean rainfall intensity is a key influence factor of the surface runoff rate.

The relationship between the rainfall duration and the runoff rate, as well as the relationship between the amount of rainfall and the runoff rate are shown in Figure 3.21 and Figure 3.22 respectively. By observing these two Figures, there is no conspicuous relevance between the rainfall duration and the runoff rate, also between amount of rainfall and the runoff rate, which can be confirmed.

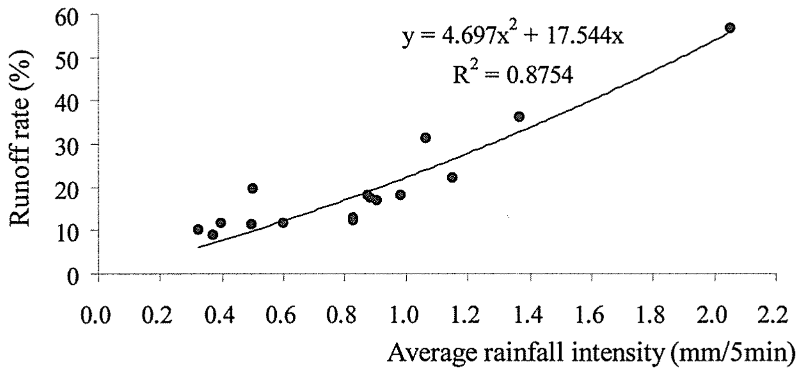

Fig 3.20 Correlation between the mean rainfall intensity and runoff rate

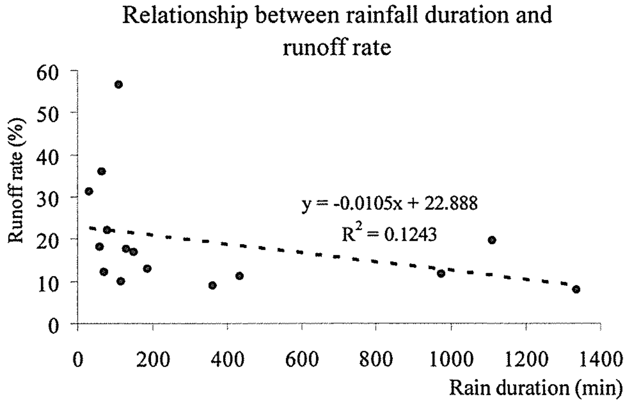

Fig 3.21 Relationship between rainfall duration and runoff rate

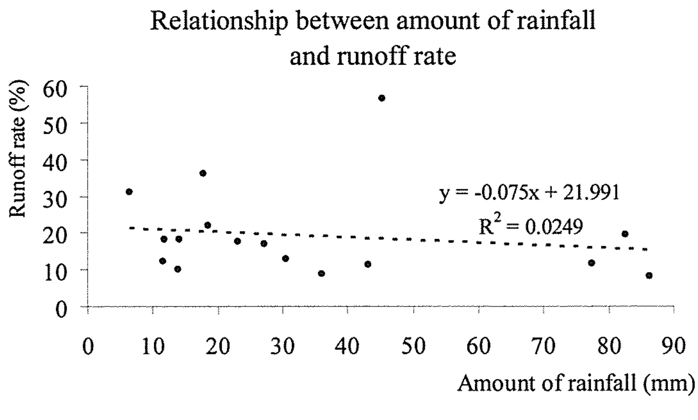

Fig 3.22 Relationship between amount of rainfall and runoff rate

3.8 Summary & Conclusions

The primary coverage of this chapter is analysis of the relationship between the rainfall and the surface runoff through analysis of the observed data. Firstly, relationship between the rainfall intensity and the surface flow generation was clarified. Next, mechanism of the surface flow generation was clarified. Then, correlation between the mean rainfall intensity and runoff rate was estimated. Some conclusions are listed as follows:

Relationships between the rainfall intensity and generation of the surface flow:

(1) The necessary condition of the surface flow generation is the rainfall intensity ≧ 0.6 mm/5min for saturated topsoil condition.

(2) The necessary condition of the surface flow generation is the rainfall intensity ≧ 2.6 mm/5min for unsaturated topsoil condition.

(3) The mean rainfall intensity is the key influence factor of the runoff rate.

Mechanisms of the surface flow generation caused by the low intensity with long duration rainfall and the high intensity rainfall were clarified respectively.

Some properties of the soil:

(1) The thickness of the topsoil is about 10 cm.

(2) The mean saturated infiltration velocity of the topsoil is slightly more than 0.6 mm/5min; the mean unsaturated infiltration velocity of the topsoil is less than 2.6 mm/5min.

(3) The average infiltration velocity of the soil layer subsequent to the topsoil is less than 0.6 mm/5min.

Additionally, distribution characteristics of the rainy events in 2007 were analyzed because the rainfall amount and the rainfall process in 2007 were approximate to the rainfall in the normal year.

Chapter 4

Numerical Calculation of the Surface Runoff

4.1 Introduction

Conventionally, various runoff analysis techniques were proposed. Some representative types such as kinematic wave model[64), 65)], tank model[66), 67)], storage routing model[68),69)], fuzzy neural network model[70)], and distributed basin model combined with a certain analysis method[71),72), 73)]. These runoff analysis models have been applied to the fields such as the runoff simulation, the runoff calculation and flood forecast and so on.

With regard to the runoff calculation methods based on lumped system model, tank model and storage routing model have simplicity and practicability compared with the distributed model. However, both tank model and storage routing model are lack of physical basis which are considered as the shortcomings[74)].

Tank model is useful for runoff analysis because it represents non-linear stream flow behavior. It is especially applicable to the long-term runoff calculation. However a comparatively large difference generally exists between the peak discharge and the simulated result merely by using tank model. In other words, a short term runoff calculation by using tank model has inaccuracy in a certain extent. Compared with tank model, as a merit of storage routing model, it is adequate for the simulation of the short-term runoff calculation. The simulated maximum discharge by using storage routing model approaches the actual peak flow primely. However, calculated accuracy of the long-term calculation simply by using storage routing model is relatively low[74), 75)].

Compared with tank model and storage routing model, kinematic wave model has extensive physical basis, and marvelously applies to runoff calculation both long-term and short-term which results in its widely applicability[65),76), 77)].

Contrasted to lumped system model, the distributed model by which spatial connective relation between each tributary of a basin can be iconically expressed. Consequently, the distributed model combined with a certain runoff calculation methods have been developed and advanced in recent years[77)]. A prior research of distributed runoff model was developed by using irregular triangular facets[72)] (Oscar Luis, P.V. and Baltasar C.R mode, 1992). Yamashita, M. and Ichikawa, A. (2005) conducted the surface flow calculation by using SCS (Soil Convention Service Curve Number Method) which promoted the applicability of the distributed model[78)]. Tang, Q.H. and Oki, T. (et al., 2006) verified a distributed biosphere hydrological model (DBHM) for a large river basin[79)]. Kinematic wave model applying to the distributed basin has been validated that could be applied to the basins of various scales.

Especially, the runoff calculation method which developed by kinematic wave theory combined with hypothetical channel network has been quickly developed due to its extensive applicability and favorable practicability[80),81),82)].

Consequently, based on taking various factors of each kind of runoff analysis model into consideration, also thinking over the actual geographical features of the study location, we adopted kinematic wave model combining with hypothetical channel network to develop a runoff calculation model for surface runoff calculation of the study basin.

4.2 Conventional studies

4.2.1 Kinematic wave model

Kinematic wave model is a physical model to some extent which demands the relationship between the flow-discharge and the water depth according to the river channel resistance law. In such model, equation of motion of the flow can be replaced by the river channel resistance law of the uniform flow. In other words, the river channel resistance law is equivalent to mean velocity formula of the flow[64), 83)]. In past few years, GIS (geographic information system) was adopted to analyze the real conditions of a basin which caused the connection of each tributary could be expressed distinctly. Specifically, the DEM (digital elevation model) is used to generate the hypothetical channel network with GIS-Arcview. Application of GIS vividly promoted the runoff analysis technique which was developed by kinematic wave theory combing with the hypothetical channel network[84), 85), 86)].

4.2.2 Hypothetical channel network

The prior automatic generation of the hypothetical channel network was tentatively conducted by Nagami, M. and Sugiwura, Y. (1986) which was followed with many relational studies conducted by many researchers[87)]. The digital elevation model (DEM) is a necessary data to generate the hypothetical channel networks and it is separated into three types, such as the grid type, the triangle type and the contour type. Meanwhile, each type of DEM has inherent advantages and shortcomings. The grid type was widely adopted due to its convenient data acquisition and data processing. Moreover, development of the hypothetical channel network by using DEM of grid type could be applied to the theory of the flow direction[88)].

4.2.2.1 Flow direction

Determination of the correct flow direction is a crucial precondition for generating the hypothetical channel network exactly. Two methods were currently suggested for determining the flow direction, the steepest slope approach and the lowest elevation method. The two methods can be briefly explained by using Figure 4.1. With regard to the steepest slope approach, the flow direction is defined from the central point P to one of the circumjacent 8 points whose gradient between the current point P is the maximum. For the lowest elevation method, the flow direction is determined from the central point P to a point whose elevation is the minimum among the circumjacent 8 points[89]. The steepest slope direction can be calculated by Equation 4.1.

$$grad = \frac{-\{Z(\mathrm{I}) - Z(\mathrm{II})\}}{\sqrt{\{X(\mathrm{I}) - X(\mathrm{II})\}^2 + \{Y(\mathrm{I}) - Y(\mathrm{II})\}^2}} \qquad 4.1$$

where, X, Y-coordinate of the mesh point, Z-elevation of the point (X, Y), I-number of the central point (the current point), II-number of the next point in the steepest slope direction.

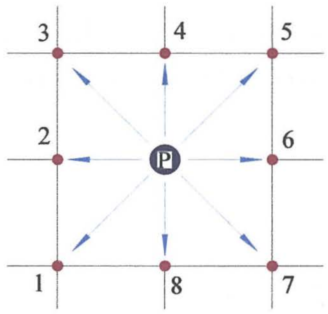

Fig 4.1 Flow-tracing direction

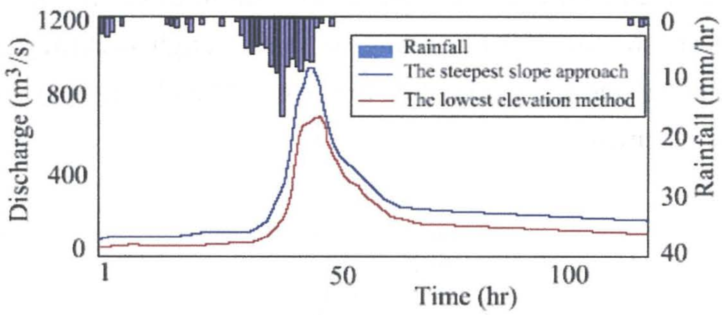

Fig 4.2 Comparison between the steepest slope approach and the lowest elevation method.[90]

Comparison between the steepest slope approach and the lowest elevation method was researched by Ao, T.Q. and Takeuchi, K. (2001). As a result, an obvious distinguishment existed in the spatial pattern of the flow direction between the steepest slope approach and the lowest elevation method. The spatial pattern of the flow direction was generally dominated by ration of the longitudinal size and horizontal size of the DEM grid-cell. Simultaneously, there is almost no distinction with an eye to the boundary of the hypothetical channel networks and the positional relation between the main stream way and every tributary. However, the difference exists in catchment area, the length of the main stream way, especially the average gradient to a certain degree. Moreover, as the influence on the runoff, the occurrence of the peak discharge achieved by the steepest slope method is slightly earlier than the lowest elevation method. The amount of runoff also shows the increased tendency by using the steepest slope method. Compared with the lowest elevation method, the steepest slope method can express the flow direction even relevantly[89), 90)].

4.2.2.2 Mesh size

Towards clarifying the responsive characteristics of runoff model varies with the different mesh size, Riku, S. and Koike, T. (et al., 1989) developed the distributed model with the mesh size of 100 m, 250 m, 500 m for the upstream of Uono River basin (area, 355 km^2) respectively. With regard to the results of the runoff calculation, almost no visible distinguishment between the mesh size of 100 m and 250 m, whereas result of mesh size of 500 m obviously distinguished from mesh size of 100 m and 250 m (Fig 4.3). Generally, parameters of the runoff model are necessarily changed with the increase of the mesh size. Furthermore, the expression of the runoff characteristics becomes even difficult with gradually increasing of the mesh size for a certain basin, which could be predicted[91)]. Takuma, T. and Kaoru, T. (et al., 1989) investigated the variation of the mesh size influencing on the expression of topographic feature with a basin whose area is about 10 km^2. The results indicated that with the mesh size increased the surface relief could not be expressed well and the calculated average gradient also diminished. In the case of the basin area of 10 km^2 with mesh size of 250 m, owing to fairly rough accuracy of the calculated length of the river channel and the gradient of the river channel, the appropriate mesh size of 50 m-100 m could be affirmed[92)].

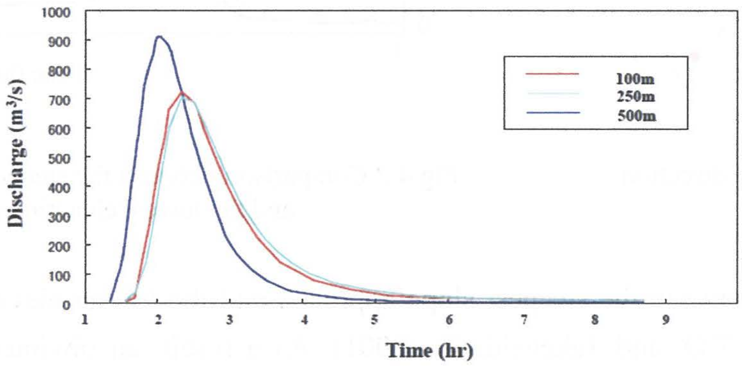

Fig 4.3 Hydrograph of different mesh sizes

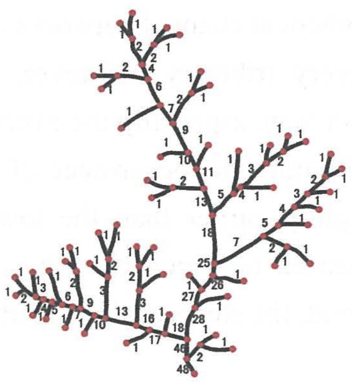

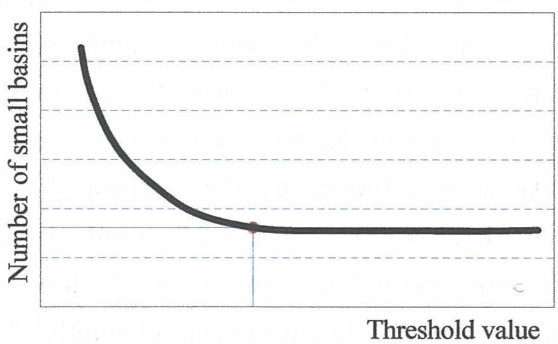

Fig 4.4 Stream order by Shreve's magnitude theory Fig 4.5 Determined method of threshold value

4.2.2.3 Stream order

An usable method for processing the flow-direction line is Shreve's magnitude theory by which the hypothetical channel network is classified into the line-group and point-group. The point-group refers to the source, junction and sink of the most downstream. The line-group refers to the river channel sector from source (external link), and the river channel sector of each junction after the source (internal link) to the edge of the most downstream[93]. The definition methods of the stream order are as follows.

(1) The external link is defined by magnitude 1.

(2) The river channel sector (internal link) is defined with magnitude $i_1 + i_2$ after junction of internal link (magnitude i_1) and internal link (magnitude i_2).

Thus, the integral hypothetical channel network can be represented by algebra addition according to Shreve's magnitude theory (Fig 4.4).

4.2.2.4 Threshold value for removing the flow-direction line

As a matter of fact, not all the flow-direction line can express the actual condition of the river channel while generating the hypothetical channel network by using DEM. Accordingly, it is necessary to remove a part of flow-direction lines felicitously. A banausic method is to set a threshold value by which a certain part of flow-direction lines can be removed. For instance, if the threshold value is set to be 10, each upstream edge of the generated hypothetical channel network has 10 mesh intersections which exist at the upside of each upstream edge. In such a manner, with increasing of the threshold value, the appearance of the hypothetical channel network will become more and more rough. Thus, how to set a felicitous threshold value is essential to generate the hypothetical channel network exactly. With regard to the method for determining the threshold value, a rectangular coordinate system can be established by plotting threshold value on horizontal axis while plotting number of small basins on vertical axis. The small basin refers to each separated basin with an eye to each junction in the hypothetical channel networks. As shown in Figure 4.5, the number of small basins almost has no change when the threshold reaches to a certain value, and this value was adopted as the threshold value to remove the flow-direction line[94), 95)].

4.2.2.5 Flowchart of generating the hypothetical channel network

In recent years, generation of the hypothetical channel network can be automatically performed by using a computer in the light of recent developments in computers. Figure 4.6 shows the general procedure for generating the hypothetical channel networks.

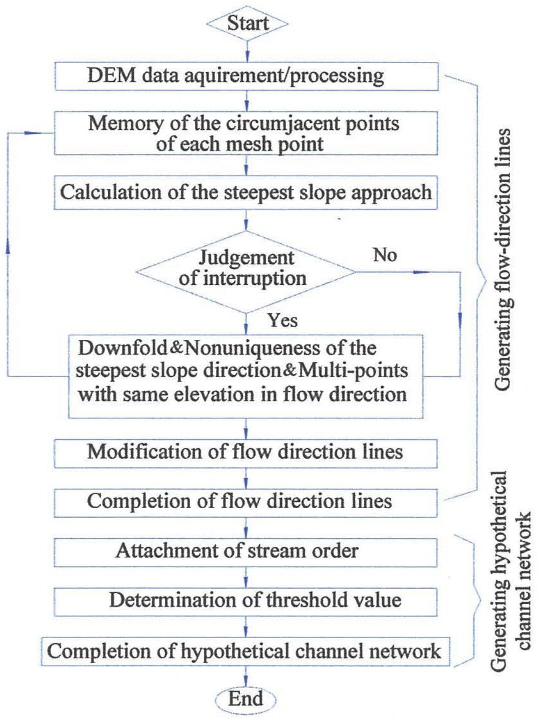

Fig 4.6 Flowchart for hypothetical channel network generation

4.2.3 Distributed-type model of a basin

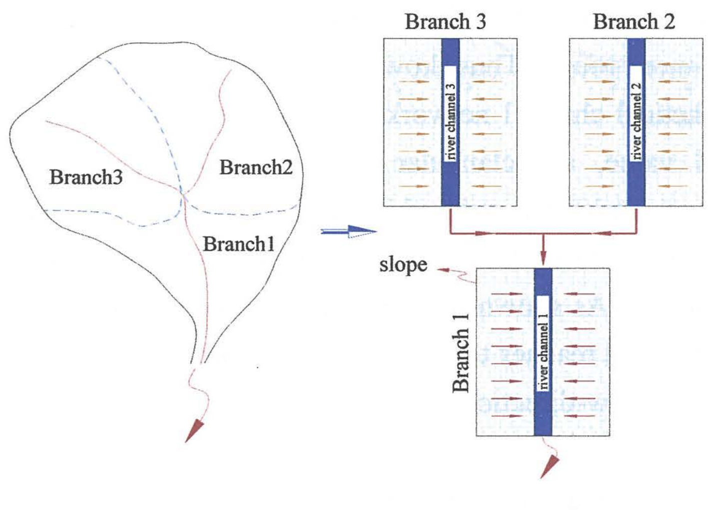

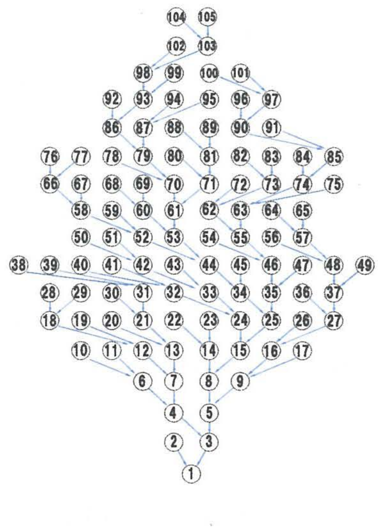

Fig 4.7 Schematic diagram of separation/combination of a distributed-type model

Fig 4.8 Modeling of a distributed basin (Arakura basin, Japan. area: 159 km^2)

A distributed basin model can express the spatial connective relation between each tributary of a basin distinctly. A basin must be separated into a number of small basins when modeling a basin into distributed type, then the whole basin can be expressed by the connection of each small basin in consideration of the mutual spatial-position. A method for basin separated is to pay attention to the junction of each branch and to confirm the relationship of water inflow of each small basin[95]. Figure 4.7 schematically depicts the separation/combination of the distributed model. Figure 4.8 shows modeling of a distributed basin which incipiently developed by Takasao, T. and Ikebuchi, S. (et al., 1977)[96].

4.3 Hypothetical channel network of the study area

4.3.1 Acquisition of DEM data

Because there is no extant available DEM data, the DEM data was acquired by using a topographic map of Liudaogou Basin which was drawn in 1982.

With respect to the acquired method of the DEM data, we established a rectangular coordinate system on the original topographic map with *X* axis in east-west direction, and *Y* axis in south-north direction, and the origin of coordinate was set on the bottom-left point, thereby every point on the topographic map was fixed. Next, inserted the lines in east-west direction by the space length of 5 m by which the elevation data of each gully can be expressed distinctly in the DEM (Fig 4.9). Then, read the intersection point of every inserted line and every contour line in regular sequence, whereafter wrote the obtained DEM data into a file (file format: *.txt).

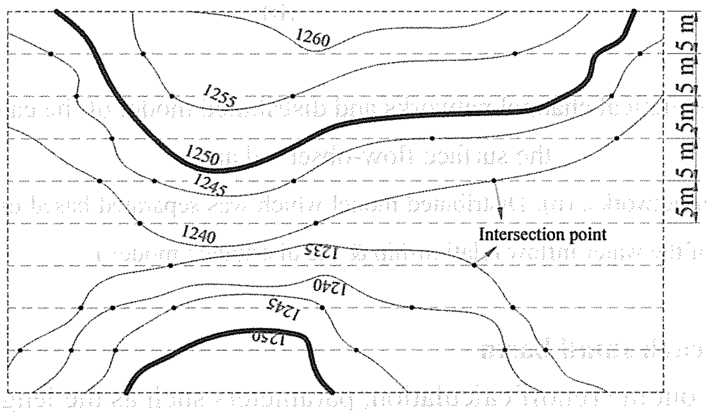

Fig 4.9 Schematic diagram of DEM data obtained method

In view of the present terrain obviously changed in some places compared with the conditions of twenty years ago, we updated the DEM data at these sites by GPS survey or leveling process with the result that the achieved DEM even more approaches the actual terrain.

4.3.2 Generation of hypothetical channel network

The hypothetical channel network is automatically generated by using GIS-Arcview (hyper-release 3.2). The threshold value of 40, by which the gullies could be clearly expressed, was adopted for generating hypothetical channel network of the study area. The achieved hypothetical channel network of the catchment of the surface-flow observed area (the upper reach of the area as shown in Fig 3.1) is shown in Figure 4.10.a. Considering the actual condition of the study area, each small basin of the left side was separated from the main stream channel by a road, thus the distributed model which was separated based on the hypothetical network is shown in Figure 4.10.b (area: about 0.10 km^2), and model of the relationship of the water inflow is shown in Figure 4.10.c.

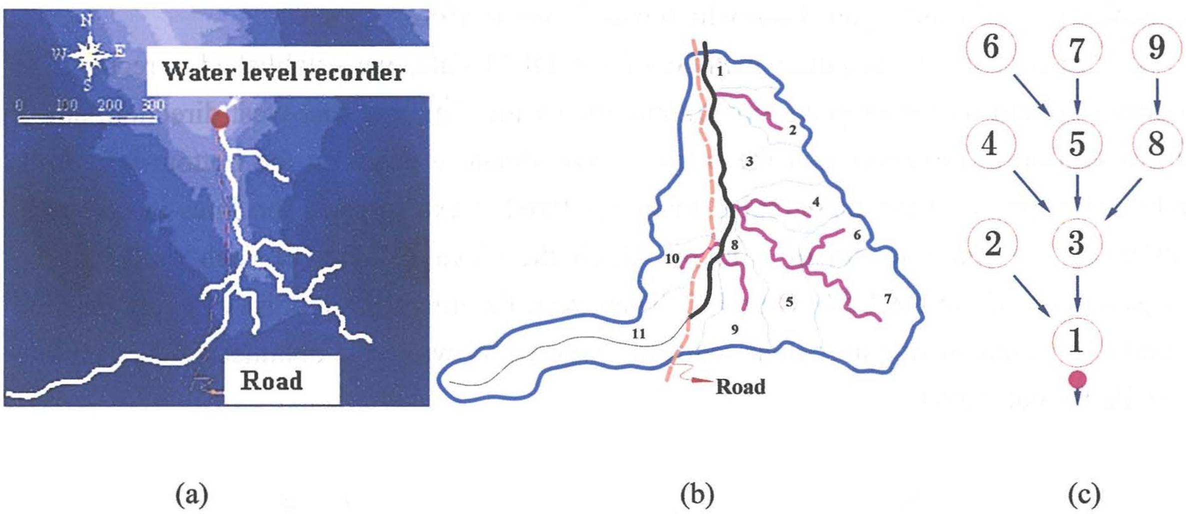

Fig 4.10 Hypothetical channel networks and distributed model of the catchment of the surface flow-observed area

((a). Hypothetical channel networks; (b). Distributed model which was separated based on hypothetical channel networks; (c). Modeling of the water inflow relationship & the distributed model)

4.3.3 Parameters of each small basin

Towards carrying out the runoff calculation, parameters such as the length of the slope and the river channel, the gradient of each slope sector and the river channel sector and etc must be determined. The determined method was mainly using the DEM, and some parameters were validated by the leveling survey. The determined parameters were listed in Table 4.1.

In consideration of the vegetation type on the slope, the crops-planting is carried out during the vegetation season. The vegetation period covers the whole rainy season which is the main time for the surface runoff calculation in the study location. Due to the influence of the vegetation cover, the coefficient of roughness on the slope sector is extremely difficult to be determined exactly. Comprehensively considering the land use pattern and the ground conditions on the slope sector, the coefficient of roughness of 0.10 was approximately adopted. In the river channel sector, coefficient of roughness was determined by the method as mentioned in Chapter section 3.4.

Table 4.1 Parameters of the slope sector and the river channel
(* Unit of the length (L): m)

Sector	The slope sector						The river channel sector		
Basin	Left side			Right side					
No.	L	i	n	L	i	n	L	i	n
1	0.0089	0.0684	0.10	0.0820	0.0767	0.10	0.04438	0.1584	0.06
2	0.0784	0.0726	0.10	0.0907	0.0809	0.10	0.1097	0.1613	0.06
3	0.0020	0.1205	0.10	0.1499	0.0152	0.10	0.1832	0.0256	0.06
4	0.0468	0.1044	0.10	0.0688	0.0944	0.10	0.1242	0.2117	0.06
5	0.1054	0.0833	0.10	0.0543	0.0756	0.10	0.1649	0.0873	0.06
6	0.0612	0.1623	0.10	0.0450	0.1322	0.10	0.0876	0.1772	0.06
7	0.1158	0.1397	0.10	0.0704	0.1184	0.10	0.1641	0.1164	0.06
8	0.0224	0.0822	0.10	0.0218	0.1017	0.10	0.07235	0.0071	0.06
9	0.0427	0.2601	0.10	0.0355	0.1855	0.10	0.1061	0.1886	0.06

(* L: length of channel; i: gradient of channel; n: coefficient of roughness)

4.4 Development of the runoff calculation model

4.4.1 Model development

The runoff calculation model was developed by kinematic wave theory. According to the investigated results of the actual ground condition, the diagram of the vertical profile from the ground surface to the sandstone stratum is extracted as shown in Figure 2.5. Based on consideration of the ground condition in Liudaogou Basin, the ground is approximately in homogeneous situation which could be confirmed. Therefore, in hydraulics, the model can be developed into a homogeneous model[38]. Towards the model development, the model was considered to be consisted of the slope sector and the river channel sector. The slope sector is composed of 2 layers. The river channel sector was considered to be composed of 1 layer from the riverbed down to the sandstone. Due to the limitations of the techniques of the present filed survey, the ground condition such as the exact thickness of the second layer in slope sector and the initial groundwater depth above the sandstone and etc are still unclear. However, because the surface flow mainly generates during the time of intensive rainfall, and generally disappears soon after the rain ending, therefore, each imprecise factor such as the thickness of the second layer and the initial groundwater depth above the sandstone layer has almost no impact on the surface runoff calculation. Consequently, the developed model in the present study is close to the actual ground condition as far as possible. And its schematic drawing is shown in Figure 4.11.

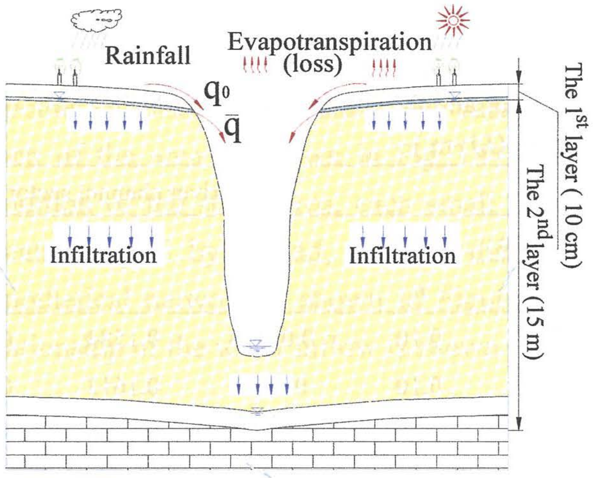

(a) Model lumping of Liudaogou Basin

(b) Typical terrain

Fig 4.11 Lumping of the runoff calculation model & Typical terrain

(In this model, the thickness of the 1st layer on the slope sector is determined by the analyzed result of the topsoil as mentioned in Chapter section 3.5; Thickness of the 2nd layer of the slope sector is approximately determined according to the result of the field survey)

4.4.2 Governing equations

The runoff calculation method in the developed model is continuous calculation in time. When carrying out the calculation, the model is separated into the slope sector and the river channel sector, the surface flow and the groundwater flow is to be calculated respectively.

4.4.2.1 Slope sector

(1) Equation of the continuity of the surface flow

$$\frac{\partial h}{\partial t}+\frac{\partial q}{\partial x}=r-\alpha\begin{cases}\alpha=f_1 & (h/\Delta t\geq f_1)\\ \alpha=h/\Delta t & (h/\Delta t<f_1)\\ \alpha=0 & (h=0)\end{cases} \qquad 4.2$$

(2) Manning's mean velocity formula (Equation of motion of one-dimensional surface flow)

$$q=\frac{1}{n}hR(h)^{\frac{2}{3}}I^{\frac{1}{2}} \qquad 4.3$$

where, h-depth of water (m), q-unit width flow rate ($m^2\cdot s^{-1}$), Δx -unit length for calculation in flow direction (m), Δt - interval of calculation time (s), r-the effective rainfall ($m\cdot s^{-1}$), f_1,

f_2-mean infiltration velocity of the 1st and the 2nd layer ($m \cdot s^{-1}$), n-coefficient of the roughness ($s \cdot m^{-1/3}$), R-hydraulic radius (m), I-gradient of the slope. α-a referenced coefficient, because f_1 is defined as a constant, however, its actual value must rely on a certain boundary condition of the water depth h (each boundary condition of the water depth is indicated in the parenthesis in Equation 4.3). Therefore, the actual infiltration velocity of the 1st layer (f_1) is determined by this referenced coefficient.

(3) Equation of the continuity of the groundwater flow (in the 1st layer)

$$\lambda \frac{\partial \bar{h}}{\partial t} + \frac{\partial \bar{q}}{\partial x} = f_1 - \beta \begin{cases} \beta = f_2 & (\lambda \bar{h} / \Delta t \geq f_2) \\ \beta = \lambda \bar{h} / \Delta t & (\lambda \bar{h} / \Delta t < f_2) \\ \beta = 0 & (\bar{h} = 0) \end{cases} \quad 4.4$$

(4) Darcy's law (Equation of motion of one-dimensional groundwater flow)

$$\bar{q} = k \bar{I} \bar{h} \quad 4.5$$

where, λ-effective porosity of the soil, $\bar{h}$-Depth of the groundwater flow (m), $\bar{q}$-discharge of the unit width of the groundwater ($m^2 \cdot s^{-1}$), k-coefficient of permeability ($m \cdot s^{-1}$), $\bar{I}$-gradient of groundwater in the 1st layer which is approximately replaced by the gradient of the slope. β-a referenced coefficient, by which determines the actual infiltration velocity in the 2nd layer (f_2) for the different groundwater depth in the first layer.

The equations for groundwater calculation in the second layer are same as equations used on calculation in the first layer, only the number of layer is changed, which are omitted here.

4.4.2.2 The river channel sector

The computing formulas of the runoff calculation in the river channel are corresponding to the slope sector respectively, only some factors are changed which results in the distinctions of the formulas in forms.

(1) Equation of the continuity of the surface flow

$$\frac{\partial A}{\partial t} + \frac{\partial Q}{\partial x} = q' + (r - \alpha) \cdot b \begin{cases} \alpha = f_1 & (h / \Delta t \geq f_1) \\ \alpha = h / \Delta t & (h / \Delta t < f_1) \\ \alpha = 0 & (h = 0) \end{cases} \quad 4.6$$

(2) Manning's mean velocity formula

$$Q = \frac{1}{n} AR(h)^{\frac{2}{3}} I^{\frac{1}{2}} \tag{4.7}$$

where, A-area of the flow-section (m^2), Q-flow discharge ($m^3 \cdot s^{-1}$), b-with of the river channel (m), q'-surface inflow from the unit width of the slope ($m^2 \cdot s^{-1}$), other factors are corresponding to those of the slope sector as above-mentioned.

(3) Equation of the continuity of the groundwater flow

$$\lambda \frac{\partial \overline{A}}{\partial t} + \frac{\partial \overline{Q}}{\partial x} = \overline{q}' + (f_1 - \beta) \cdot b \begin{cases} \beta = f_2 & (\lambda \overline{h} / \Delta t \geq f_2) \\ \beta = \lambda \overline{h} / \Delta t & (\lambda \overline{h} / \Delta t < f_2) \\ \beta = 0 & (\overline{h} = 0) \end{cases} \tag{4.8}$$

(4) Darcy's law

$$\overline{Q} = k \overline{I} \overline{A} \tag{4.9}$$

where, $\overline{Q}$-discharge of the groundwater flow ($m^3 \cdot s^{-1}$), $\overline{A}$-area of the groundwater flow-section (m^2), $\overline{q}'$-groundwater inflow from the unit width of the slope sector ($m^2 \cdot s^{-1}$), f_1-mean infiltration velocity of the soil-layer above the sandstone ($m \cdot s^{-1}$), f_2-infiltration velocity of the sandstone stratum, and it is tininess and approximately evaluated by a loss coefficient (1.0×10^{-8} $m \cdot s^{-1}$), $\overline{I}$-gradient of the groundwater (approximately replaced by the gradient of the river channel), other factors are corresponding to the above mentioned.

4.4.3 Differencing and algorithm

4.4.3.1 Differencing

Towards carrying out the runoff calculation, the equations of the continuity both of the surface flow and the groundwater flow must be differenced (discretization in time). The differencing method is the upstream-difference scheme[97)]. Taking the slope sector as an example, the difference formulas of the Equation of continuity of the surface flow and the Equation of the continuity of the groundwater flow are as follows.

(1) Difference formula of the Equation of the continuity of the surface flow

$$h_i^{n+1} = h_i^n + dt \left[r(t) - \alpha - \frac{q_i^n - q_{i-1}^n}{dx} \right] \tag{4.10}$$

(2) Difference formula of the Equation of continuity of the groundwater flow

$$\overline{h}_i^{n+1} = \overline{h}_i^{n} + \frac{dt}{\lambda}\left[(f_1 - \beta) - \frac{\overline{q}_i^{n} - \overline{q}_{i-1}^{n}}{dx} \right] \quad 4.11$$

where, n-time step of calculation (1 s), i-grid No., other factors are corresponding to the above mentioned.

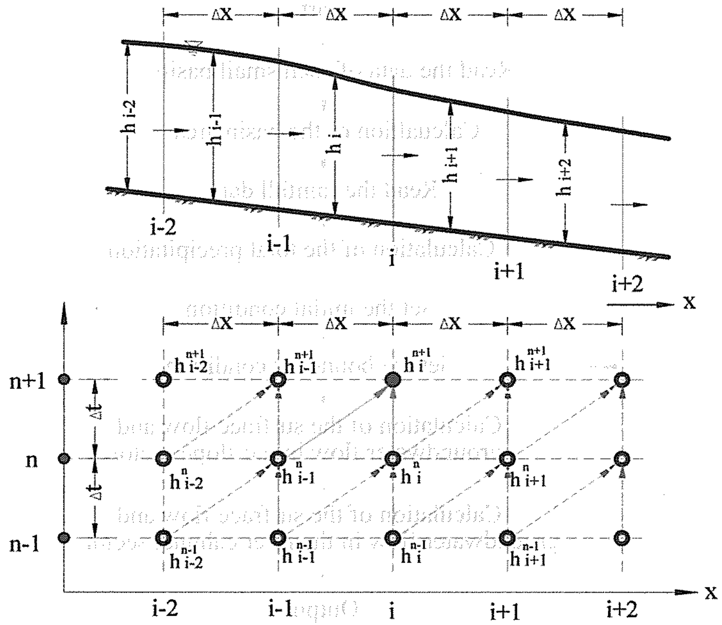

Fig 4.12 Schematic drawing of algorithm

4.4.3.2 Algorithmic method

The algorithmic method of the upstream-difference scheme can be explained by using Figure 4.12. The calculation starts from the original point (the source of the edge of the upstream) with the interval of time of 1 s. The interval of length in x direction (flow direction) is set to be 5 m. The flow tracks in the developed calculation model as shown in Figure 4.11. By setting a certain initial conditions and the boundary conditions for the numerical calculation, the runoff calculation was ensured as the spatio-temporal continuous calculation.

4.4.3.3 Boundary condition

(1) Vertical direction The boundary conditions in the vertical direction, in other words, the water input and output in each layer are listed in the bracket in Equation 4.2 and Equation 4.4 of the slope sector (the second layer is omitted), and in Equation 4.6 and Equation 4.8 of the river channel sector.

(2) The upstream edge The inflow of the upstream edge in the slope sector is set to be 0.

For the river channel sector, if there is a catchment at the upside, the discharge at the lower end of this catchment is regarded as the boundary condition of the upper end of the river channel sector.

4.4.3.4 Procedure

The main procedure of the runoff calculation is shown in Figure 4.13.

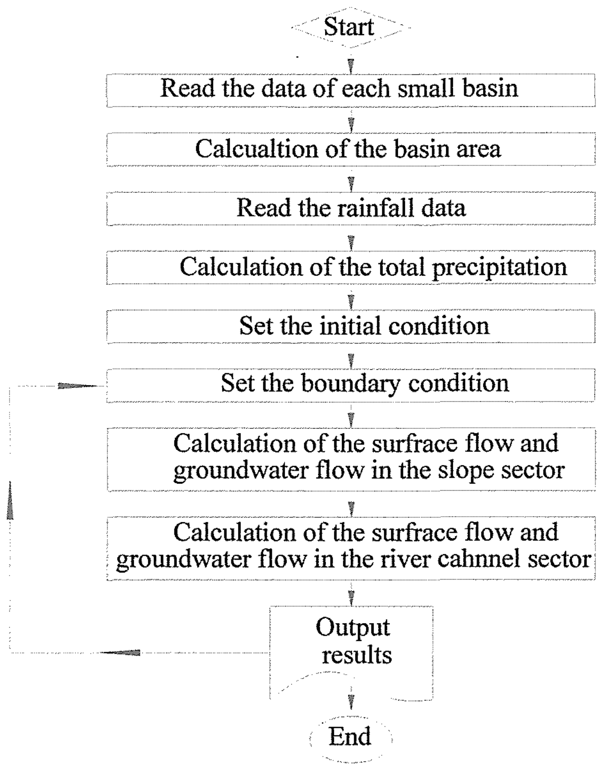

Fig 4.13 Flow chart of the runoff calculation

In the current study, the numerical calculation model was developed by programming language FORTRAN 90/95. The actual process of the program compiling is omitted here.

4.4.4 Parameter determination

With the aim to achieve the precise numerical calculation results, the value of every necessary parameter must be accurately determined as much as possible. In the current study, the main methods for determining the parameters are as follows.

(1) Some parameters such as the thickness of the topsoil, the mean infiltration velocity of the first layer were approximately confirmed according to the analyzed results of the relationship between the rainfall intensity and the surface flow generation such as expounded in Chapter section 3.5. The parameters determined by such method were regarded as the exact values.

(2) The coefficient of roughness and effective porosity of the topsoil were determined by the actual survey combined with referencing relational studies conducted on Liudaogou Basin. Each parameter which was determined by such method was considered as approximately the exact value.

(3) Towards determining the other parameters whose value are uncertain, firstly, each of such parameter was experimentally given a value within a reasonable range. Next, we carried out the runoff calculation by using the developed numerical model, and the calculated result of the surface runoff was named by the calculated-flow (C-flow in Figure 4.14). Inevitably, there is a difference between the calculated-flow and the observed-flow (O-flow in Figure 4.14). The observed-flow was regarded as the accurate value which was achieved by the method as introduced in Chapter section 3.4. To lessen the difference between the observed-flow and the calculated-flow, we adjusted the value of each unconfirmed parameter and repeated the runoff calculation many times. Finally, a certain group of parameters, by which the minimum difference among all the calculated results was produced, was adopted and used to perform the numerical calculation.

The main parameters determined by the methods as above mentioned are listed in Table 4.2.

Table 4.2 Main parameters

Coefficient roughness	Slope		0.10	$sm^{-1/3}$
	Channel		0.06	
Coefficient permeability	Slope	1st layer	1.0×10^{-3}	m/s
		2nd layer	4.5×10^{-5}	
	Channel	1st layer	3.0×10^{-5}	
Infiltration velocity	Slope	1st layer	3.0×10^{-6}	m/s
		2nd layer	4.0×10^{-7}	
	Channel	1st layer	3.0×10^{-6}	
Loss coefficient	……..		1.0×10^{-8}	m/s
Thickness	Slope	1st layer	0.10	m
		2nd layer	15	
	Channel	1st layer	5	
Initial degree of saturation	Slope	1st layer	0.10	……
		2nd layer	0.20	
	Channel	1st layer	0.20	
Porosity	……		0.30	……

A loss coefficient was adopted to approximately estimate the evapotanspiration which mainly involves the loss of vegetation interception during the rainfall time, the evaporation and the transpiration. In fact, because the surface flow is merely generated by the intensive rainfall and with short-lived, the loss of rainfall is mostly through the way of the vegetal interception. Either the evaporation or the transpiration has almost no impact on the surface runoff during the rainfall time. In other words, except the rainfall time, the loss coefficient is used to roughly estimate the soil evaporation and vegetation transpiration.

In spite of the methods for parameter determination as introduced above, an inevitable problem is that the condition of the soil changes dynamically. Therefore, the real-time value of each parameter is impossibly to be determined exactly. Consequently, the runoff calculation is the approximate calculation based on kinematic wave theory.

4.5 Applicability validation

4.5.1 Numerical simulation

Validity and applicability of the runoff calculation model was tested and verified by numerical simulation of the observed-flow. With regard to the observed data of the surface flow, there was almost no long-last intensive rainfall occurred in the year of 2005 which resulted in the rainfall in 2005 was short of representativeness. In 2006 and 2007, the observed data was deficiency. The available observed data of the surface flow were obtained both in 2004 and 2008. The numerical simulation results of the surface runoff combined with the corresponding rainfall are shown in Figure 4.14.a-Figure 4.14.d.

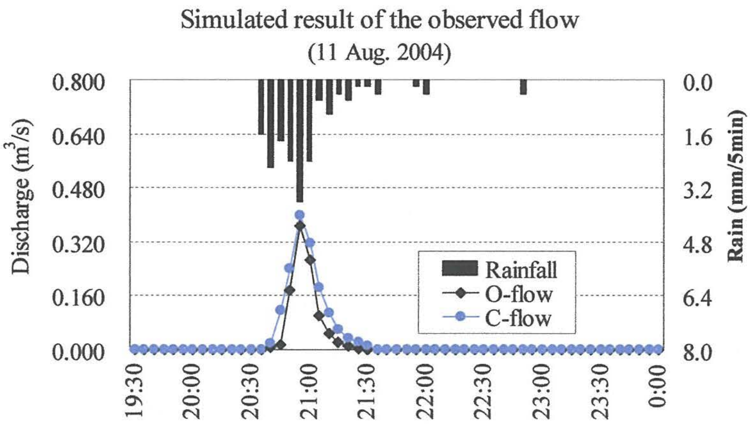

(a) Simulated result on 11 Aug. 2004

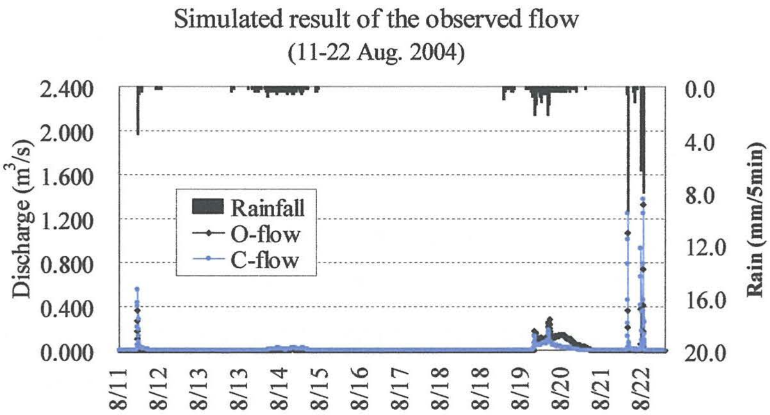

(b) Simulated result from 11 Aug. to 22 Aug. 2004

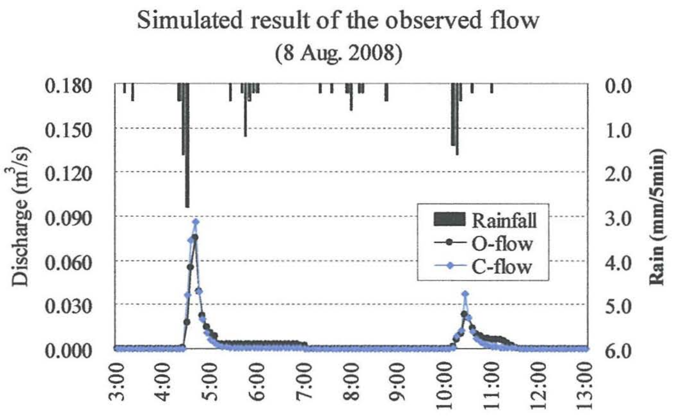

(c) Simulated result on 8 Aug. 2008

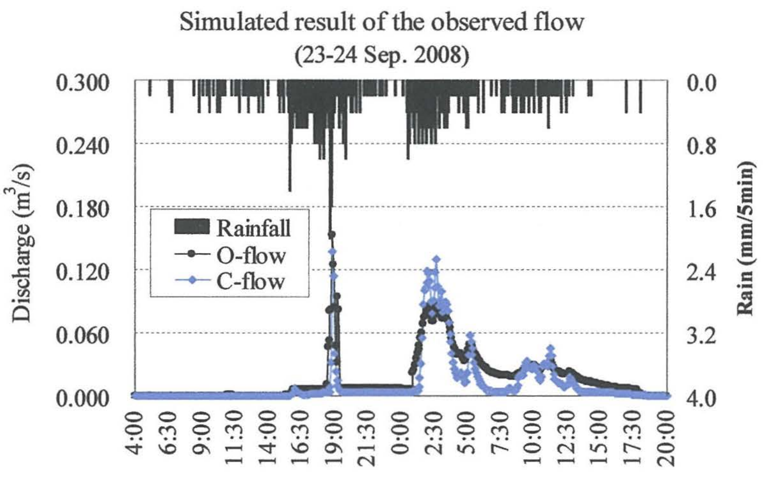

(d) Simulated result on 23-24 Sep. 2008

Fig 4.14 Results of the numerical simulation

4.5.2 Difference analysis and evaluation

4.5.2.1 Difference analysis

By observing the simulated results as shown in Figure 4.14, we can understand the numerical results reproduced the observed flow well though the obvious error still exist between the observed-flow and the simulated result in some period of times. By considering the actual observation of the surface flow, the main reasons which caused the obvious error were analyzed as follows.

The observation of the water depth (water level) of the surface flow was achieved through a sensor (inside a small-size hole) which was set close to the bottom on the water level recorder. For the working principle of the water level recorder, firstly, the hydraulic pressure is measured. Then, data of the hydraulic pressure is automatically converted into the data form of the water depth. Principle of data transformation between the hydraulic pressure and the depth of water is expressed by Equation 4.14.

$$P(t) = \rho h(t) g \qquad 4.12$$

where, P-hydraulic pressure (Pa), ρ-density of water (=1.0×10^3 kg·m^{-3}), g-gravitational acceleration (=9.81 m·s^{-2}), h-water depth (m). P and h are the functions of the time factor t.

Liudaogou Basin is located at the water-wind erosion crisscross region on the northern Loess Plateau where the severe land erosion occurs in the time of every intensive rainfall, as a result, the sand and soil content in the flow is higher than the fresh-water flow. And at certain times during the observed period, the sediment flowed into the small hole on the water level recorder which impacted on the sensor for observation and caused the pressure increase distinctly. Accordingly, the water depth which was converted from the hydraulic pressure of these certain times was higher than the actual value, and the relatively distinct error was generated such as the simulated results on 20 August, 2004 (Figure 4.14.b) and during the time 6:00-8:00 on 24 September, 2008.

Theoretically, if we consider the impact of the sediment content on observation, the flow-discharge calculated by the observed data of the water level would be higher than the fresh-water flow to some extent. However, because the depth of water on the surface flow observed section was mostly less than 20 cm with a few large discharges (refers to $Q > 0.5$ m^3/s herein) occurred during the observed time from August, 2004 to September, 2008, the sediment content had no significant influence on the calculated results of the surface runoff. In other words, the calculation of the observed-flow could be approximately replaced by the calculation of the fresh-water flow. Therefore, except a few situations where the observation was significantly effected by the sediment, the acceptable simulated results were achieved both manifesting in the scale of the flow and temporal process.

4.5.2.2 Difference evaluation

Evaluation of the difference between the observed flow and the simulated results was performed by using Equation 4.13[98)].

$$E = \frac{1}{n}\sum_{i=1}^{n}\left\{\frac{Q_o(i) - Q_c(i)}{Q_{op}}\right\}^2 \qquad 4.13$$

where, E-difference, n-number of the calculation times, $Q_o(i)$-the observed flow at moment i (m^3·s^{-1}), $Q_c(i)$-the calculated flow at moment i (m^3·s^{-1}), Q_{op}-the maximum discharge of the observed flow during the calculated time.

According to this evaluation criterion, when the error is no more than 3 %, the numerical calculation method can be proposed.

Error calculation was randomly carried out for the simulated results (include the results of Figure 4.14), the results indicated that for the short-last intensive rainy event as depicted in Figure 4.14.a, the difference between the O-flow and the C-flow is no more than 3 %. In the case of the long-last rainy event, the difference is also no more than 3 % (Figure 4.14.c). With regard to the simulated results in a certain period with several rainy events such as shown in Figure 4.14.b, there was situation that the observation impacted by the sediment, the error increased to some extent. If there is no such situation, the error is less than 3 %.

On the other hand, the sediment merely impact on the observed flow by way of impacting on the observation of the water depth occasionally. However, the sediment could not influence the simulated result which was calculated by the rainfall data without using the observed data of the water depth. Therefore, under the condition of the better simulated results achieved as shown in Figure 4.14, the simulated result (C-flow) during the sediment influenced period as depicted in Figure 4.14.b is considered as more accurate than the observed-flow. Consequently, the difference between the O-flow and C-flow can be considered as no more than 3 %.

Based on the results of the numerical simulation and the difference evaluation, it is concluded that the numerical calculation model can be applied to the calculation of the surface runoff in the study basin.

4.6 Numerical calculation

4.6.1 Results of numerical calculation

Because the surface runoff mainly occurs in the rainy season and there is almost no surface runoff in other seasons, in each calculated year, the selected time for runoff calculation covered the entire time of the surface runoff generated. The calculated results in recent four years (2005-2008) are shown in Figure 4.15.a-Figure 4.15.d respectively.

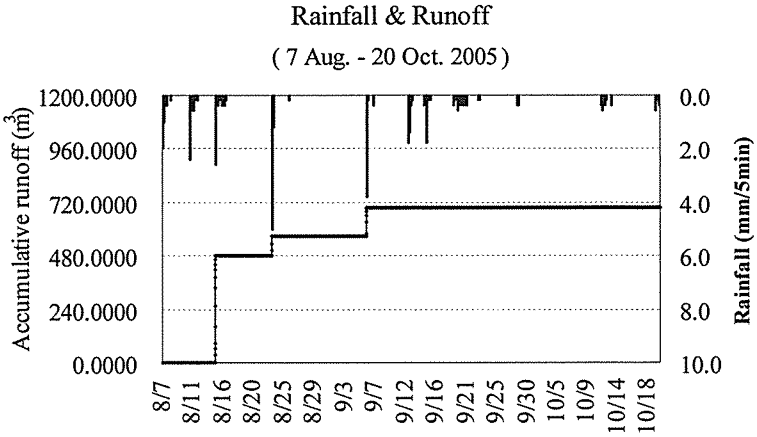

(a) Rainfall-runoff hydrograph in 2005

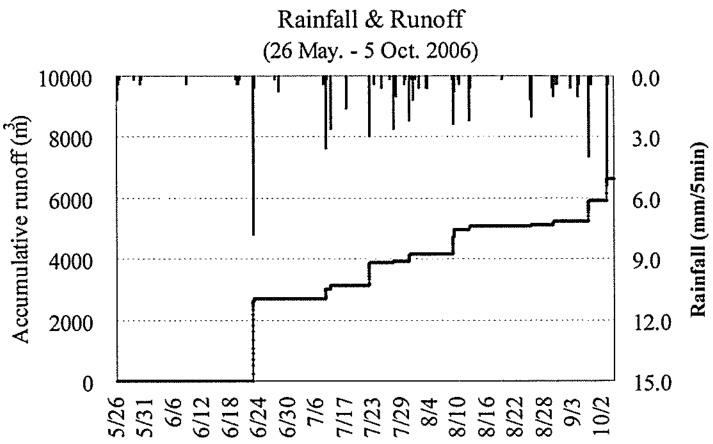

(b) Rainfall-runoff hydrograph in 2006

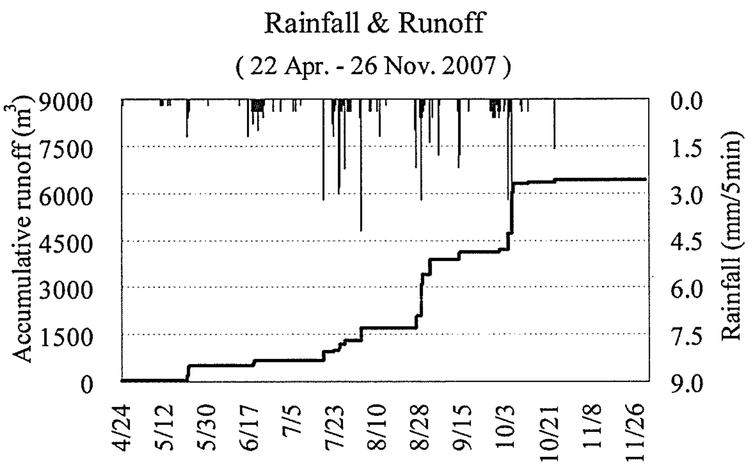

(c) Rainfall-runoff hydrograph in 2007

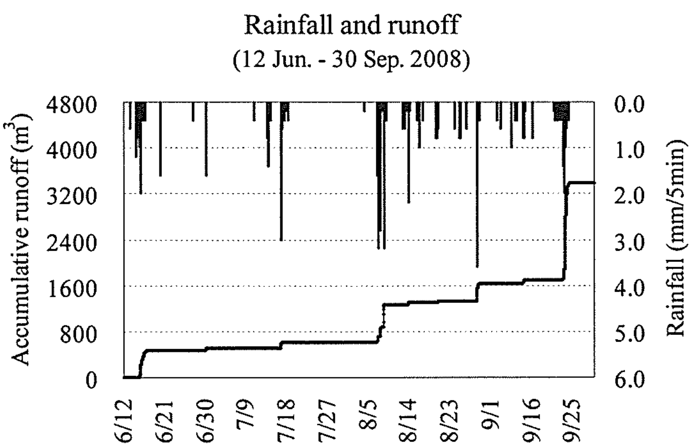

(d) Rainfall-runoff hydrograph in 2008

Fig 4.15 Rainfall-runoff hydrographs

The relational results of the rainfall and runoff corresponding to the Figure 4.15.a-Figure

4.14.d are listed in Table 4.3.

Table 4.3 Annual rainfall and runoff in recent years

Given year	Total precipitation (mm)	Amount of runoff (m^3)	Runoff rate (%)
2005	315.0	710	2.3
2006	386.0	6600	17.0
2007	481.0	6500	13.5
2008	502.0	3500	7.0

* The calculated area is the catchment of the surface flow observed area (about 0.10 km^2).

4.6.2 Discussion

In the year of 2005, due to the total precipitation (315 mm) was lower than the annual mean rainfall (430 mm) obviously, and there was almost no intensive rainfall occurred with the result that the surface runoff only occurred three times and the runoff rate was very low, only 2.3 %.

In 2006, though amount of precipitation was slightly less than the mean annual value, however the rainfall mainly concentrated in the rainy season and the intensive heavy rainfall occurred several times which resulted in the relatively high runoff rate.

In 2007, the amount of rainfall was slightly more than the annual mean precipitation, and the annual distribution of rainfall also had characteristics of the normal year, thus the runoff rate in 2007 was approximate to the normal value of accumulated year.

In 2008, the total rainfall was higher than the annual average value. However, owing to the scanty heavy rainfall in the rainy season, the runoff rate was less than the normal year.

According to the above analyzed results, the following two points can be concluded.

(1) Both the annual rainfall and its temporal distribution impact on the annual runoff rate.

(2) If the annual rainfall is approximate to the mean annual value and its yearly distribution has representativeness of the normal year, the annul runoff rate can be estimated to be 10 % - 15 % in the study location.

4.7 Summary and Conclusions

The main contents in this chapter are summarized as follows:

(1) Introduced the developed method of the runoff calculation model.

(2) Based on the actual conditions of the study location, a numerical calculation model for the surface runoff calculation was developed.

(3) Provided the general methods for determining the parameters of the runoff calculation.

(4) Validated the applicability of the runoff calculation model through numerical simulation of the observed flow.

(5) Carried out the numerical calculation of the surface runoff.
(6) Evaluated some runoff characteristics according to the results of the numerical calculation.

Some conclusions:
(1) Both annual rainfall and its temporal distribution significantly impact on the annual runoff rate.
(2) The surface runoff mainly occurs in the rainy season, in other words, there is almost no surface runoff except intensive rainfall time in the rainy season.
(3) The runoff rate in the normal year is approximately 10 % - 15 %.

Additionally, the developed runoff calculation model applies to the surface runoff calculation of the study location.

Chapter 5

Index of annual water balance

5.1 Introduction

The water balance relationship at the earth's surface is complex and dynamic. The relationship involves interactions between atmosphere, surface, soil, plant and groundwater[99]. The general hydrologic processes are precipitation, runoff, infiltration, evapotranspiration (evaporation and transpiration). Analysis of the water balance is the basis for realizing the scientific evaluation and appropriate allocation of the water resources in a basin[100]. The water balance in a basin generally has three connotations. The first connotation is the water balance of the "rainfall-runoff" which refers to the water balance in hydrological circle in a basin. The second one is the balance of the water income (precipitation and inflow) and expenditure (water consumption and outflow). And the third connotation refers to the equilibrious relationship between water supply and demand which is a water balance between the natural available water resources and the demand of water resources of the socio-environment. The significance between the three concepts of the water balance is different but interrelated[100), 101]. Analysis of the water balance of the "rainfall-runoff" expresses the conservation of matters between the precipitation, the evapotranspiration and the runoff, and it is one of the basic principles of the hydrological research. For a closed basin, the water balance may be simply expressed by Equation 5.1[101), 102].

$$P = R + \Delta W + ET \tag{5.1}$$

where, P-precipitation, R-runoff which includes the surface runoff and the groundwater (GWT) outflow, ΔW-change of the water storage in a basin which commonly manifests in the variation of the soil water content and change of the GWT within a certain period of time, and its annual mean value approximates to 0, ET-evapotranspiration.

In the state of nature, the water resources in a basin keep the sustainable state of the normal circle, and maintain a dynamic balance. However, if the water balance in a basin is interfered from the water resources development by the human activities, such as the GWT overdraft, farmland irrigation, the change of water storage ΔW (in Equation 5.1) will be led to negative value or deficit state. If the deficit of the water storage cannot achieve restoration in a long-term, the ecological environment in a basin will be damaged such as the GWT recession, the vegetation degradation, the land desertification and the runoff reduction and etc. Thereby, the sustainable development and utilization of the water resources in a basin will be endangered[103].

In consideration of Liudaogou Basin has various representative features such as the hydrology, the topography, the land use patterns, also the water utilization in the northern Loess Plateau, in the current study, based on the results of field survey and numerical calculation of the surface runoff, index of annual water balance and index of monthly water income and expenditure for an unit area (1.0 km^2) were established respectively. Further, annual available water resources were approximately estimated.

5.2 Index of annual water balance

5.2.1 Brief introduction of annual water balance

As mentioned previously (in Chapter 2), the mean yearly precipitation in the study location is about 430 mm/y which is theoretically as the amount of water income in the normal year. In the study location, deep ground water generally perches at the depth of dozens of meters or over 100 m which is difficult to be exploited. Even if such deep groundwater has once developed to be used, we have to evaluate how long water can be supplied until drying up as there is almost no effective recharge from the rainwater infiltration. At present, in the study location, annual water consumption includes the domestic water and the irrigation water. The domestic water and irrigation water are mainly provided by the shallow GWT (phreatic water) which generally perches at the depth less than 10 m below the ground surface in the valley floor[60), 104)].

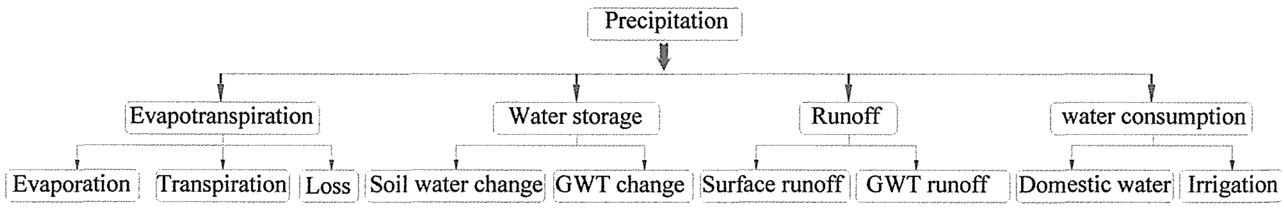

Fig 5.1 Diagram of annual water balance in the study area

The components of the water expenditure in Liudaogou Basin commonly include the runoff (the surface runoff and the GWT outflow), the evapotranspiration (*ET*), and the water consumption. Though the irrigation water can be regarded as a part of *ET* in theory, however, with an aim to evaluate the actual water consumption in the study location, the total of the domestic water and the irrigation water is considered as a specific component of the water expenditure. Accordingly, when performing the analysis of the annual water balance of the study location, a component of the water consumption ought to be added into Equation 5.1. Equation used for estimating the annual water balance is as below.

$$P = R + \Delta W + ET + U \qquad 5.2$$

where, U- water consumption, an component of the water expenditure includes the domestic water and the irrigation water. Other factors are corresponding to the above mentioned. Figure 5.1 shows every component of annual water balance in the study location of the current situation.

In the study location, owing to the low temperature in winter, the upper ground is frozen and the shallow GWT flow is also stopped from December to the end of the next February. The moisture exchange between the soil from the ground surface to the depth of 100 cm and the atmosphere approximately keeps equilibrium in winter[44), 104)]. Therefore, the main annual period for the water budget analysis is from March to November. The diagram of annual water income and expenditure (except the item of water consumption) is shown in Figure 5.2.

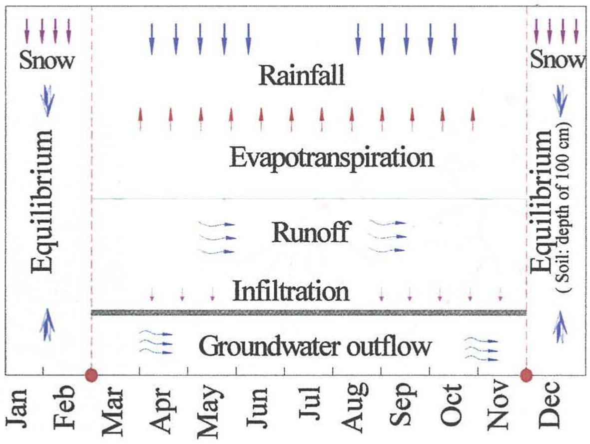

Fig 5.2 Diagram of the water income and expenditure in the study area

5.2.2 Components of annual water budget

Towards estimating each component of the annual water budget, the relational results which were achieved by the field observation from 2005 to 2008, and from the numerical calculation of the surface runoff were chosen and used.

5.2.2.1 Water income

For a closed basin, the amount of annual water income refers to the annual precipitation. The average annual precipitation in the study location is about 430 mm, thereby in Liudaogou Basin (area: 6.89 km^2), the amount of water income in the normal year can be estimated to be 2.96×10^6 m^3. In the unit area of 1 km^2, the annual amount of water income is equivalent to 4.30×10^5 m^3.

5.2.2.2 Surface runoff

Annual surface runoff is approximately estimated based on the results of the numerical calculation of the surface runoff in the year of 2005, 2006, 2007 and 2008 (results were shown in Chapter 4, Fig. 4.15). As the surface runoff rate has been estimated to be 10 %-15 % in the normal year, in the current study, the annual surface runoff rate of 12 % is adopted to approximately evaluating the surface runoff. In the unit area, it is transferred to 5.2×10^4 m^3.

5.2.2.3 GWT outflow

Observation of the GWT flow was also carried out in Liudaogou Basin through opportunity of each time of the filed survey. A relatively stable GWT flow occurs on the sandstone layer at comparative lower altitude in the gully floor. The GWT runoff observed site is shown in Figure 5.3.

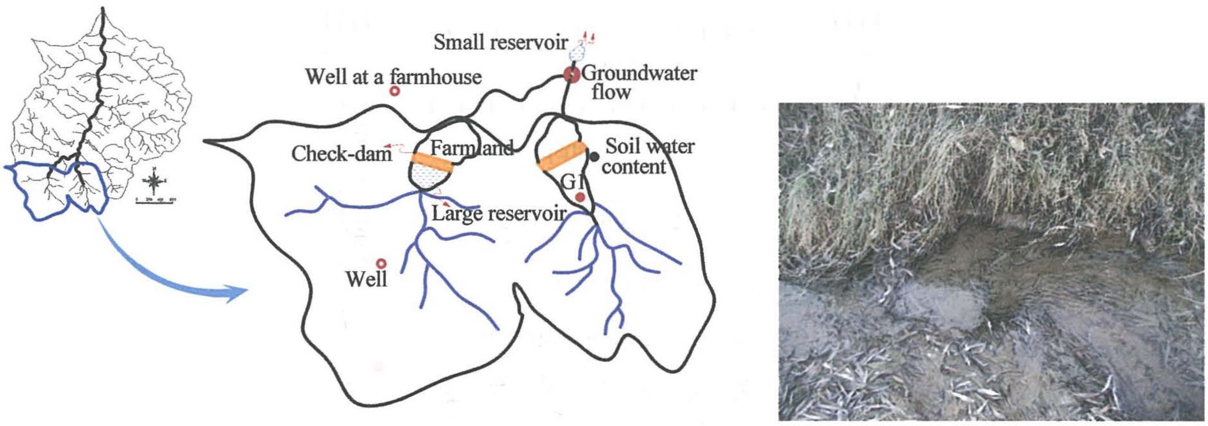

Fig 5.3 GWT flow observed point & A photo of the GWT flow (Nov. 2005)

The GWT flow increases gradually from the observed point to the downstream direction. On the observed point, the observed discharge is shown in Figure 5.4. The average discharge is about 1800 cm^3/s.

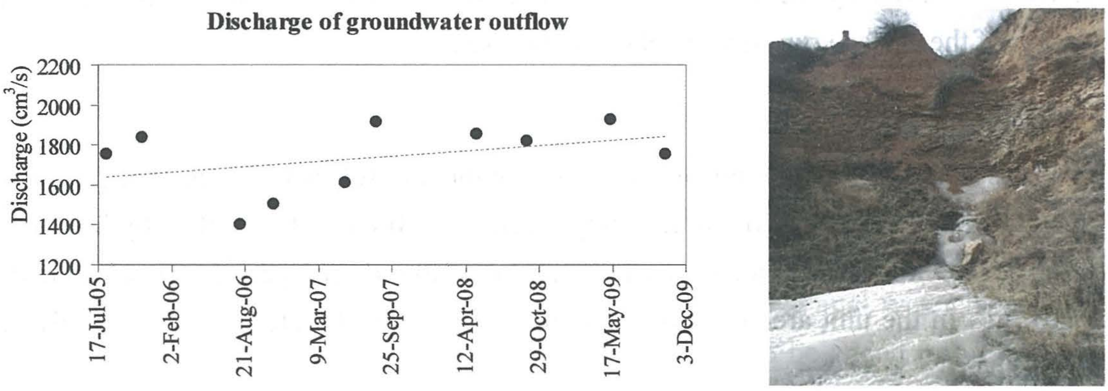

Fig 5.4 Discharge of the GWT flow on the observed point

(A photo shows the GWT flow is frozen in the winter)

Because the ground condition in Liudaogou Basin is in homogeneous situation, the GWT flow is considered as uniformly generating from each tributary. Because the catchment area which ends at the discharge observed point accounts for about 15 % (1.04 km^2) of the total basin area, the mean discharge of the GWT flow from Liudaogou Basin was approximately estimated to be 1.2×10^4 cm^3/s. Annual amount of GWT outflow was estimated to be 2.8×10^5 m^3 except winter, with the result that annual GWT outflow from the unit area is approximate to 4.1×10^4 m^3.

5.2.2.4 Groundwater fluctuant characteristics

In the study location, the deep GWT has not been exploited and has almost no annual replenishment from the rainwater infiltration. Annual water storage was considered to mainly manifest in the variation of the soil water content and change of the shallow GWT (phreatic water).

Observation of the shallow GWT was conducted on several points such as in a well at a farmhouse and on G1 point at the sediment filled area in front of a check dam (Figure. 5.3). Figure 5.5.a and Figure 5.5.b show the observed GWT level in a well at a farmhouse and on G1 respectively.

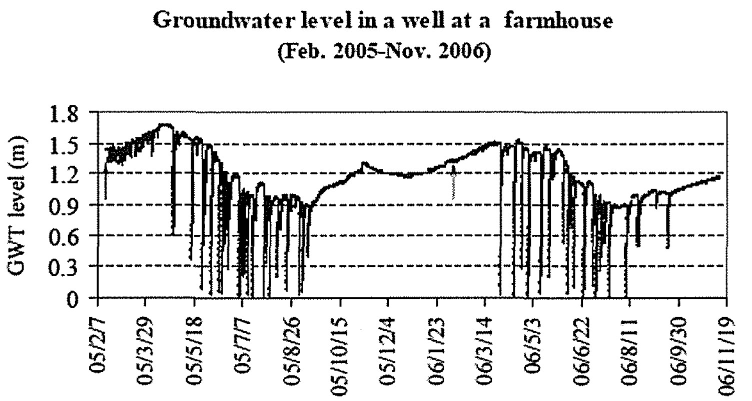

(a)

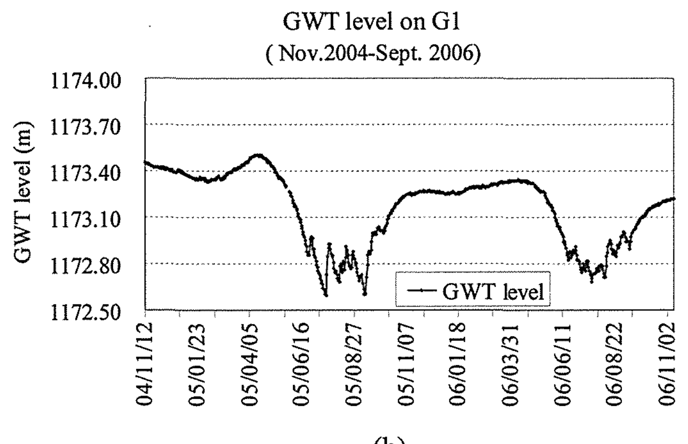

(b)

Fig 5.5 GWT fluctuation in the study area

By observing Figure 5.5.a and Figure 5.5.b, the short-term fluctuant characteristics and annual fluctuant characteristics of the GWT can be tersely summarized as below.

(1) Before and after the vegetation period, (Annual vegetation period in the northern Loess Plateau is from May to September) the GWT level increases gradually owing to the replenishment from the rainwater infiltration. The annual maximum GWT stage generally occurs before the start of the vegetation period.

(2) After the start of vegetation period, the GWT level decreases distinctly, especially during the rainy season, though the rainfall is more than other seasons, the GWT level has no obvious increment and maintains annual relatively low level.

(3) The GWT level has no distinct difference at annual corresponding time, and almost maintains the same level. In other words, the GWT keeps approximately equilibrium at annual corresponding time. Therefore the annual change of GWT is approximately 0.

Additionally, the maximum GWT stage in 2005 was slightly higher than in 2006. A main reason was that the total precipitation in 2004 (427.4 mm) was more than the total precipitation in 2005 (315 mm) which resulted in the different GWT recharge in 2005 and in 2006. This result indicates that the different annual precipitation would impact on annual GWT recharge to some extent.

5.2.2.5 Annual variation of the soil water content

The soil water content observed site was shown in Figure 5.3. In the study location, the evapotraspiration impacts on the infiltration at the maximum depth of 60 cm from the ground surface, the soil water content keeps relatively stable state below the depth of 1 m[44]. Observation of the soil water content was conducted at 4 cm, 10 cm, 26 cm, 34 cm, 42 cm, 50 cm, 58 cm, 66 cm, and at the maximum depth of 100 cm respectively. Results of the average soil water content of the various depths are shown in Figure 5.6. Figure 5.6 represents the mean soil water content keeps approximately equilibrium at the beginning and end of each year. Thus the annual water storage responses to the variation of the soil water content can be approximately estimated to be 0.

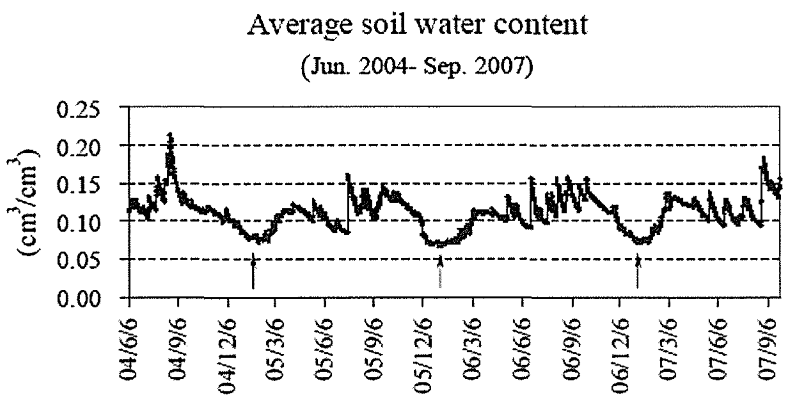

Fig 5.6 Average soil water content

5.2.2.6 Annual water storage

Based on the analyzed results of the annual GWT fluctuation characteristics and the annual variation of the soil water content, the annual water storage in Liudaogou Basin is roughly estimated to be 0 because the annual change of the GWT and annual change of the soil water content are both approximate to 0.

5.2.2.7 Annual water consumption

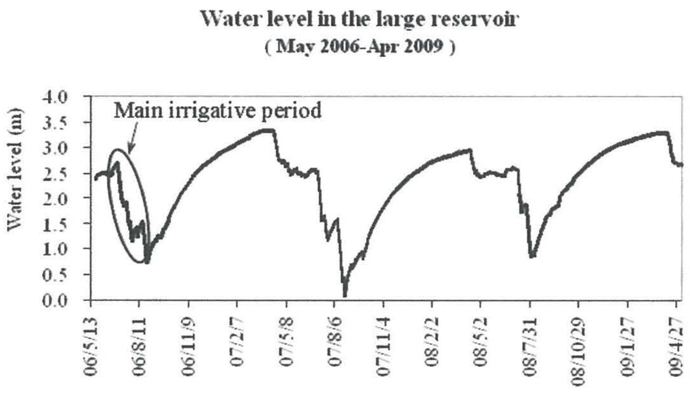

(a) Water level in the large reservoir

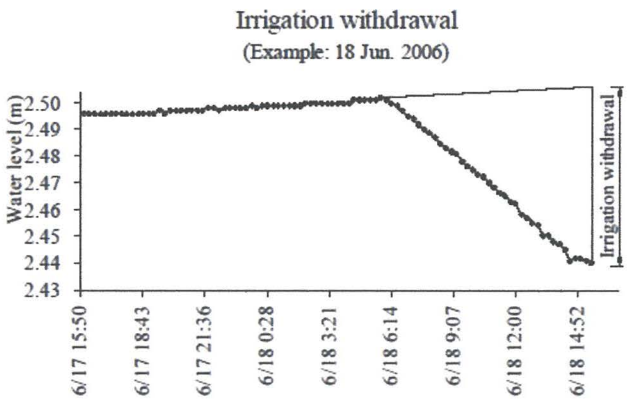

(b) Irrigation withdrawal

A photo of the large reservoir

Fig 5.7 The observed water level in the large reservoir & Irrigation withdrawal

(1) Irrigation water

The irrigated area in Liudaogou Basin was 20.6 ha in recent years. Irrigation withdrawal is provided by the two reservoirs, large and small one as shown in Figure 5.3. According to the actual investigation, annual irrigative period is from the late April to September which almost covers the whole annual growing period. The large reservoir and the small one provide the annual irrigation water of 70 % and 30 % respectively. The main irrigation method is the surface flooding. The irrigation water was approximately estimated by analyzing the change of the water level in the large reservoir. Area of this large reservoir is about 5330 m^2. The observed water level in the large reservoir is shown in Figure 5.7.a. The method for estimating the actual irrigation withdrawal of each time is depicted in Figure 5.7.b.

For the large reservoir, the monthly accumulative curves of the irrigation water in the year of 2006, 2007 and 2008 are shown in Figure 5.8 respectively. Figure 5.8 represents that the amount of annual irrigation water in recent years has no obvious change though some distinguishments manifest in the monthly distribution. Based on the analyzed results of the irrigation withdrawal in the large reservoir, the amount of irrigation water from the small reservoir in the corresponding year is roughly estimated to be 9950 m^3 in 2006, 10020 m^3 in 2007 and 10600 m^3 in 2008. By considering the analyzed results of the irrigation water in recent years and the irrigated farmland area, the mean annual amount of irrigation water in Liudaogou Basin was approximately estimated to be 3.5×10^4 m^3. Because the irrigated area is translated to 3.0 ha/km^2 in the unit area, so the annual amount of irrigation water is approximately to be 0.51×10^4 m^3 in the unit area of 1 km^2.

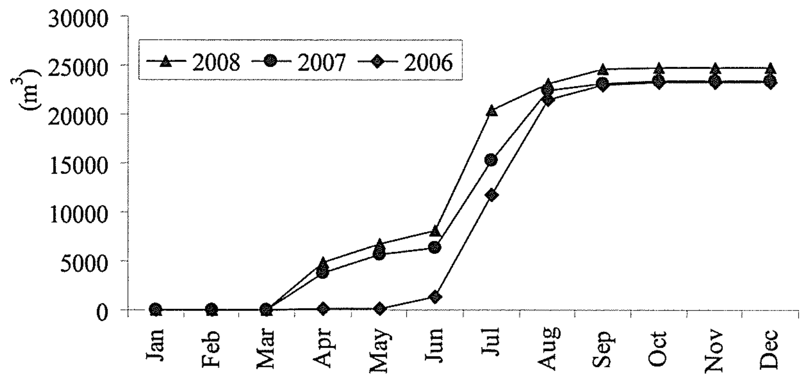

Fig 5.8 Monthly accumulative irrigation withdrawal from the large reservoir

(2) Domestic water

Domestic water normally includes water supply for residents and cattle. According to the results of targeted investigation, the domestic water is fetched from an artesian well which is located at upstream in Liudaogou Basin (Fig 5.3). The water in this well also belongs to the unconfined groundwater (phreatic water). Normally, diurnal domestic water was about 200 m^3/d which increased to about 300 m^3/d in summer (from July to September). Therefore, total annual domestic water is roughly estimated to be 8.2×10^4 m^3 in Liudaogou Basin, and the annual domestic water in the unit area is around 1.2×10^4 m^3.

5.2.2.8 Evapotranspiration

Evapotranspiration normally refers to the sum of evaporation from ground surface and vegetation transpiration. In view of the complicated geomorphological features such as the bare land, the crops, and sparse distributed vegetation with various types, estimation of the actual evapotranspiration is almost impossible. Because the annual water storage which manifests in the variation of the soil water content and the change of the GWT was approximately to 0, annual evapotranspiration was roughly estimated by subtracting annual surface runoff, annual GWT outflow and annual water consumption from the annual precipitation. As the result, annual evapotranspiration is about 3.2×10^5 m^3/y.

5.2.3 Results of annual water balance

Result of each component of annual water budget in the unit area is listed in Table 5.1, and based on the results in Table 5.1 index of annual water balance was established as shown in Figure 5.9.

Table 5.1 Analyzed results of annual water balance (unit area: 1 km^2)

Item	Precipitation *P*	Evapotranspiration *ET*	Runoff *R*		Water utilization *U*		Water storage ΔW
			Surface	GWT	Domestic	Irrigation	
Amount ($\cdot 10^4$ m)	43.0	32	5.2	4.1	1.2	0.51	0
Percentage (%)	100	74.4	21.6		4.0		0

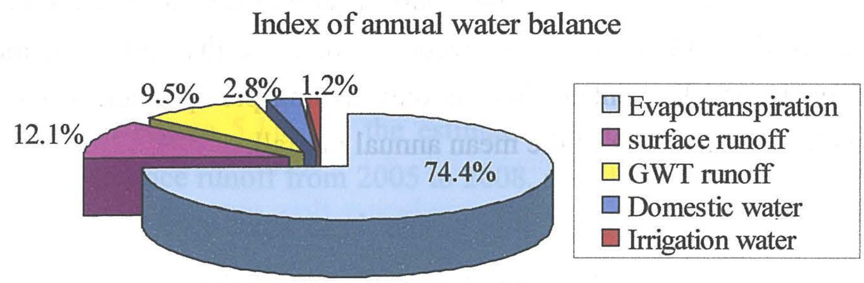

Fig 5.9 Index of annual water balance

5.2.4 Analysis of results

In the opinion of the analyzed results of the annual water balance, the following points can be summarized or concluded.

(1) The total runoff (surface and GWT) accounts for slightly more than 20 % of the annual precipitation in the normal year.

(2) The annual water consumption only accounts for 4.0 % of the annual precipitation.

(3) The annual evapotranspiration occupies over 70 % of the annual precipitation which is in predominant status among all components of the annual water expenditure.

In the study area, due to the complicated landform and the uneven distribution of the annual rainfall, the surface runoff is difficult to be effectively stored and used with a large amount. The surface runoff is simply intercepted by the check dam in some gullies, and the dammed-up surface water commonly keeps a short existence owing to strong infiltration capacity of the topsoil and intense evapotranspiration. Only a small part of infiltrated water can be expected to recharge the GWT due to the strong soil evaporation and vegetation transpiration.

As there are seldom technologic measures to store the surface water effectively except the check dam, the GWT and its outflow has become very significant available water in the study area, also in the northern Loess Plateau region. According to the analyzed results of the annual water balance, under the condition of the annual GWT approximately maintains balance, the GWT outflow which accounts for about 9.5 % of the annual rainfall is expected easily to be used. Additionally, the available water resources are also expected to increase by the means of storing more surface water.

5.3 Index of monthly water income and expenditure

5.3.1 Monthly precipitation

Based on the annual mean precipitation (about, 430 mm/y) and data of the yearly/monthly rainfall from 1956 to 2007, the monthly distribution of the rainfall is estimated as shown in Figure 5.10. The main part of rainfall is centralized in the rainy season. The rainfall received in July and August accounts for more than 50 % of the annual total. Whereas, in January and December, there is only trifling precipitation in the form of snow which accounts for less than 1 % of the mean annual rainfall.

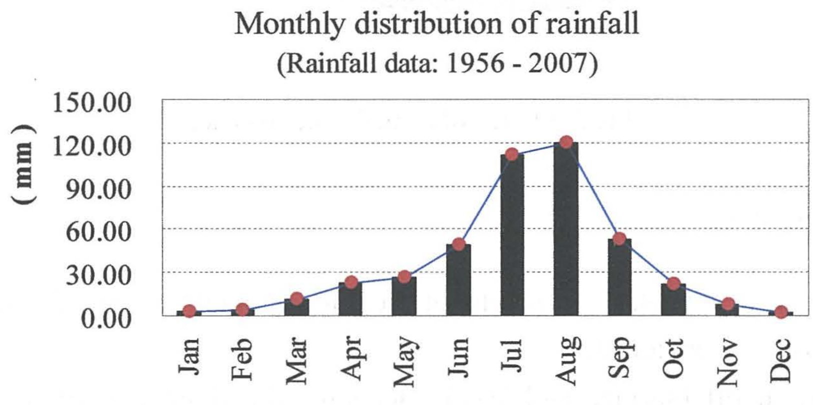

Fig 5.10 Monthly rainfall distribution

5.3.2 Each component of monthly water expenditure

5.3.2.1 Monthly surface runoff

Monthly surface runoff was estimated by analyzing the runoff calculated results of the surface runoff in recent four years (2005-2008, Chapter section 4.6). For these four years, the mean annual rainfall is 421 mm and average runoff rate is approximately 10 % which are approximate to but slightly less than the normal value of accumulated year respectively. It is considered that the rainfall and runoff process in 2007 has representativeness in the normal year though amount of rainfall in 2007 is slightly higher than the mean annual value.

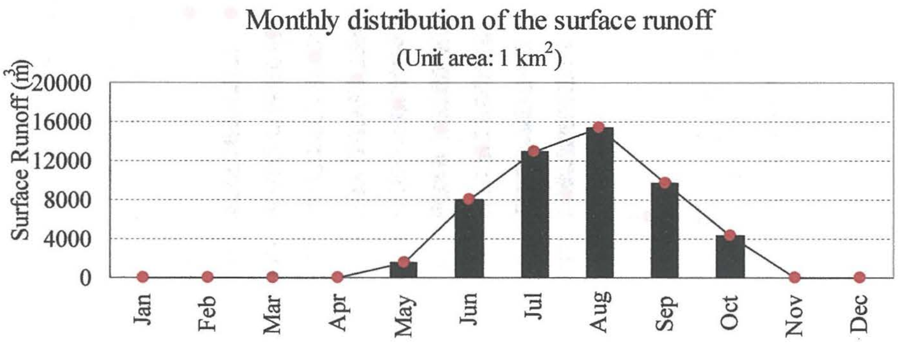

Fig 5.11 Monthly surface runoff distribution

In the current study, based on analysis of the runoff calculated results in recent four years (from 2005 to 2008), the runoff rate of 12 % was adopted to approximately evaluate the surface runoff in the normal year. The monthly distribution of the surface runoff was estimated as shown in Figure 5.11. For the estimation method, firstly, based on the mean value of the monthly surface runoff from 2005 to 2008, distribution of the monthly runoff rate (%) was estimated. Then, by using annual rainfall of 430 mm and annual runoff rate of 12 % (5.2×10^4 m^3/y), the amount of surface runoff in each month was estimated. Thereby monthly distribution of the surface runoff in the unit area (1 km^2) was ascertained. By observing Figure 5.10 and Figure 5.11, the monthly distribution of the surface runoff responses to the distribution of the monthly rainfall, which can be affirmed. Except the annual period from May to October, there is no surface runoff generation in the study location.

5.3.2.2 Monthly GWT outflow

The observed results of the GWT flow are shown in Figure 5.4. The discharge in those months, in which the GWT flow was not observed, was approximately estimated by the interpolation method. For example, the average discharge in June and July, in which there is no observed data, was estimated by considering the observed results in May and in August using the interpolation method. The estimated monthly amount of GWT outflow from the unit area is shown in Figure 5.12.

Figure 5.12 represents that the GWT outflow keeps relatively stable state from March to

November. As the shallow GWT maintains relatively low level during the annual vegetation period from May to September (Fig 5.5), the GWT outflow should be less than the other months to some extent. However, Figure 5.12 shows the GWT outflow during the rainy season mainly from June to September is a bit higher than other months. A main reason which results in this situation is considered as below.

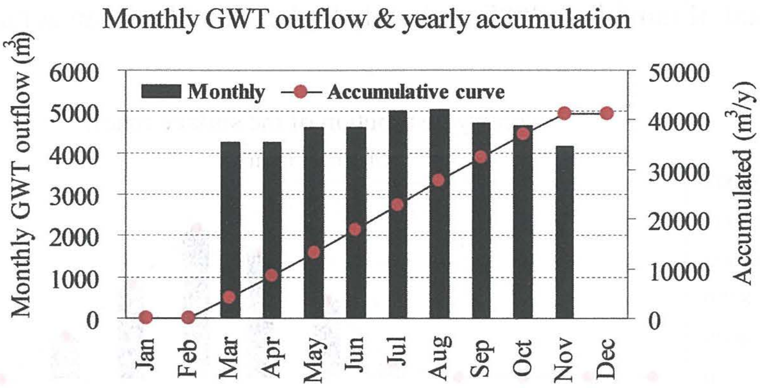

Fig 5.12 Monthly GWT flow & Yearly accumulated (Unit area: 1 km^2)

In the study area, the elevation gradually decreases from the upstream to the downstream with a relatively steep gradient. Also in every tributary, the terrain lowers gradually from the upper extremity to the lower extremity on the slope, and there is a gully generally at the lower extremity. After start of the rainy season, in a certain period with the several intensive rainfalls, the topsoil may attain saturated condition and the temporary groundwater may be generated at the lower part in the topsoil (Referencing: Fig. 4.11: Runoff calculation model). Due to the tendency of the terrain of the slope, the groundwater flow may occur at the lower end of the slope sector and flow into the river channel (gully) which results in the increment of the GWT flow in the rainy season.

5.3.2.3 Monthly change of water storage

The monthly change of water storage is approximately estimated by analyzing the monthly change of the GWT and the monthly variation of the soil water content.

(1) Monthly change of the GWT

Towards evaluating the monthly change of GWT, the observed results in a well at a farmhouse, and the GWT observed point (G1) at the sediment filled area in front of a check dam (position: Fig 5.3, results: Fig 5.5) were selected for analysis. Through data analysis, the estimated results of the monthly change of the GWT level on the two observed sites are shown in Figure 5.13 respectively. Figure 5.13 shows the similar changed process of the monthly GWT on the two sites. The change of GWT in annual January and December approximates to 0.0 which verifies the annual GWT almost keeps balance.

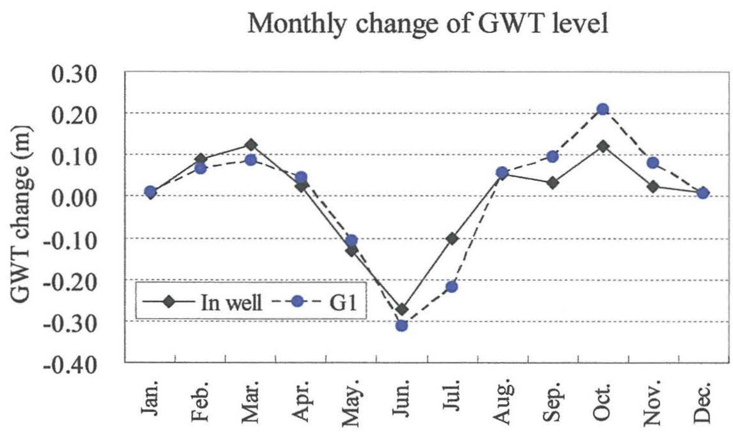

Figure 5.13 Monthly change of GWT level

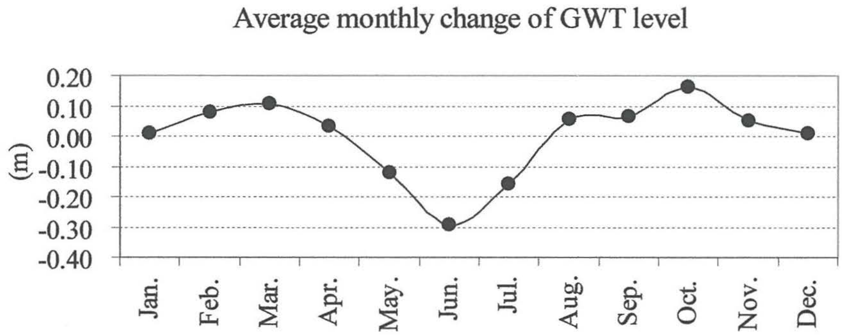

Fig 5.14 Monthly average change of the GWT level

Based on the analyzed results of the monthly change of the GWT level on the two observed sites as shown in Figure 5.13, the monthly change of the GWT level was estimated as the mean value of GWT level change of the two observed sites as shown in Figure 5.14.

(2) Monthly variation of the soil water content

The monthly variation of the soil water content was evaluated by analyzing the observed data of the soil water content. The data observed site is shown in Figure 5.3, and the observed results are shown in Figure 5.6.

Generally, the soil water content in annual rainy season was higher than other time. The soil water content shows the similar variational process at annual corresponding time in the year of 2005 and 2006. However, during the rainy season in 2004 and 2007, the maximum soil water content was higher than the corresponding time in 2005 and 2006 to some extent. Despite of the difference at annual corresponding time, the monthly variation of the soil water content was estimated by the following steps.

Firstly, the monthly increment of the soil water content between the adjacent two months throughout the observed period (June, 2004-September, 2007) was estimated by analyzing the observed data. For instance, the increment of the soil water content in June 2005 was estimated by comparison of the average soil water content in June 2005 and in May 2005.

Secondly, the mean increment of the soil water content between the adjacent two months within a year was estimated by using the results obtained in the first step. For example, the average variation of the soil water content in June was estimated by averaging the values in the corresponding month throughout the observational span (from 2004 to 2007).

Finally, the obtained results in the second step, in other words, the mean variation of the soil water content between every two adjacent months were adopted as the results of the monthly variation of the soil water content (Fig 5.15).

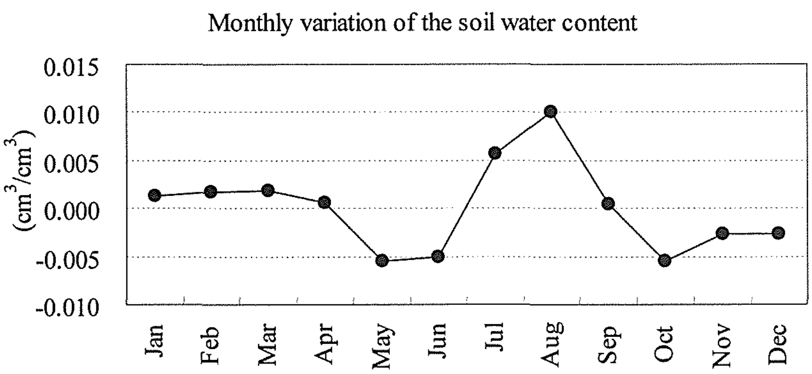

Fig 5.15 Average monthly variation of the soil water content

Figure 5.15 represents that the increment of the soil water content in July and in August are more prominent than other months due to the much precipitation. Whereas in winter, because the upper ground was frozen, the soil water mainly exists in form of the solid state, and the soil water content had almost no obvious change and approximately keeps balanced state.

5.3.2.4 Monthly water consumption

(1) Domestic water

According to the actual investigation, the number of inhabitants in Liudaogou Basin remained relatively stable in recent years, which were 533 in the year of 2007. In the opinion of this number, the populations in unit area (1 km^2) are 77 which approximates to the mean value of 50-100/km^2 in the northern Loess Plateau region (http://www.eku.cc, April in 2009: China's population distribution). Because the diurnal domestic water in the study basin is about 200 m^3/d (about 300 m^3/d in summer), so the diurnal water consumption of a person can be estimated to be about 0.38 m^3/d (0.56 m^3/d in summer). Thus, the monthly distribution of the domestic water in the unit area was estimated as shown in Figure 5.16.

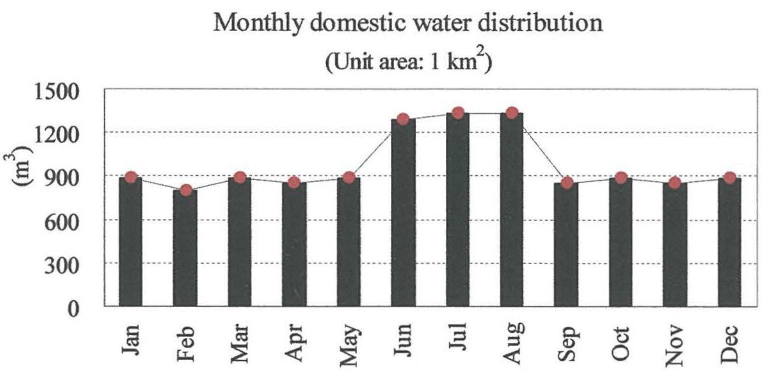

Fig 5.16 Monthly distribution of the domestic water

(2) Irrigation water

In the study location, the irrigated area is 20.6 ha which has almost no change in recent years. The annual irrigation time almost covers the whole growing period, and the annual irrigated process is similar. The distribution of monthly irrigation water was ascertained by analyzing the estimated results of the irrigation water in 2006, 2007 and 2008 in the study basin (Fig 5.17). The irrigated area in 1 km^2 is equivalent to 3.0 ha. Figure 5.18 shows the monthly irrigation water in the unit area which was estimated by analyzing the monthly irrigation water from 2006 to 2008.

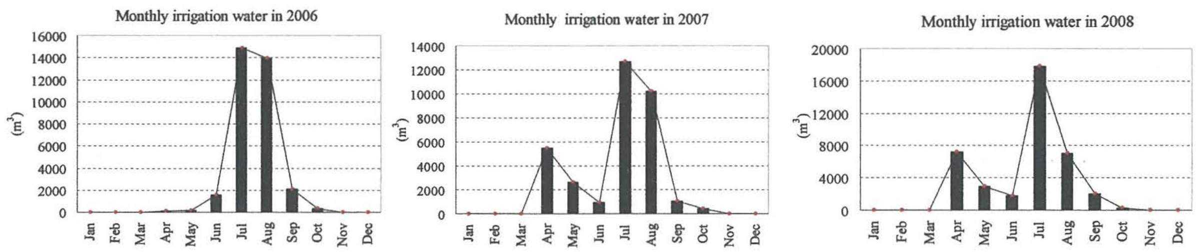

Fig 5.17 Monthly irrigation water (2006-2008) (unit: m^3)

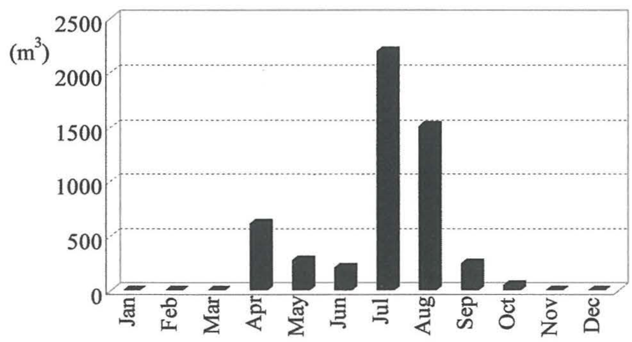

Fig 5.18 Monthly distribution of the irrigation water in unit area

Figure 5.17 and Figure 5.18 represent that the irrigation water in July and August are generally more than other months during the period of time for annual irrigation.

5.3.2.5 Monthly evapotranspirtation

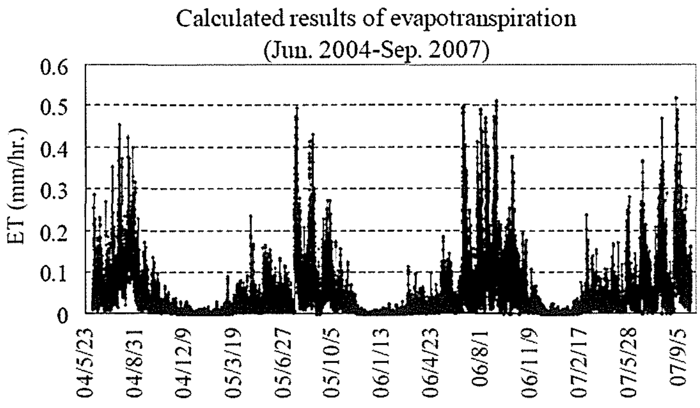

Fig 5.19 The calculated results of ET over the grassland

The evapotranspiration (*ET*) was estimated by the *ET* calculation model as introduced in Chapter section 6.5.1. The selected land-use pattern for *ET* calculation is grassland with the average vegetation height of 15 cm which accounts for more than 30 % of the total vegetation covering area in Liudaogou Basin. The adopted thickness of the soil-layer for *ET* calculation is 1.0 m below which the soil water content keeps relatively stable state. The *ET* calculated period is from June, 2004 to September, 2007 (more than 3 years). The calculated results are shown in Figure 5.19 which represents the annual temporal process of the *ET* is similar. The *ET* mainly focuses on the vegetation period whereas obviously decreases in winter.

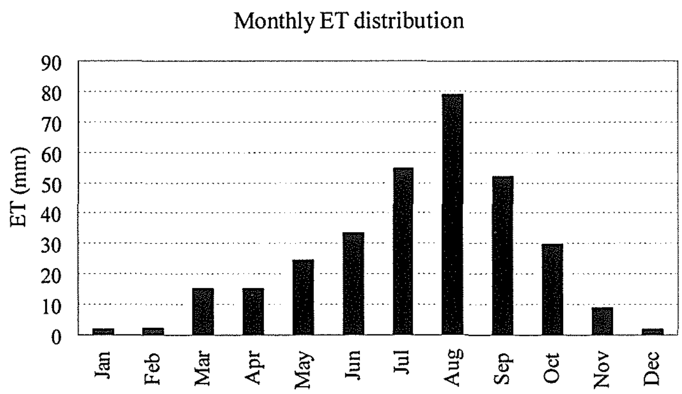

Fig 5.20 Monthly ET distribution

In consideration of the various vegetation covers in the study location such as the natural meadow (grass), the nudation, the shrub land, the farmland and etc, the actual *ET* is impossible to be estimated accurately. The *ET* over the grassland is generally lower than that of the farmland and nudation, also the shrub land to some extent. The *ET* simply over the grassland accounts for 69.7 % of the yearly precipitation which is lower than the actual value of *ET* to some extent (about 74 % of yearly precipitation in Fig. 5.9). Therefore, the monthly *ET* merely estimated over the grassland must be adjusted by considering the annual *ET* as listed in Table 5.1. For the adjusted method, the result of *ET* over the grassland in each month was multiplied by a factor of 1.06 which was the specific value of the two results of annual *ET* (74 % / 69.7 % = 1.06). The estimated results are used as the actual monthly *ET* in the study area are shown in Figure 5.20 (listed in Table 5.2).

Table 5.2 Every component of the monthly water income and expenditure
(unit: $10^3 \cdot m^3$, Area: 1 km^2)

Item →	Preci-pitation *P*	Runoff *R*			Water utilization *U*			Water storage ΔW			Evapo-transpiration *ET*
		Surface	GWT	Sum	D.W	I. W.	Sum	GWC	S.W	Sum	
Jan	2.52	0.0	0.0	0.0	0.88	0.0	0.88	2.52	1.25	3.77	1.8
Feb	3.62	0.0	0.0	0.0	0.80	0.0	0.80	23.32	1.70	25.02	2.4
Mar	11.02	0.0	4.26	4.26	0.88	0.0	0.88	31.44	1.80	33.24	15.2
Apr	22.43	0.0	4.26	4.26	0.85	0.62	1.47	10.20	0.60	10.80	15.3
May	26.64	1.53	4.62	6.15	0.88	0.28	1.16	-35.70	-5.50	-41.20	24.5
Jun	49.09	8.03	4.62	12.65	1.29	0.21	1.50	-87.67	-5.10	-92.77	33.3
Jul	111.34	12.94	5.02	17.96	1.34	2.20	3.54	-47.87	5.61	-42.26	54.6
Aug	119.78	15.37	5.05	20.42	1.34	1.51	2.85	16.56	10.05	26.61	78.9
Sep	52.61	9.75	4.73	14.48	0.85	0.25	1.10	19.50	0.5	20.00	51.9
Oct	21.52	4.37	4.65	9.02	0.88	0.05	0.93	49.28	-5.50	43.78	29.7
Nov	7.8	0.0	4.15	4.15	0.85	0.0	0.85	15.80	-2.6	13.20	9.1
Dec	1.63	0.0	0.0	0.0	0.88	0.0	0.88	2.62 $\Sigma \approx 0.0$	-2.71 $\Sigma 0.1$	-0.09	2.0
Σ	430	93.9			16.8			0.1			319
%	100	21.8			3.9			≈0.0			74.2

- In Table 5.2, D.W-Domestic water; I.W-Irrigation water; S.W-Variation of the soil water content; GWC-Groundwater change.

5.3.3 Index of monthly water income and expenditure

Every component of the monthly water income and expenditure is summarized as listed in Table 5.2. The established index of the monthly water income and expenditure is shown in Figure 5.21.

Based on the results as listed in Table 5.2 and shown in Figure 5.21, some characteristics of the monthly water income and expenditure can be generalized as follows.

1) After the start of the vegetation period, the water storage decreases distinctly. The *ET*

also shows the gradually incremental tendency.

2) In summer, especially in July and August, with increasing of the rainfall, each component of the water expenditure changes significantly.
3) The soil water content obviously increases in July and August, whereas the GWT is effectively recharged in the periods from August to October and from February to March.
4) The total annual water storage is approximate to 0.0.
5) The *ET* accounts for more than 70 % of the annual precipitation.

With regard to the analyzed results of the water storage, variation of the water content is only estimated from the observed results at the maximum depth of 100 cm, variation of the soil water content in the soil layer from the depth of 100 cm to the shallow GWT had not been analyzed due to the data deficiency. On the other hand, the water exchange between the soil water and the shallow GWT, the exchange between the soil water content and the atmospheric moisture are in dynamically changing state. Therefore, the analyzed results of the annual water balance and the monthly water income and expenditure are approximate to the actual condition with a certain degree of error.

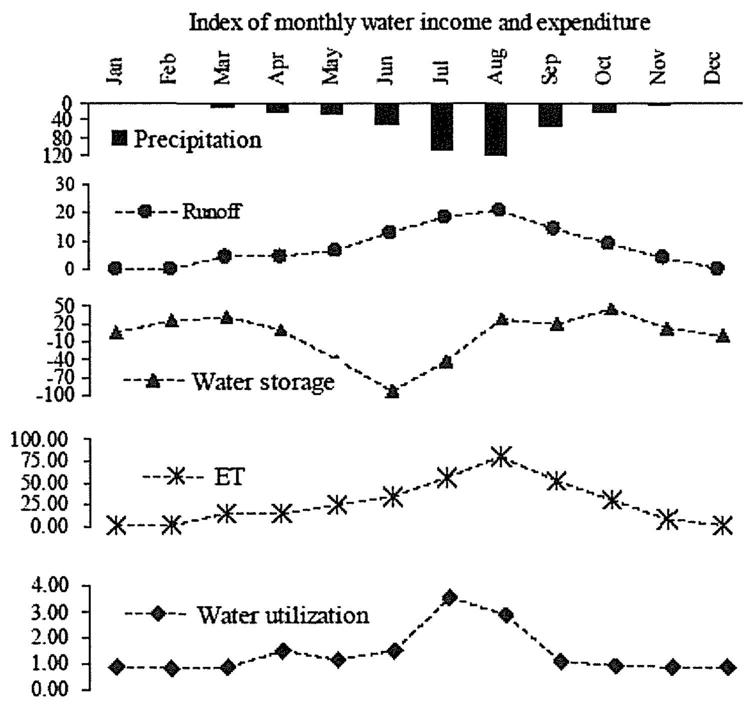

Fig 5.21 Index of the monthly water income and expenditure (Area: $1km^2$, unit: $10^3 \cdot m^3$)

5.4 Summary

In Chapter 5, index of annual water balance and index of monthly water income and expenditure of the study area have been approximately established. The processes of annual water income and expenditure have been clarified to some extent.

Additionally, the GWT fluctuant characteristics in the study location were clarified to some extent through analysis of the observed data of GWT level.

From view point of total hydrological cycle, the annual irrigation water is commonly regarded as a part of yearly evapotranspiration. Based on the estimated results of the annual water balance, if the annual irrigation water (about 5.12 mm) is added to the annual *ET*, the *ET* attains approximately 76.0 % of the annual rainfall. Cotemporaneously, the annual domestic water can be considered as a part of GWT outflow with the result that the yearly runoff reaches to about 24.0 % of the yearly precipitation. Thereupon, the annual precipitation can be approximately separated into two main components of the water expenditure, as the runoff (24.0 %) and the evapotranspiration (76.0 %).

In the current study, with an eye to evaluate the annual water consumption, further to estimate the annual available water, the water consumption was considered as a specific component of the monthly/annual water expenditure.

Theoretically, although all the precipitation can be used by means of the proper methods, but it is thought as impossible with the present technical means. Especially in view of the existing conditions in the study location such as the complicated landform, intense evapotranspiration in summer, the relatively backward economic conditions and etc, effective collections of the rainfall and surface runoff are extremely difficult to be implemented. Therefore, the shallow GWT combining with its outflow has become very significant available water for the agricultural production and people's lives. Under the condition of the present annual water balance, the GWT outflow which accounts for about 9.5 % of the annual rainfall is considered as the most important available water resources in the study location. Additionally, the available water resources are also expected to increase by the means of storing more surface water.

Chapter 6

Effects of the check dam system

6.1 Introduction

Loess plateau, as the most severe soil and water loss area in the world, over 60 % of the land in Loess Plateau has been subjected to soil and water loss[37)]. The severe land erosion (the slope erosion and gully erosion) causes the vast sediment yield every year. Sediment from Loss Plateau results in the siltation of many reservoirs, lakes and rivers, the approximately 90 % of Yellow River sediment comes from Loess Plateau[32),105),106)]. Since 1950s, large efforts on soil erosion control and ecosystem restoration were made by the Chinese Government, and after years efforts, though the land erosion has been alleviated to some extent, however it is still in serious condition[107), 108)]. A series of soil conservation practices are being implemented on Loess Plateau, especially on the hilly-gully region[109)]. It is indicated that construction of the check dam system is one of the most important engineering measure to conserve soil and water in Loess Plateau[31), 110)].

Fig. 6.1 Check dam (earth-fill dam) in Loess Plateau for mitigating the soil erosion and the sediment transportation

On the other hand, it was pointed out that overextraction of groundwater in Loess Plateau has led to continuous decline of the groundwater table and diminishing of the groundwater resource. Constructing many reservoirs on the Loess Plateau, and dikes around the farmland to collect rainfall for infiltration into the ground provides additional resources of groundwater[111)]. As a primary function, the check dam system effectively mitigating the gully erosion and sediment yield. Simultaneously it also plays an important role on decreasing and redistributing the surface runoff in every small basin. In the wind-water erosion crisscross region at the northern Loess Plateau, scare amount and uneven distribution of rainfall in addition to intense evapotranspiration causes the deficiency of the annual water resources.

The shallow groundwater which is formed in the sediment filled area at the upstream-side of the check dam and the shallow groundwater flow which occurs at the downstream-side of the check dam becomes an important part of available water in every small basin[60), 104)].

In the current study, with an aim to clarify the effects of the check dam system on runoff redistribution, observation of the shallow groundwater (GWT) was conducted at the sediment filled area in front of a check dam in Liudaogou Basin. A numerical calculation model for runoff calculation of the sediment filled area was developed according to the actual topographic and ground conditions of the study area. Applicability of the developed model was validated by fit to the observed data of GWT level. The runoff calculation for three cases such as the original condition without a check dam (Case 1), an assumed case with a dam but no sediment filled area (Case 2) and the present situation with a check dam system (Case 3) were carried out respectively. Through comparison of the numerical calculation results of the three cases in given year of 2006, effects of the check dam system were clarified from the view of runoff redistribution.

6.2 Outline of topographic form of the gully-check dam area

Basing on the field survey, the general gully-check dam topographic profile in the northern Loess Plateau is extracted as depicted in Figure 6.2.

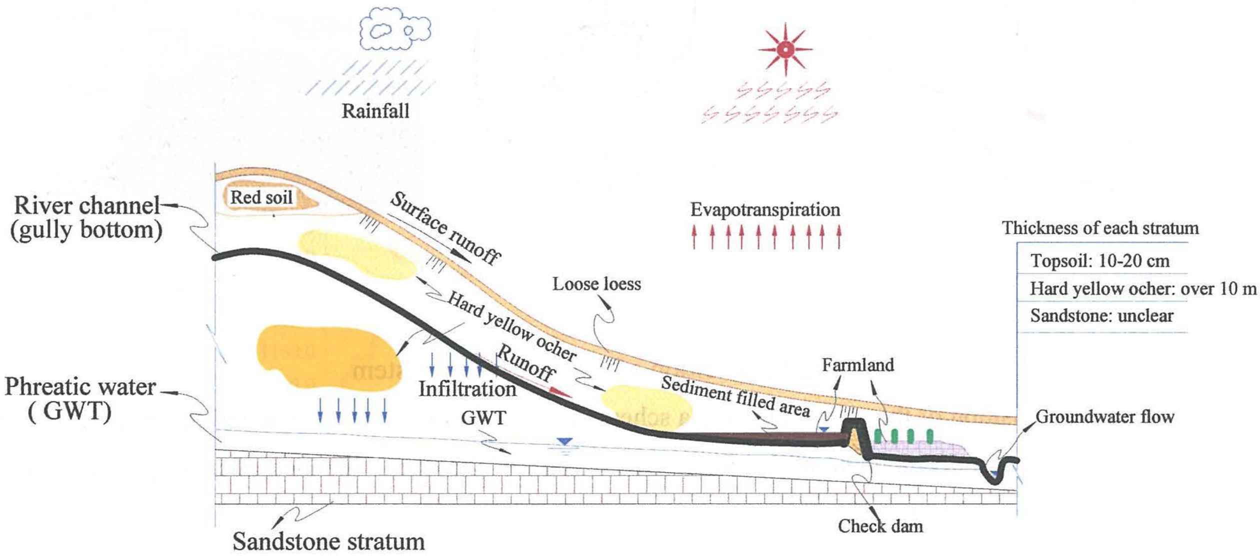

Fig. 6.2 Longitudinal profile of the general gully-check dam topography

Outline of the gully-check dam geographic profile formed process could be simply summarized as follows:

(1) Firstly, a large gully had been formed mainly by the long-term severe land erosion.

(2) In order to reduce the soil erosion and sediment transportation, a check dam (earth-filled

dam) was constructed at the suitable location at the downstream in a gully.

(3) Due to the sedimentation in front of the check dam, a small scale alluvial plain had been formed after 20-30 years of construction of the check dam.

Naturally, the check dam intercepted the major part of the surface runoff which generated at the upstream area. The dammed-up surface water was infiltrated and evaporated in front of the check dam. And a part of infiltrated water became the shallow groundwater (phreatic water) in the sediment filled area. A relatively stable groundwater flow generally occurs at the downstream-side of the check dam with a fairly small scale.

As the check dam system significantly impacts on the redistribution of the runoff, clarification of the effects of the check dam system is significant for reasonable development and utilization of the water resources in each small basin, also in the northern Loess Plateau region.

6.3 General situation of the check dam system in the study location

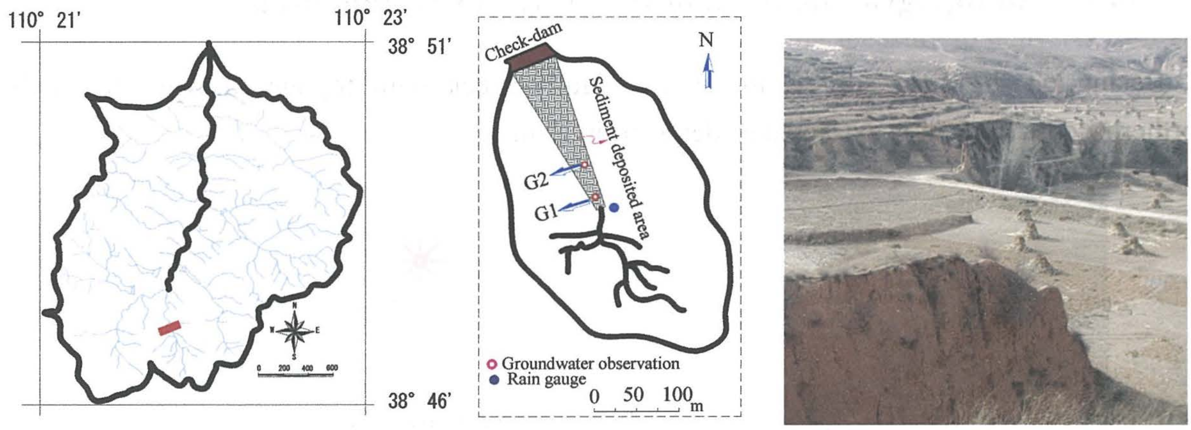

(a) (b) (c)

Fig 6.3 Position of the check dam system

((a) the actual position of the check dam; (b) a schematic drawing of the study area and the arrangement of the field observation ; (c) a photo of the check dam system . It shows the situation after the growth period, the check dam is used as a road.)

The check dam system is the shortened form of the check dam combined with the sediment filled area which formed in front of the check dam. In the study location, a check dam was constructed about 30 years ago at the lower reach in a gully which belongs to the upstream of Liudaogou Basin. The field observation of the GWT was conducted at the sediment filled area, (G1 and G2 in Fig 6.3). A linn which drop height is about 8.0 m exists at the downstream-side of the surface flow observed site as shown in Fig 6.5. The width of the sediment filled area broadens little by little from the bottom of the linn to the check dam. Due to the severe sedimentation, a small scale fluvial plain has been formed at the upstream-side of the check dam. In recent years, the crops such as the maize and soybean were planted at a side on the sediment filled area approaching the check dam (Fig. 6.3).

Elevation of the sediment filled area is 1171.74 m-1175.28 m, the longitudinal length is about 450 m, area is about 1.8×10^4 m^2. The orthographic plan and the longitudinal profile of the sediment filled area are shown in Figure 6.4 and Figure 6.5 respectively.

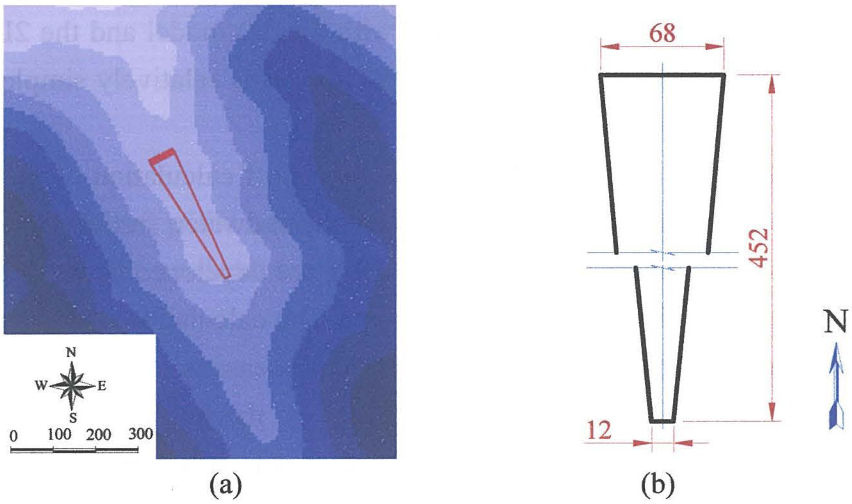

Fig 6.4 Orthographic plan of the sediment filled area

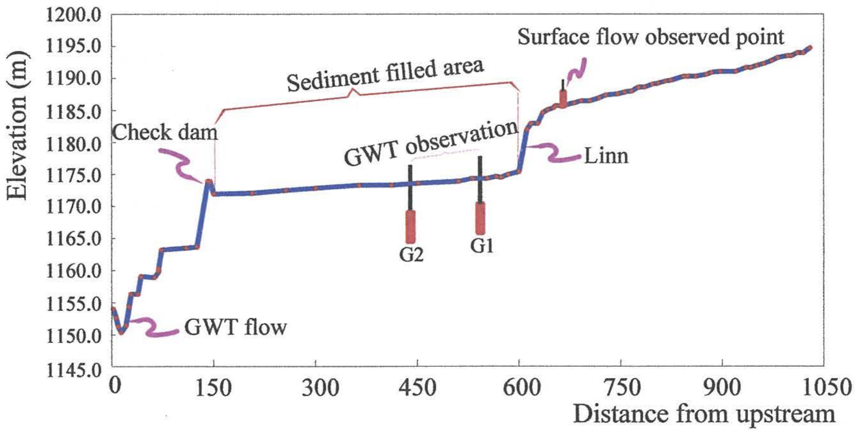

Fig 6.5 Longitudinal profile of the check dam system

6.4 Runoff calculation model of the sediment filled area

6.4.1 Introduction

Various models on calculation of the groundwater have been put forward conventionally.

Krüger S. and Rutschmann, P. (2006) proposed modeling 3D supercritical flow with extended shallow-water approach[112]. Saito, Y. and Suzuki, A. (et al., 2006) developed a quasi-three dimensional model (WCAP: Water Circle Analysis Program) for GWT calculation by using finite element method[113]. The two instances of the two dimensional model (2D model) with the unstructured finite volume method as respectively proposed by F.ASCE, and Kang, S.K., (et al., 2004) and Nguyen, D.K. and Shi, Y.E. (et al., 2006)[114), 115)]. There are many examples of the one-dimensional GWT calculation which were commonly carried out combined with the calculation of the surface runoff such as a latest instance conducted by Hunukumbura, P.B. and Tachikawa, Y. (et al., 2009)[116]. Compared with the 3D model and the 2D model, one of the obvious features of the one-dimensional GWT model is relatively simple and easy to be developed.

In the current study, with an aim to achieve the runoff calculation of the sediment filled area which involves the surface runoff and shallow groundwater, further to clarify the effects of the check dam system on the runoff redistribution, we developed a one-dimensional runoff calculation model for the chosen check dam system. The calculation model was developed as one-dimensional model owing to the following principle reasons.

(1) Due to the limited opportunities of the field survey, the investigation of the topography and the ground condition of the sediment filled area is still scant. Such as the hydraulic properties of the soil-layer which is subsequent to the topsoil both in the slope sector and in the sediment filled area have not been ascertained. As perception of the ground conditions of the chosen sediment filled area is not in-depth, development of the 3-dimensional or 2-dimensional hydraulic model becomes extremely difficult.

(2) The check dam system is situated at the downstream in a gully and spatially links to the area of the surface runoff calculation. The calculated results of the surface runoff and the groundwater flow of the runoff calculated area (Chapter section 4.3, Fig. 4.10) respectively become the boundary condition of the surface runoff calculation and groundwater calculation at the upper end of the sediment filled area. The adopted method for model development of the sediment filled area is similar to the development of the surface runoff calculation model (expounded in Chapter section 4.4).

6.4.2 Model development

By considering the actual topography and ground conditions of the chosen check dam system, lumping of model for runoff calculation has been developed as shown in Figure 6.6. Based on the results of the leveling survey, the longitudinal profile of the sediment filled area was ascertained as shown in Figure 6.7.

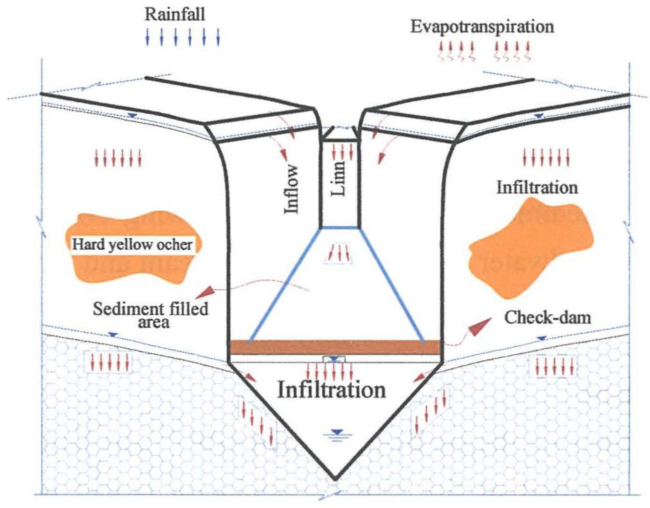

Fig 6.6 Lumping of the runoff calculation model of the sediment filled area (includes the slope sector of the both sides)

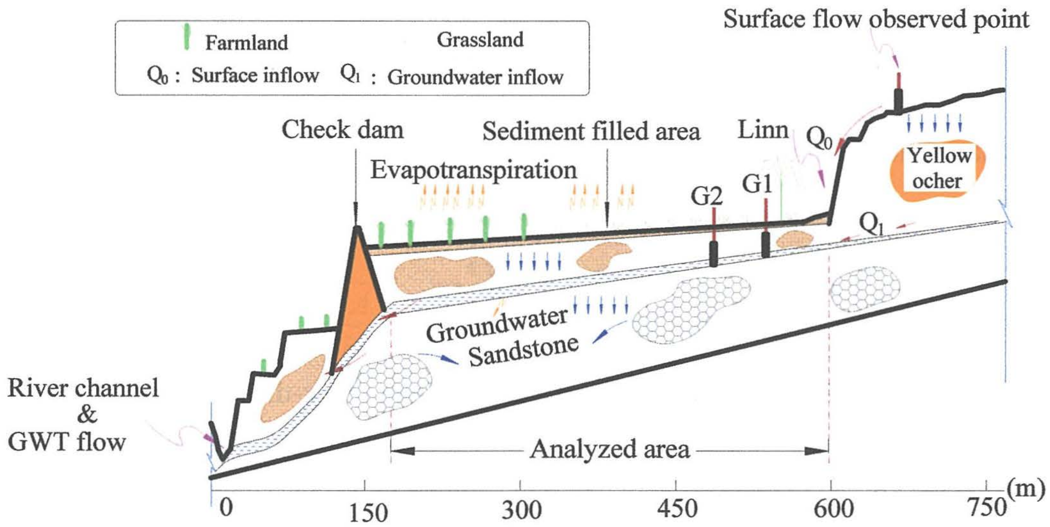

Fig 6.7 Longitudinal profile of the sediment filled area

Lumping of the model is composed of the slope sector and the river channel sector (sediment filled area) which is similar to the surface runoff calculation model in structure. Because the check dam was constructed on the original river channel which formed in the sandstone layer, the lateral section of the sediment filled area was considered as the connection of the triangle and the rectangular. The triangle refers to the quondam river channel which formed in the sandstone stratum, and the rectangular refers to the sectional part above the surface of the sandstone layer. The groundwater (phreatic zone) exists at lower part in the second soil layer (above the sandstone layer) which was clarified by the field survey.

On both sides of the check dam is the farmland. The two GWT observed points are adjacent to the upstream extremity at the sediment filled area.

The main components of the water input and output include the rainfall, the surface runoff, the GWT flow, evapotranspiration, and infiltration in both the slope and the sediment filled area. With regard to the sediment filled area, the inflowing components also include the surface inflow and the groundwater inflow from the upstream and the slope sector of the both sides (as indicated in Fig 6.6 and Fig 6.7).

6.4.3 Governing equations

The governing equations on the surface flow and GWT calculation in the slope sector are same as the numerical method of the runoff calculation model which was introduced in Chapter section 4.4.

· Slope sector

(1) Equation of the continuity of the surface flow

$$\frac{\partial h}{\partial t}+\frac{\partial q}{\partial x}=r-f_1 \qquad 6.1$$

(2) Formula of the mean velocity

$$q=\frac{1}{n}Rh^{\frac{5}{3}}I^{\frac{1}{2}} \qquad 6.2$$

where, h-depth of water (m), q-unit width flow rate ($m^2 \cdot s^{-1}$), x-distance in flow direction (m), t- interval of calculation time (s), r-the effective rainfall ($m \cdot s^{-1}$), f_1, -mean infiltration velocity of the 1st layer ($m \cdot s^{-1}$), n-coefficient of the roughness ($s \cdot m^{-1/3}$), R-hydraulic radius (m), I-gradient of the slope.

(3) Equation of the continuity of the GWT flow in the first layer

$$\lambda\frac{\partial \bar{h}}{\partial t}+\frac{\partial \bar{q}}{\partial x}=f_1-f_2 \qquad 6.3$$

(4) Darcy's law (One-dimensional motion equation of the infiltration flow)

$$\bar{q}=k\bar{I}\bar{h} \qquad 6.4$$

where, λ-effective porosity of the soil in the slope sector, $\bar{h}$-Depth of the groundwater flow (m), $\bar{q}$-discharge of the unit width of the groundwater ($m^2 \cdot s^{-1}$), k-coefficient of permeability

($m \cdot s^{-1}$), $\overline{I}$-gradient of the 1st layer which is approximately replaced by the gradient of the slope, f_2-mean infiltration velocity of the 2nd layer ($m \cdot s^{-1}$).

The equations used on calculation in the second layer are same as the equations which are used on calculation in the first layer, only footnote of some factors are changed which leads to the difference in form. The relational contents are omitted herein.

· Sediment filled area

(1) Equation of the continuity of the surface flow

$$\frac{\partial A}{\partial t}+\frac{\partial Q}{\partial x}=(r-EW-f_1)\cdot B_i+q_s \qquad 6.5$$

(6) Manning's equation of mean velocity

$$Q=\frac{1}{n}R^{\frac{2}{3}}I^{\frac{1}{2}}A(i) \qquad 6.6$$

where, A- sectional area of the surface flow (m^2), Q-flow discharge ($m^3 \cdot s^{-1}$), B_i-with of the sediment filled area at grid No. i (m), I-gradient of the sediment filled area, q_s-sum of surface inflow and GWT inflow in the first layer from the slope sector ($m^2 \cdot s^{-1}$). EW-evaporation from the water surface ($m \cdot s^{-1}$). Other factors are corresponding to the surface flow calculation in the slope sector as above mentioned.

(7) One-dimensional equation of the continuity of the GWT flow in the first layer

$$\lambda_1(1-S_{r1})\frac{\partial \overline{A_1}}{\partial t}+\frac{\partial \overline{Q_1}}{\partial x}=(f_1-f_2-ET)\cdot \overline{B_i} \qquad 6.7$$

(8) Darcy's law

$$\overline{Q_1}=k_1\overline{I}\,\overline{A_{1i}} \qquad 6.8$$

where, λ_1-mean porosity of the soil in the 1st layer, S_{r1}- degree of saturation in the first layer, ET-evapotranspiration over grassland which is corresponding to the vegetation type on the GWT observed point G2 ($m \cdot s^{-1}$), $\overline{A_1}$-sectional area of the GWT flow in the 1st layer (m^2), $\overline{Q_1}$-discharge of the GWT flow in the 1st layer ($m^3 \cdot s^{-1}$), f_2-mean infiltration velocity of the 2nd layer ($m \cdot s^{-1}$), k_1-coefficient of permeability in the 1st layer ($m \cdot s^{-1}$), $\overline{B}$-width of the GWT table in the 1st layer which is corresponding to the width of the river bed at the same section (m), $\overline{I}$-gradient of the GWT table in the first layer which proximately replaced by gradient of the river channel, other factors are corresponding to the above mentioned.

(9) Equation of the continuity of the GWT flow in the second layer.

$$\lambda_2(1-S_{r2})\frac{\partial \overline{A_2}}{\partial t}+\frac{\partial \overline{Q_2}}{\partial x}=f_2\overline{B_i}-f_3\overline{B_{gi}}+q_{sg} \qquad 6.9$$

(10) Darcy's law

$$\overline{Q_2}=k_2\overline{I}\,\overline{A_2} \qquad 6.10$$

(11) Sectional area of the GWT flow in the 2nd layer

$$\overline{A_{2i}}=\frac{1}{2}\overline{B}_{gi}\overline{H_{gi}} \qquad 6.11$$

where, λ_2-mean porosity of the soil in the 2nd layer, $\overline{A_2}$-sectional area of the GWT flow in the 2nd layer (m^2), $\overline{Q_2}$-GWT flow discharge in the 2nd layer ($m^3\cdot s^{-1}$), f_3-infiltration velocity of the sandstone layer ($m\cdot s^{-1}$), q_{sg}- the GWT inflow from the second layer of the slope sector ($m^2\cdot s^{-1}$), k_2-coefficient of permeability in the 2nd layer ($m\cdot s^{-1}$), $\overline{B_{gi}}$-width of the GWT flow in the 2nd layer at grid No. i (m), $\overline{H_{gi}}$-depth of the GWT flow in the 2nd layer at grid No. i (m), S_2-degree of the saturation in the 2nd layer. Other factors are corresponding to the above mentioned.

6.4.4 Differencing and algorithm

6.4.4.1 Differencing

The differencing method of the upstream-difference scheme is conventionally adopted to perform the calculation. Because the sectional form of the phreatic zone is triangle in the second layer, the area factor was adopted for differencing. As a result, the achieved differential formulas are relatively uncomplex.

(1) Differencing of the continuity equation of the surface flow

$$A_i^{n+1}=A_i^n+dt\cdot\left[(r(t)-f_1-EW)B_i+q_s-\frac{Q_i^n-Q_i^{n-1}}{dx}\right] \qquad 6.12$$

(2) Differencing of the continuity equation of the GWT in the 1st layer

$$\overline{A_{1i}}^{n+1} = \overline{A_{1i}}^{n} + \frac{dt}{\lambda_1(1-S_{r1})}\left[(f_1 - f_2 - ET)\overline{B_i} - \frac{\overline{Q_{1i}}^{n} - \overline{Q_{1i}}^{n-1}}{dx}\right] \quad 6.13$$

(3) Differencing of the continuity equation of the GWT in the 2nd layer

$$\overline{A_{2i}}^{n+1} = \overline{A_{2i}}^{n} + \frac{dt}{\lambda_2(1-S_{r2})}\left[f_2\overline{B_i} - f_3\overline{B_{gi}} - \frac{\overline{Q_{2i}}^{n} - \overline{Q_{2i}}^{n-1}}{dx} + q_{sg}\right] \quad 6.14$$

where, n-unit time on calculation (1s), i-grid No., other factors are corresponding to the above mentioned.

6.4.4.2 Algorithmic method for the infiltration calculation in the sediment filled area

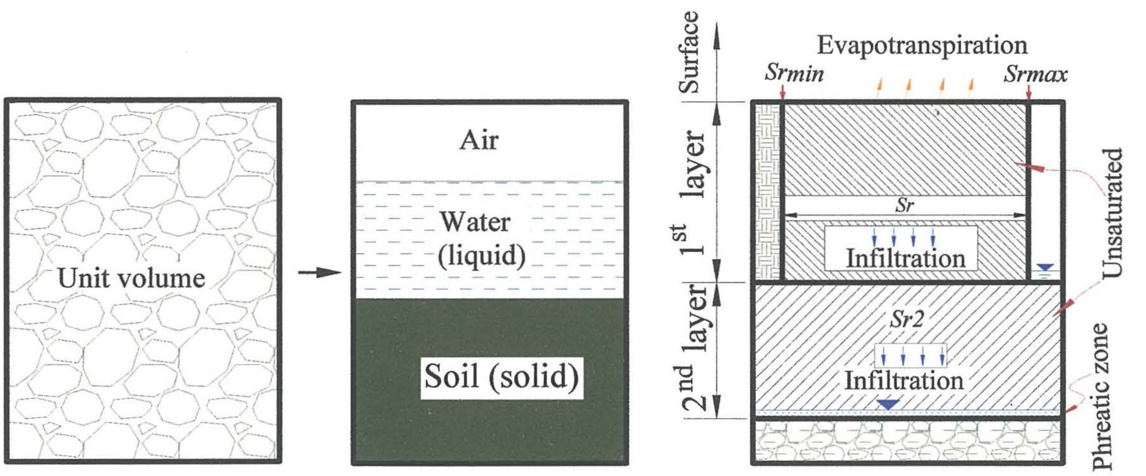

(a) Natural soil (b) Three phase (c) Condition of soil layer on calculation

Fig 6.8 Condition of soil layer on calculation

The natural soil can be extracted as depicted in a schematic drawing of Figure 6.8.a. Figure 6.8.b depicts the three-phase soil model which is composed of the solid soil grain, the water in liquid state and air[117)]. According to the actual conditions of the sediment filled area, condition of the soil layer on calculation which is extracted from the Figure 8.a and Figure 8.b is shown in Figure 6.8.c.

The algorithmic method for the infiltration calculation in vertical direction in the first layer and the second layer can be simply explained using a diagram as Figure 6.8.c. In the soil model as depicted by Figure 6.8.c, the minimum and the maximum degree of saturation in the first layer are represented as S_{rmin} and S_{rmax} respectively. When the degree of saturation in the first layer attains S_{rmax}, the groundwater is generated in the first layer and the infiltration from the first layer to the second layer takes place. Evapotranspiration is commonly considered as to occur from the first layer. If the degree of saturation in the first layer drops to S_{rmin}, the evapotranspiration is assumed to be 0. When the degree of saturation in the first layer varies within a range of $S_{rmin}<S_{r1}<S_{rmax}$, the groundwater in the first layer and the infiltration from the first layer to the second layer cannot occur, and the soil water movement in the first layer mainly manifests in the exchange with the atmospheric moisture. In the study location, the soil evaporation normally impacts on the infiltration down to the maximum depth of 60 cm from the ground surface, and the saturation of degree maintains relatively stable state below this depth. Thus the degree of saturation in the second layer (S_{r2}) at the sediment deposited area was assumed to be an invariable. The actual infiltration velocity into the second layer varies with the different depth of GWT in the first layer and changes within a range of $0 \leqq \alpha \leqq f_2$ (α-a referenced factor).

6.4.4.3 Number of grids for calculation in the longitudinal direction

Towards the runoff calculation, the sediment filled area is necessary to be segmented in the longitudinal direction from the upstream extremity to the check dam. The selected unit length for segmenting is 4 m with the result that the total length of the sediment filled area (452 m) has been divided into 113 grids. The slope sectors on the both sides have also been divided into the same number in the lateral direction.

When performing the runoff calculation, the sum of the surface inflow and GWT inflow from the first layer of the slope sector (q_s in Equation 6.12) becomes a component of surface flow calculation in the sediment filled area at every corresponding grid. Simultaneously, the inflow from the second layer of the slope sector (q_{sg} in Equation 6.14) becomes a component of GWT calculation in the second layer in the sediment filled area at each corresponding grid.

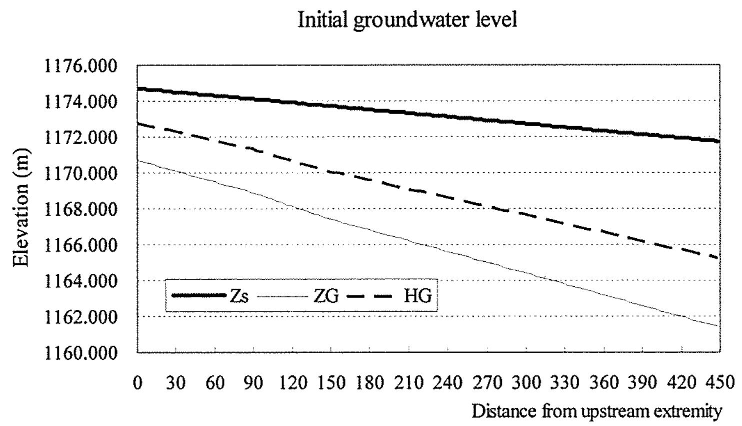

Fig 6.9 Initial water level in the 2nd layer in the sediment filled area
(Zs-the ground line of the sediment filled area; ZG-the baseline of the buried channel (the original river bed); HG- the initial surface curve of the GWT)

6.4.5 Initial conditions & Boundary conditions

6.4.5.1. Initial conditions

The initial degree of saturation in the first layer was determined by considering the observed mean soil water content on 1 January, 2006.

The degree of the saturation in the second layer was determined based on considering the observed data of the average soil water content at the depth 1.0 m.

The initial depth of GWT in the second layer was ascertained by the observed data of the GWT level. In the longitudinal profile of the second layer, the initial depth of GWT is shown in Figure 6.9.

6.4.5.2. Boundary conditions

In the slope sector, the discharge of the surface flow and GWT flow are both assumed to be 0.0 at the upstream extremity.

In the sediment filled area, the surface inflow and GWT inflow from the upstream are set to be as the boundary condition for the calculation of the surface flow and GWT flow in the second layer respectively.

6.5 Evapotranspiration

6.5.1 Evapotranspiration over the grassland

The evapotranspiration (*ET*) used on the runoff calculation at the sediment filled area was estimated by using a reference crop evapotranspiration (ET_0) (mm/h) by Allen (et al.,1998), which is expressed as follows[118)].

$$ETF = \frac{ET_{inst}}{ET_{0inst}} \tag{6.15}$$

$$ET_{0inst} = \frac{0.408\Delta(R_n - G) + \gamma(37/T)u(e_s - e_a)}{\Delta + \gamma(1 + 0.34u)} \tag{6.16}$$

where *ETF*-the fraction at the satellite image time, ET_{inst}-the estimated *ET* for the target pixel at the satellite image time ($mm \cdot h^{-1}$), ET_{0inst}-the reference crop *ET* at the selected weather station at the satellite image time ($mm \cdot h^{-1}$), Δ – the slope of the saturation vapor-pressure at air temperature ($kPa \cdot {}^{o}C^{-1}$), γ–the psychometric constant ($kPa \cdot {}^{o}C^{-1}$), e_s-saturated vapor-pressure at air temperature (kPa), R_n- net radiation ($MJ \cdot m^{-2} \cdot h^{-1}$), *G*-soil heat flux ($MJ \cdot m^{-2} \cdot h^{-1}$), e_a- Actual vapor-pressure (kPa), *u*-average hourly wind speed at height of 2 m ($m \cdot s^{-1}$), *T*-mean hourly temperature (^{o} C).

Kimura, R. (et al., 2007) proposed the methods for estimating the *ET* over Liudaogou Basin based on the original Penman-Monteith Equation by assuming the *ETF* equals to the 24-h *ETF*, the 24-h *ET* can be estimated with the equations as below[119), 120)].

$$ET_{24} = ETF \cdot ET_0(24) \qquad 6.17$$

$$ET_{0(24)} = \frac{0.408\Delta(R_n - G) + \gamma \frac{900}{T+273} u(e_s - e_a)}{\Delta + \gamma(1 + 0.34u)} \qquad 6.18$$

Towards estimating the actual hourly *ET* from the grassland, the vegetation height is assumed to be 0.15 m as vegetation cover around the GWT observed point G2. Method for *ET* calculation proposed by Kimura, R. (et al., 2005, 2007) can be referenced due to the studies were conducted on the same study area[10), 119), 120)]. The data used in the calculation of the *ET* included sunshine duration, the hourly mean temperature and wind speed, the hourly average specific humidity and the mean soil water content at the depth of 1 m. The computational process of each necessary factor and *ET* are as below.

$$lET = \frac{\Delta(R_n - G) + c_p \rho \frac{(e_s - e_a)}{r_a}}{\Delta + \gamma(1 + \frac{r_s}{r_a})} \qquad 6.19$$

where, lET -latent heat flux in the soil (MJ$\cdot$m$^{-2}\cdot$h^{-1}), l-the latent heat of vaporization (MJ$\cdot$kg^{-1}), ET-actual evapotranspiration (mm$\cdot$h^{-1}), c_p-specific heat of air 1.0×10^{-3} (MJ$\cdot$kg$^{-1}\cdot$°C^{-1}), ρ –air density at constant pressure (kg$\cdot$m^{-3}), r_a-aerodynamic resistance (s$\cdot$m^{-1}), r_s-the surface resistance (s$\cdot$m^{-1}).

Each necessary factor in Equation 6.19 can be calculated as follows:

$$R_n = (1 - ref)S^{\downarrow} + L^{\downarrow} - L^{\uparrow} \qquad 6.20$$

ref-the surface albedo (0.23), $S^{\downarrow}$ -global radiation (MJ$\cdot$m$^{-2}\cdot$h^{-1}), $L^{\downarrow}$ -the downward long-wave radiation (MJ$\cdot$m$^{-2}\cdot$h^{-1}), $L^{\uparrow}$ -the upward long-wave radiation (MJ$\cdot$m$^{-2}\cdot$h^{-1}).

The G can be approximately calculated by the following method[118)].

$G = 0.1R_n$ in the daytime and $G = 0.5R_n$ in the nighttime.

$$\Delta = \frac{4098 \times \left[0.6108 \exp(\frac{17.27T}{T+237.3})\right]}{(T+237.3)^2} \qquad 6.21$$

$$\rho = 1.293 \times \frac{273.15}{273.15+T}\left(\frac{P}{101.3}\right) \times \left(1-0.378\frac{e_a}{P}\right) \quad 6.22$$

Here, P- atmospheric pressure (kPa) which can be expressed as

$$P = 101.3 \times \exp(-Alt/8200) \quad 6.23$$

Alt-altitude (m), the altitude of the No. 2 water lever recorder installed point (G2) is 1173.59 m.

$$\gamma = 0.665 \times 10^{-3} P \quad 6.24$$

$$r_a = \frac{\ln\left(\frac{z-d}{z_{0m}}\right) \cdot \ln\left(\frac{z-d}{z_{0h}}\right)}{k^2 u} \quad 6.25$$

where, z-height of measurements (m) which is equal to 2.0 m, d-the zero-plane displacement height (m), z_{0m}, z_{0h}- designate the roughness length governing momentum, heat, and vapor transfer (m), k-the von Karman's constant (0.41).

$$d = \frac{2}{3}H_c \ ; \ z_{0m} = 0.123H_c \ ; \ z_{0h} = 0.1z_{0m} \quad 6.26$$

H_c-Plant height (m), about 0.15 m on the GWT observed area.

The surface resistance r_s ($s \cdot m^{-1}$) was parameterized following Dickinson and Jarvis as below[121), 122)].

$$r_s = \frac{r_{s\min}}{LAI}(F_1F_2F_3F_4)^{-1} \quad 6.27$$

where, LAI-index of the leaf area. F_1, F_2, F_3, F_4-functions related to solar radiation, vapor-pressure deficient, temperature, soil water content. r_{smin}-the minimum surface resistance ($s \cdot m^{-1}$). Nonlinear regression analysis by the least-squares method was used for determining F_1, F_2, F_3, F_4. Kimura, R. (et al., 2005) suggested the r_s for ET calculation over the grassland in Liudaogou Basin can be determined by an equation as below[10)].

$$r_s = 108439 \cdot \exp(-38.344 \cdot \theta) \quad 6.28$$

θ –average soil water content at a certain depth ($cm^3 \cdot cm^{-3}$).

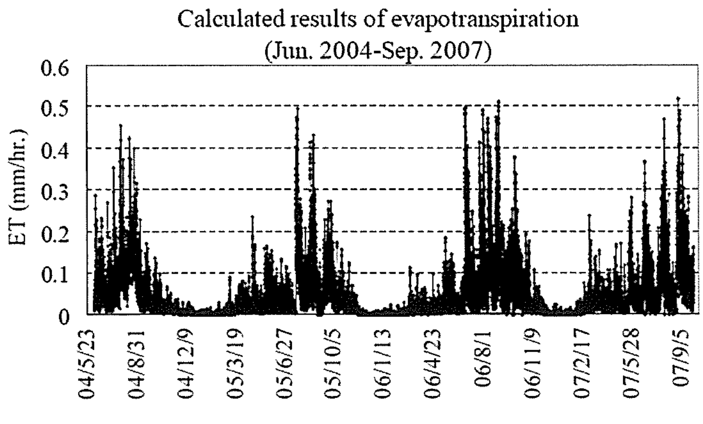

Fig 6.10 Results of the hourly *ET* over the grassland in Liudaogou Basin

6.5.2 Results of evapotranspiration

The calculated results of the hourly *ET* over the grassland during the period from May, 2004 to September, 2007 are shown in Figure 6.10 (same as Fig. 5.19).

The ratio between the *ET* and the rainfall in the calculated year of 2005 and 2006 are listed in Table 6.1. The annual *ET* over the grassland accounted for approximately 70 % of the yearly precipitation both in 2005 and in 2006. In view of the estimated results of the annual *ET* in Chapter section 5.2 (analysis of the annual water balance), the annual *ET* exceeded 70 % of the total yearly precipitation in Liudaogou Basin. As the *ET* varies with the different type of vegetation cover, the daily *ET* over grassland is general less than the *ET* over the shrub and the irrigated farmland, the results of *ET* over the grassland could be considered as reasonable[119)].

Table 6.1 Ratio between annual ET over the grassland and annual rainfall

Year	Rainfall (mm)	ET (mm)	Ratio (ET/Rainfall) %
2005	315	218	68.6
2006	386	265	69.2

The *ET* shown in Figure 6.10 was estimated by using the mean soil water content data which was observed on the slope at the maximum depth of 1 m. Because degree of saturation in the sediment filled area is higher than the slope sector in the most of annual time, when performing the runoff calculation of the sediment filled area, the achieved *ET* over the grassland in the slope sector must be adjusted. With regard to the method for data correction, firstly, the runoff calculation of the sediment filled area was carried out with the developed model using the results of *ET* of the slope sector. Next, the calculated results of the saturation degree in the first layer of the sediment filled area were chosen to recalculate the *ET* over the sediment filled area. The calculated results of the *ET* over the grassland of the slope sector and the sediment filled area in the year of 2006 are shown in Figure 6.11 respectively. This figure shows evapotranspiration over the grassland at the sediment filled area was generally higher than that of the slope.

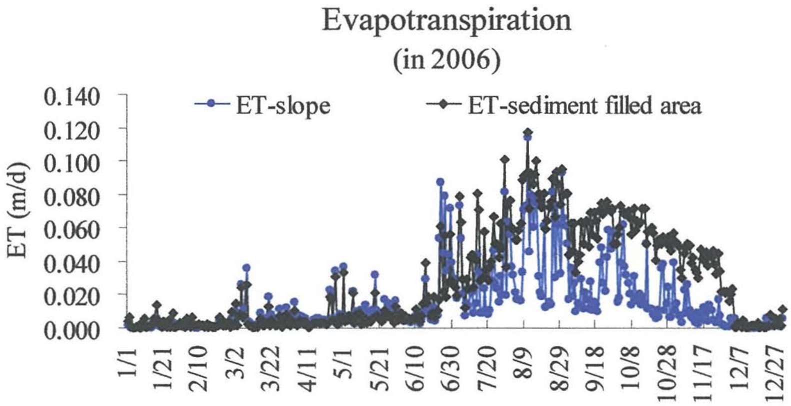

Fig 6.11 *ET* over the grassland on the slope & the sediment filled area

6.5.3 Water surface evaporation

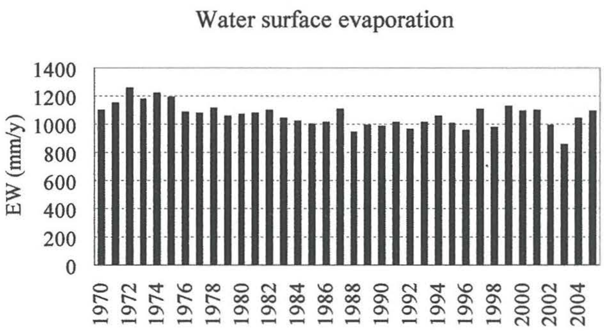

(a) Annual water surface evaporation

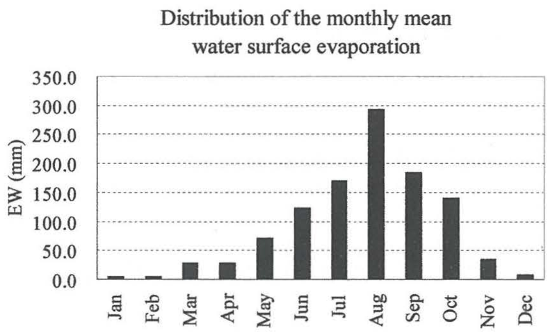

(b) Monthly distribution

Fig 6.12 Water surface evaporation
(EW- water surface evaporation)

If there is surface water in the sediment filled area, the main form of the *ET* is considered as the water surface evaporation. Due to the data deficiency of the actual water surface evaporation, the water surface evaporation in the calculated year of 2006 was approximately replaced by the mean annual value of the water surface evaporation in the study location. Because the temporal process of the water surface evaporation is similar to the *ET* over the grassland, the monthly distribution of the water surface evaporation was ascertained by considering the monthly distribution of the *ET* over the grassland in 2006. The annual water surface evaporation and the monthly distribution are shown in Figure 6.12.a and Figure 6.12.b respectively.

In given year of 2006, the surface flow only generated in June, July, August and September (Chapter section 4.6: surface runoff calculation). When performing the runoff calculation of the sediment filled area, the actual water surface evaporation is approximately adopted as the average value in each month in which the surface runoff occurred, such as in July, its value was about 5.5 mm/d.

Table 6.2 Main parameters

Parameter	Sediment filled area		Slope		Unit
Length	450		L: 206	R: 100	m
Roughness coefficient	0.08		0.12		$s \cdot m^{-1/3}$
Gradient	0.0078		……		…….
Thickness	1st	2.0	1st	0.50	m
	2nd	………	2nd	20	
Porosity	1st	0.45	1st	0.30	……
	2nd	0.35	2nd	0.30	
Coefficient of permeability	1st	1.0×10^{-3}	1st	1.0×10^{-3}	$m \cdot s^{-1}$
	2nd	5.0×10^{-5}	2nd	3.0×10^{-5}	
Infiltration velocity	1st	8.0×10^{-6}	1st	3.0×10^{-6}	$m \cdot s^{-1}$
	2nd	2.5×10^{-7}	2nd	2.0×10^{-7}	
	3rd	1.2×10^{-8}	3rd	1.2×10^{-8}	
Minimum saturation degree	1st	0.10	…….		…..
Initial saturation degree	1st	0.25	…..		…..
Maximum saturation degree	1st	0.85	……		…..
Saturation degree in 2nd layer	0.50		……		……

* L-left side, R-right side, 1st-the first layer, 2nd-the second layer, 3rd-sandstone layer

6.6 Parameters determination

The dimensional parameters were determined by leveling such as the longitudinal length of the extent of the sediment filled area. The elevation of the main datum points were determined by GPS. Some parameters related to the soil hydraulic properties such as the infiltration velocity of the topsoil and the coefficient of the permeability were determined by referencing to the corresponding parameters used in the calculation of the surface runoff (Chapter section 4.4). The initial soil water content (degree of saturation) in the sediment filled area was determined by the observed data. Some parameters such as the porosity of the topsoil in the sediment filled area, the maximum degree of saturation and the minimum degree of saturation were approximately determined by referencing to the relational studies which conducted on Liudaogou Basin[41),44),123)].

With regard to the other undetermined parameters such as the porosity of the second soil layer and the infiltration velocity of the sandstone layer under the sediment filled area and etc, the determined method of such parameters is in accordance with the following steps.

Firstly, each parameter was experientially given an initial value which was approximate to the actual condition as much as possible. For instance, the porosity of the second soil-layer is commonly less than the first layer, and the infiltration velocity of the sandstone layer is very small whose order is $\leqq 10^{-8}\ m \cdot s^{-1}$.

Next, carrying out the runoff calculation by using the developed calculation model and the obtained results of the GWT level was named by the calculated result. The observed results of GWT level were regarded as the exact value, and a difference must exist between the exact value and the calculated result. To lessen the difference, we adjusted the value of each undetermined parameter and repeated the calculation many times. Finally, a certain group parameters, by which the minimum difference in all the calculated results was produced, were adopted and used in the runoff calculation (Table 5.2).

6.7 Computational procedure

The program of the numerical calculation model was developed by programming language Fortran 90/95. The main computational procedure is shown in Figure 6.13.

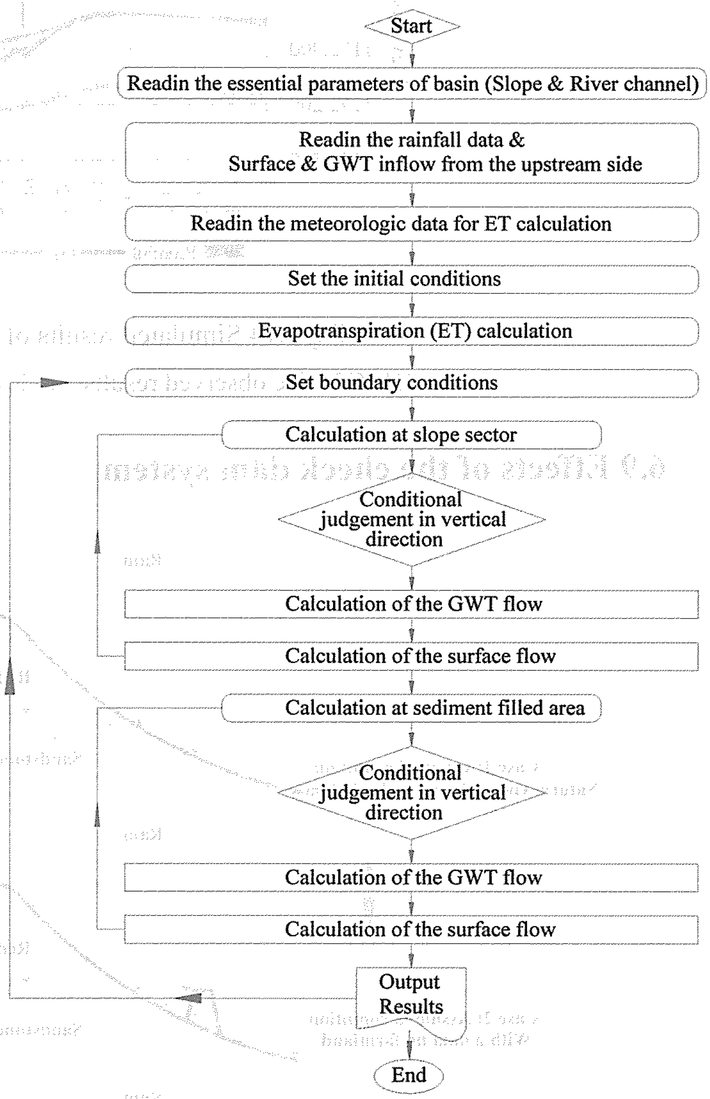

Fig 6.13 Flow chart of the calculation model

6.8 Numerical simulation

Applicability of the developed calculation model was validated by numerical simulation of the observed GWT level in 2006. Figure 6.14 shows the simulated results and the observed results (G1 and G2: shown in Figure 6.5 and Figure 6.7). As the simulated results reproduce the observed results well, the developed runoff calculation model applies to the actual conditions of the sediment filled area, which can be confirmed.

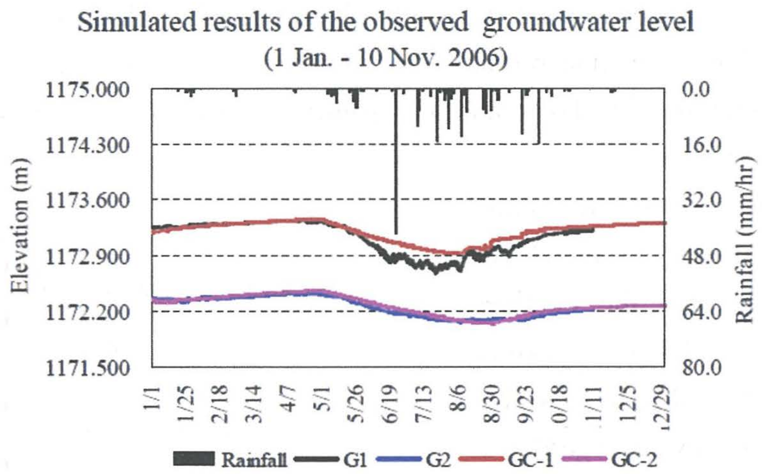

Fig 6.14 Simulated results of GWT level in 2006
(G1, G2: The observed results, GC1, GC2: The calculated results)

6.9 Effects of the check dam system

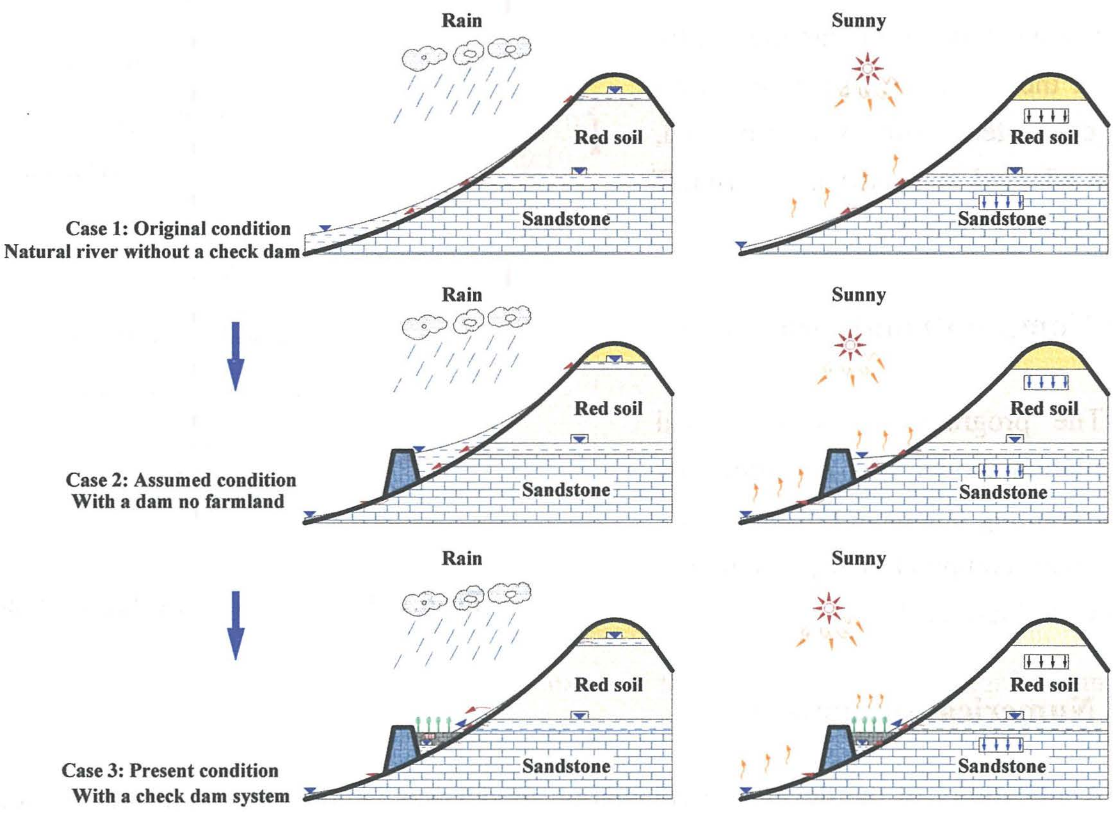

Fig 6.15 General situations in different case

6.9.1 Three cases for calculation

To evaluate the effects of the check dam area on runoff redistribution, the runoff calculation for the following three cases were carried out respectively.

Case 1 is considered as the original condition without check dam and sediment filled area.

Case 2 is considered with a check dam and a reservoir in front of the check dam. In other words, Case 2 is an assumed case which represents the condition during the time after the construction of the check dam and before the farmland came into being.

Case 3 is the present condition with a check dam system.

The schematic drawing of the three cases are shown in Figure 6.15 respectively. The common situations of runoff in different case during the time of rainy and sunny are depicted in Figure 6.15 respectively.

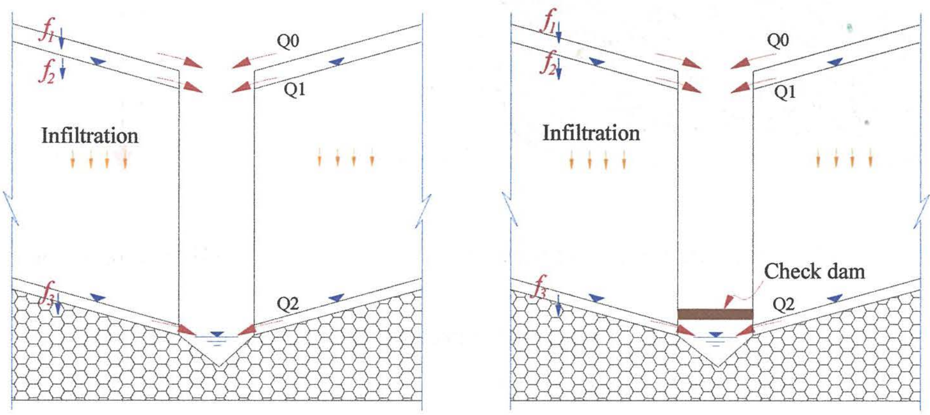

(a) Original situation of the river channel (b) Present situation of the river channel

Fig 6.16 Comparison of the original and present conditions of the river channel

Figure 6.16.a and Figure 6.16.b separately represents the situation of the river channel of Case 1 without a check dam and Case 3 with the check dam system. With regard to the original condition of the channel, the surface runoff and the GWT runoff were naturally discharged to the downstream. Compared with the original situation, the surface inflow and GWT inflow from the slope sector combined with the surface inflow and GWT inflow from the upstream-side of the sediment filled area are generally redistributed at the sediment filled area in the present situation.

6.9.2 Case 1: Original condition

6.9.2.1 Calculated area

Case 1 is considered as the original situation before construction of the check dam.

The runoff components in Case 1 include the surface runoff and GWT flow. The runoff calculation was carried out by using the developed numerical calculation model introduced in Chapter section 4.4. The calculated area is the catchment of the upstream of the check dam whose hypothetical channel networks and distributed-type basin model is shown in Figure 6.17.a. and Figure 6.17.b separately.

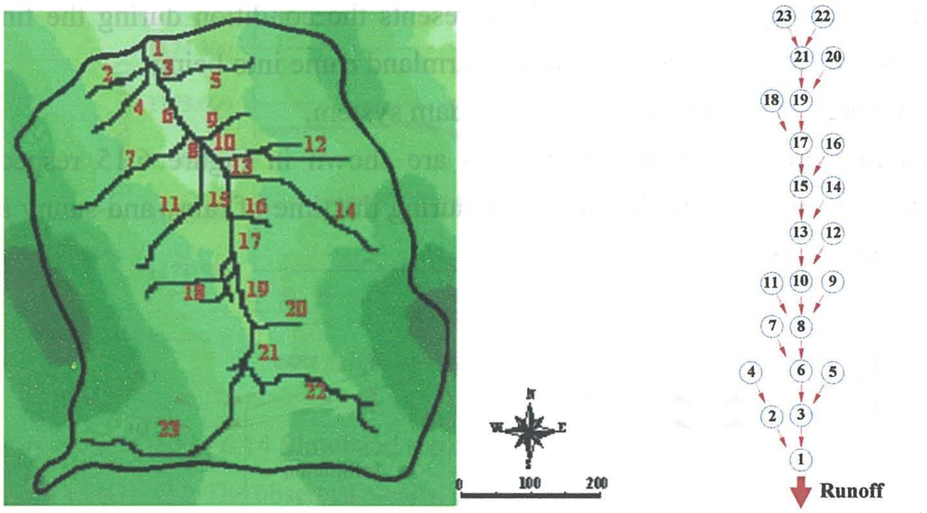

(a) Hypothetical channel networks (b) Distributed-type basin

Fig 6.17 Calculated area of the Case 1 (area: 0.43 km^2)

6.9.2.2 Results and analysis

(1) Results

The given is 2006. The calculated results of the surface runoff and GWT outflow are shown in Figure 6.18.a and Figure 6.18.b respectively. The total surface runoff was 2.84×104 m^3 and the GWT outflow was about 0.80×103 m^3.

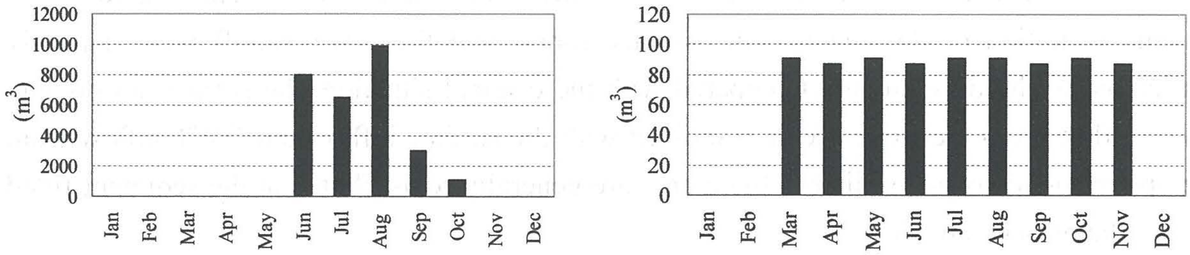

(a) Monthly surface runoff (b) Monthly GWT outflow

Fig 6.18 Runoff calculation results of Case 1

(2) Analysis

The calculated results shows that the surface runoff was concentrated on the rainy season and the monthly GWT outflow had no distinct change from March 2006 to November 2006. The GWT flow was relatively stable with a discharge of 3.4$\times 10^{-5}$ m^3/s. The GWT flow in

Case 1 was also considered to be frozen in winter by considering the actual situation of GWT flow in winter of Case 3.

In Case 1, the width of the river channel was assumed to be narrow thereby both the evapotraspiration and the infiltration were neglected.

According to the runoff calculated results of Case 1, the surface runoff and GWT outflow naturally discharged to the downstream from the calculated area. In other words, the total inflow was equal to the total runoff in Case 1.

6.9.3 Case 2: With a check dam and a reservoir

6.9.3.1 Calculated area

As above introduced, to mitigate the loss of the soil and water, a check dam was constructed at the downstream in a gully about thirty years ago. Based on the target survey, a reservoir was formed in front of the check dam because the area of the upstream-side of the check dam was widened and deepened by using a mechanical digger.

When performing the runoff calculation, the area of the quondam reservoir was considered to be same as the present sediment filled area (Fig 6.4).

6.9.3.2 Method for calculation

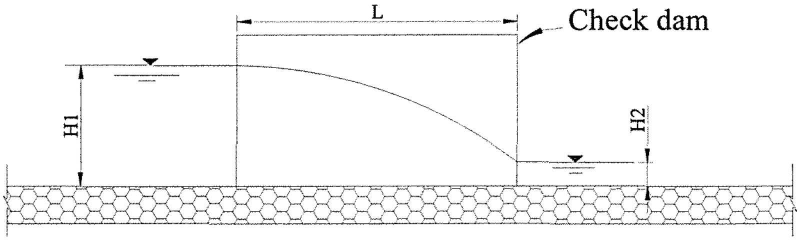

Fig 6.19 Seepage through the dam body

The calculation method of Case 2 was determined by referencing to the developed runoff calculation model of the sediment filled area (Fig. 6.6 & Chapter section 6.4-6.6). Compared with the lumping of the model as shown in Figure 6.6, the present sediment filled area is replaced by a reservoir in Case 2. Figure 6.19 depicts the seepage through the check dam body in Case 2. A simple method on the seepage calculation is as follows (Equation 6.29-Equation 6.30)[124].

· Continuity equation

$$\frac{d^2(h^2)}{dx^2} = 0 \qquad 6.29$$

· The seepage discharge through a section of lengthwise direction (perpendicular to the plane drawn in Fig. 6.19) is approximately calculated by Equation 6.30.

$$Q = \frac{kB(H_1^2 - H_2^2)}{2L} \qquad 6.30$$

With the boundary conditions: $x = 0 : h = H_1$, $x = L : h = H_2$.

where h-depth of water (m), x-distance in the calculated direction (m), Q-seepage discharge through the dam body ($m^3 \cdot s^{-1}$), k-coefficient of permeability ($m \cdot s^{-1}$). B-dam length (m), L-width of dam (m), H_1, H_2-repectively represents the boundary condition of the water depth at upstream-side and downstream-side of the check dam (m).

As to the determination of the coefficient of permeability (k) in the dam body, the coefficient of permeability of the soil used for dam construction was assumed to be same as the hard yellow ocher of the second layer in the slope sector because the local soil was used for the dam construction. As the soil must be compacted when the check dam built, the coefficient of permeability of the compacted soil is significantly lower than that of the original condition. For the soil whose original coefficient of permeability was the order of 10^{-5} m/s, the order was down to 10^{-6} m/s by using proper compaction methods[125), 126)]. Therefore, the coefficient of permeability of the dam body was roughly set to be 2.5×10^{-6} m/s.

When carrying out the calculation, the initial condition of the water depth in front of the check dam was assumed to be 2.0 m, H_2 was roughly assumed to be 0.20 m, L was approximately determined to be 10 m.

6.9.3.3 Results and analysis

(1) Results

According to the runoff calculation results of Case 2 in the year of 2006, each component of water input and output was estimated as shown in Figure 6.20. The difference between monthly water input and output of Case 2 are shown in Figure 6.21.

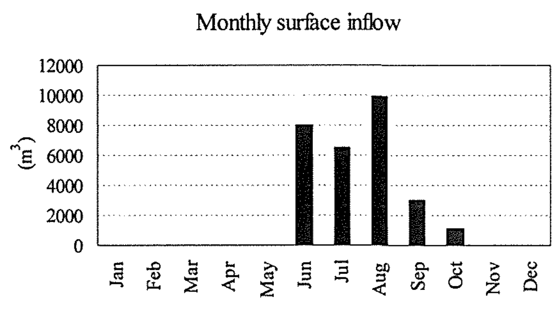

(a)

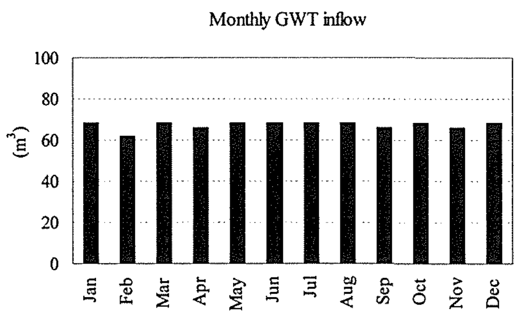

(b)

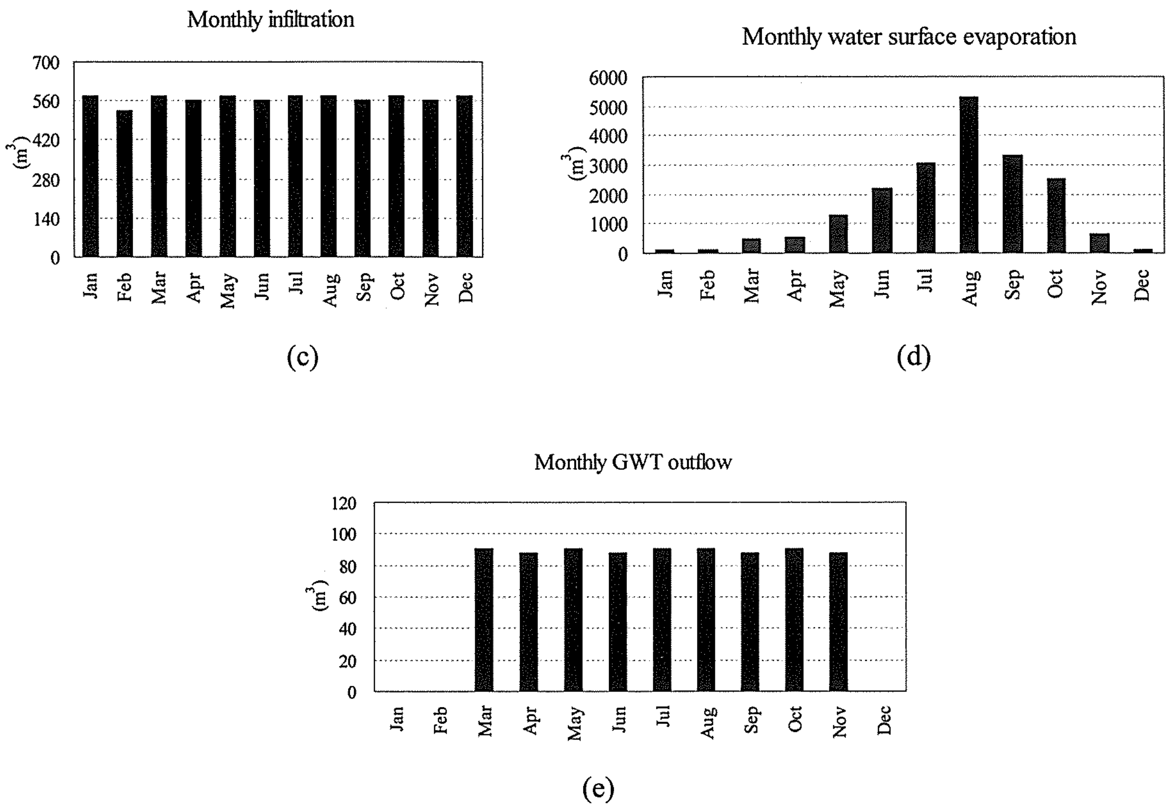

Fig 6.20 Each component of water input and output of Case 2
(a-b, input components; c-e, output components)

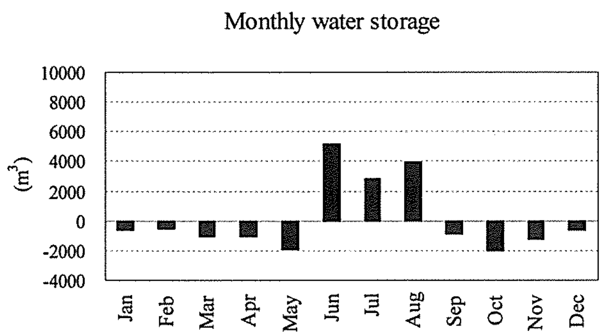

Fig 6.21 Difference between monthly input and output (Case 2)

(2) Analysis

Generally, the surface runoff at the location of the check dam could not occur in Case 2. If the water depth in front of the check dam exceeds the bottom of an effluent cave, which was built at the rightmost side in the dam body, the surface runoff will be naturally discharged. The bottom of the effluent cave was about 8 m above the original river bed at transversal profile of the downstream extremity of the present sediment filled area.

The assumed initial depth of water (2.0 m) at the downstream extremity of the reservoir was considered to be lower than the bottom of the effluent cave in Case 2. Because there was no surface inflow generated before June, the infiltration and the evapotranspiration caused the depth of water decreased gradually. According to the calculated results, the surface inflow occurred in June replenished the drawdown thereby there was no surface runoff occurred in June. In July and August, the surface inflow caused the increase of the water depth exceeding the assumed initial value for some time.

According to Figure 6.21, we know the difference between monthly water input and output in the reservoir showed the negative value except the rainfall centralized time from June to August. According to the runoff calculated results in Case 2, in July and August, it was also considered that the surface runoff from the reservoir could not occur because the maximum depth of water in front of the check dam was less than 2.5 m. The dammed-up surface water in July and August was considered to supply the amount of the water output in July, August and after the rainy season. The difference value between the amount of water input and total output was considered as the annual water storage in the reservoir, which was 1.98×10^3 m^3 in 2006.

In Case 2, GWT inflow, GWT outflow, and the infiltration show the relatively stable state, whereas in rainy season, evaporation was salience.

Compared with the calculated results of Case 1, the calculated results of Case 2 showed the effects of the check dam and the reservoir as interception of the surface runoff, and increase of the evaportranspiration, infiltration and water storage (Table 6.3).

6.9.4 Case 3: with a check dam system

A small scale alluvial plain had been formed due to sedimentation in front of the check and it was commonly used as farmland in recent years. Naturally, the check dam combined with the sediment filled area (farmland) significantly impacts on the annual runoff redistribution.

6.9.4.1 Calculated results

The numerical calculation of Case 3 was performed by using the developed calculation model as introduced in Chapter section 6.4-Chapter section 6.6. The calculated year was 2006 which was corresponding to the Case 1 and Case 2. According to the numerical results, each component of water input and output was estimated and the monthly distribution as shown in Figure 6.22.a – Figure 6.22.g respectively.

6.9.4.2 Analysis

The monthly distribution of each inflow component is same as the Case 1 and Case 2. The GWT flow has slightly increased compared with the corresponding results of Case 1 and Case 2. However, the other components of water output obviously distinguished from the corresponding results of Case 2.

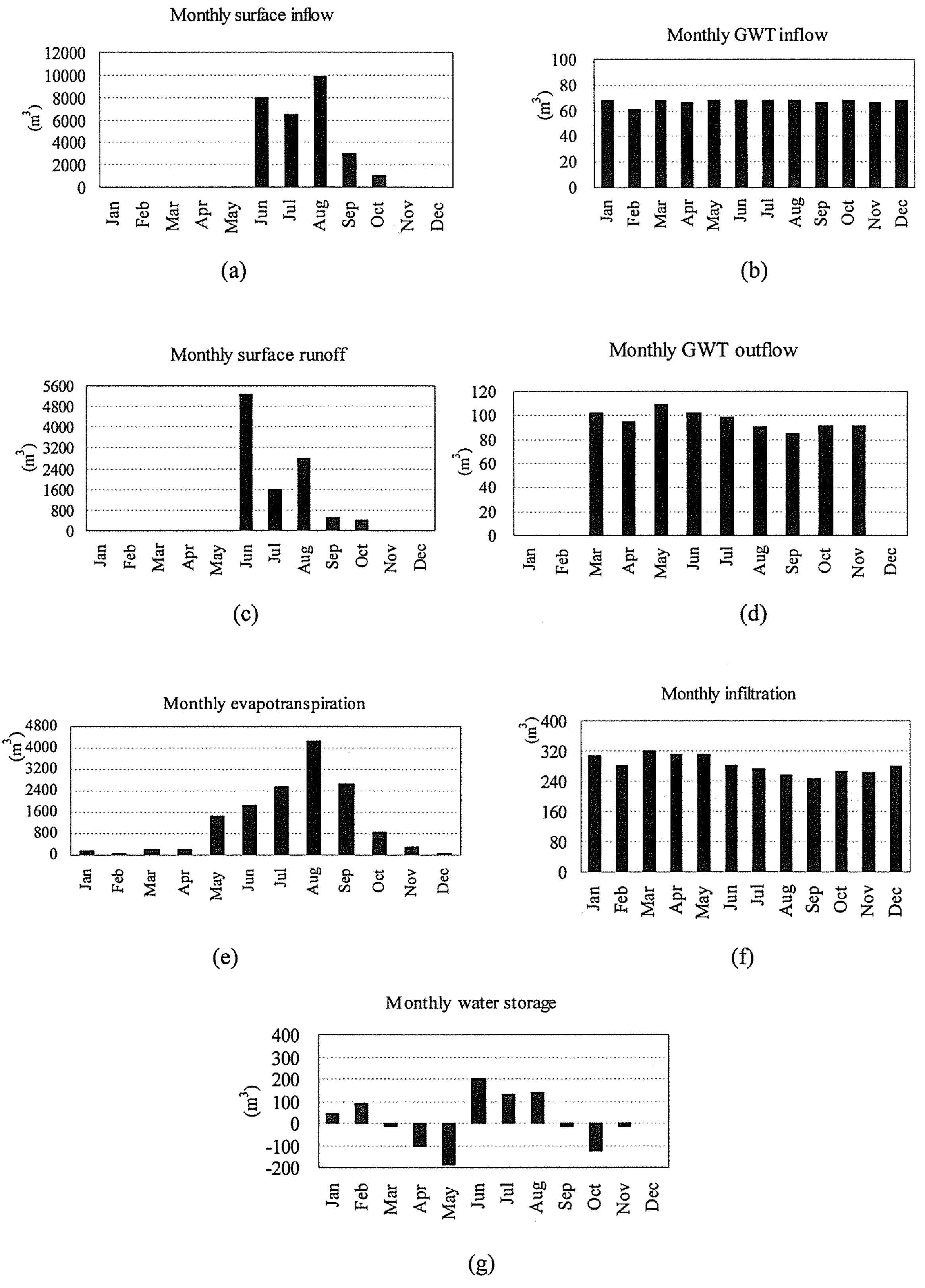

Fig 6.22 Each component of water input and output of Case 3

(Water storage is the sum of the variation of the soil water content and the change of GWT)

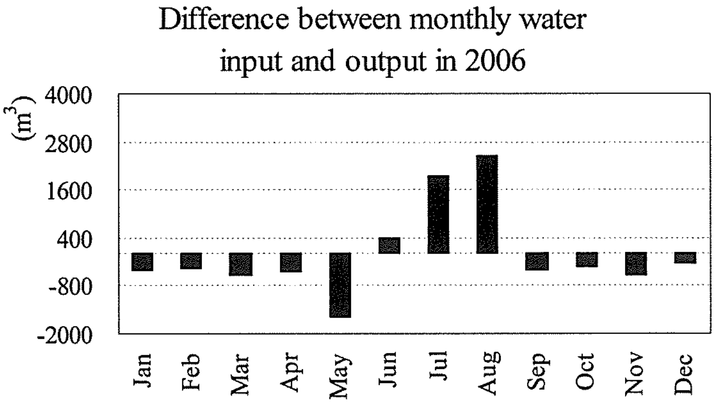

Fig 6.23 Difference between monthly water input and output of Case 3

The temporal process of the monthly evapotranspiration and infiltration in Case 3 is similar to Case 2, but the value is less than the corresponding component of Case 2.

In Case 3, the surface runoff occurring in the rainy season is about 10.5×10^3 m^3 in total. Though the amount of rainfall in June was less than in July and in August, however, the surface runoff generated in June (5.23×10^3 m^3) was more than in July (1.57×10^3 m^3) and in August (2.8×10^3 m^3). The reason which caused this situation was an intensive heavy rainy event happened on 23 June (42.0 mm within 1 hour with maximum intensity of 7.8 mm/5min and average intensity of 3.5 mm/5mmin). The amount of the surface runoff of this single rainy event attained 5.23×10^3 m^3.

With regard to the monthly water storage manifested in the variation of the soil water content and the change of the GWT (Fig 6.22.g), the results show positive value during the rainfall centralized time from June to August. Because the GWT level in the rainy season keeps annual relatively low level, the water storage mainly manifests in the increment of the soil moisture in the first layer in the sediment filled area during the rainy season. On the other side, at the beginning and end of 2006, the water storage had no obvious change which means the water input and output was approximate to equilibrium. Before and after the rainfall centralized time of June, July and August, because the evpaotranspiration was much prominent than the infiltration and the GWT recharge, the water storage showed the negative situation. The annual amount of water storage was approximately 0.

With regard to the difference between monthly water input and output in Case 3 as shown in Figure 6.23, the results indicates the monthly water input is lower than the output to some extent except in June, July and August. The annual difference between the water input and output is also approximate to 0.

6.9.5 Results comparison

6.9.5.1 Summary of the numerical results

The numerical results of the Case 1, Case 2 and Case 3 are tersely summarized as listed in Table 6.3.

Table 6.3 Components of water input and output in each case

Item	Income (10^3 m^3)		Expenditure (10^3 m^3)				Storage (10^3 m^3)
	Surface	GWT	ET	Infiltration	Surface	GWT	
Case 1	28.4	0.80	……	……	28.4	0.80	0.0
Case 2	28.4	0.80	19.60	6.80	……	0.82	1.98
Case 3	28.4	0.80	14.41	3.40	10.52	0.87	0.0

6.9.5.2 Results comparison

In Case 1, as the evapotranspiration and infiltration were neglected, the water income was equal to the water expenditure.

In Case 2, with the assumed computational conditions (Chapter section 6.9.3), the surface runoff generated in the upstream of the check dam was dammed-up by the check dam and stored in the reservoir. It was assumed that evapotranspiration was the water surface evaporation over the reservoir. The evaporation attained 1.96×10^4 m which is the maximum among the three cases. The infiltration in Case 2 is also higher than that of Case 3. The water storage in Case 2 was estimated to be 1.98×10^3 m^3 in given year of 2006.

In Case 3, the surface runoff was more than that of Case 2 but less than Case 1 distinctly. The total water storage was approximate to 0. Compared with Case 1 and Case 2, the GWT outflow slightly increased.

Compared with the original condition (Case 1), effects of the check dam system on runoff redistribution can be summarized as follows.

(1) The surface runoff was significantly reduced to 40 % of the original condition.

(2) The total water inflow was redistributed in the sediment filled area. Redistribution ration to evapotranspiration and infiltration from the runoff was 49.3 % and 11.6 % respectively.

On the other side, the deep groundwater outflow occurs at the downstream of Liudaogou basin and is conveniently used as irrigation water and domestic water. The infiltrated water at the sediment deposited area (11.6 % of the total water inflow in 2006) effectively recharged the deep groundwater which causes the increase of the deep groundwater outflow to some extent.

Additionally, due to general increase of the soil water content in the sediment filled area during the rainy season, crop planting has been carried out at the lower reach on the sediment filled area in recent years (Fig 6.24).

Fig 6.24 Crops planting on sediment filled area in front of the check dam

6.9.6 Effects of the check dam system

By 2002, about 113,500 check-dams had been built in Loess Plateau[31)]. According to the analyzed results of the check dam system on runoff redistribution in this study combined with the related studies of the check dam system on reduction of the soil erosion, the effects of the check dam system mainly manifests in the following areas[31),127)].

(1) Increase the available water resources and rainfall probability

The infiltration in the sediment filled area recharges the GWT effectively so that the annual available water in every basin has been increased to some extent. Simultaneously, the evapotranspiration increases the amount of water into local hydrological cycle which results in the increase of the atmospheric moisture, thereby the rainfall probability is also increased to some extent within the range of Loess Plateau.

(2) Reduce soil erosion and sediment transportation

The check dam systems in Loess Plateau intercept a total of 700 million m^3 of sediments that pour into the Yellow River. The check-dam system is the most important and well-known project to conserve soil and water in Loess Plateau.

(3) Create the farmland and promote agricultural production

The check dam system created the farmland with high productivity (Total: 3,200 km^2 in Loess Plateau). The benefits of the check dam system are attached for the local people by virtue of developing agriculture production.

6.10 Summary

In this chapter, based on the actual conditions of the study area, an one-dimensional runoff calculation model was developed with an aim to evaluate the effects of the check dam system on runoff redistribution. The model was applied to the observed data and verified. To evaluate the effects of the check dam system, runoff calculations for a control cases of the original condition without the check dam (Case 1), a assumed case with a check dam and a reservoir (Case 2), and the present condition with the check dam system (Case 3) in the year of 2006 were carried out. Through comparison of the numerical results between the original condition

(Case 1) and the present condition (Case 3), the effects of the check dam on runoff redistribution were clarified to some extent.

Results of the check dam system impacted on runoff redistribution are as follows.

(1) The annual total water inflow was redistributed by the check dam system. New components of the water output were generated such as the evapotranspiration and the infiltration.

(2) The surface runoff was significantly reduced to 40 % of the original condition in 2006.

(3) Evaportransipation and infiltration accounted for 49.0 % and 11.6 % of the total inflow in 2006 respectively.

As an attached effect of the check dam system, the crops planting can be carried out on the sediment filled area.

According to the analyzed results of the check dam system on runoff redistribution in this study combined with the related studies of the check dam system on reducing the soil erosion, the effects of the check dam system mainly manifests in the followings.

(1) Increase the available water resources in every basin and increase rainfall probability within the range of Loess Plateau.

(2) Reduce soil erosion and sediment transportation

(3) Create the farmland and promote the agricultural production

For the GWT calculation model

The developed numerical calculation model applied to the runoff calculation of the sediment filled area in Liudaogou Basin. The research approach on the runoff calculation of the sediment filled area can be generalized to other check dam systems in the northern Loess Plateau.

Chapter 7

General Summary and Conclusions

7.1 Summary of every chapter

Chapter 1 is the general introduction of this study.

In Chapter 2, the general situation of the study location was introduced.

In Chapter 3, the main items of the field survey and the arrangement of the field observation were introduced firstly. Next, the distribution of the rainy events in 2007 was analyzed because the rainfall amount and the rainfall process in 2007 was approximate to the normal year. Then, the relationships between the rainfall intensity and the surface runoff were clarified by analyzing the observed data of the rainfall combined with the corresponding surface runoff. The main analyzed contents are follows:

(1) Relationship between the rainfall intensity and the surface flow generation for the saturated topsoil condition and unsaturated topsoil condition respectively.

(2) Mechanism of the surface flow generation for the low intensity with long duration rainfall and the high intensity rainfall respectively.

(3) Relationship between the mean rainfall intensity and the runoff rate.

Some conclusions achieved in Chapter 3 as follows.

(1) Necessary condition of the surface flow generation for saturated topsoil condition is the rainfall intensity $\geqq$ 0.6 mm/5min.

(2) Necessary condition of the surface flow generation for unsaturated topsoil condition is the rainfall intensity $\geqq$ 2.6 mm/5min.

(3) The mean rainfall intensity is a key influence factor on the surface runoff rate.

Moreover, mechanism of the surface flow generation caused by low intensity with long duration rainy event and by high intensity rainy event was clarified respectively.

Additionally:

(1) The thickness of the topsoil is about 10 cm.

(2) For the topsoil, the mean saturated infiltration velocity is slightly more than 0.6 mm/5min; the mean unsaturated infiltration velocity is less than 2.6 mm/5min.

(3) The average infiltration velocity of the soil layer subsequent to the topsoil is less than 0.6 mm/5min.

In Chapter 4, firstly, kinematic wave model was introduced. Next, based on the actual conditions of the study area, a numerical calculation model of the surface runoff was developed by kinematic wave theory combined with hypothetical channel networks. Applicability of the model was validated by numerical simulation of the observed surface flow. Finally, the numerical calculation of the surface runoff was carried out in recent four years (2005-2008).

Some conclusions of Chapter 4 are as below.

(1) Both annual rainfall and its yearly distribution impacts on the annual runoff rate.

(2) The runoff rate in the normal year is approximately 10 %-15 %.

(3) The developed runoff calculation model applies to the surface runoff calculation of the study location.

In Chapter 5, the annual water budget and the monthly water income and expenditure of the study basin were estimated based on analysis of the results obtained from the field observation and the numerical calculation of the surface runoff. Index of the annual water balance and index of monthly water income and expenditure were established respectively. Moreover, the annual available water was also approximately estimated according to the analyzed results of the index of annual water balance.

Additionally, the groundwater (GWT) fluctuant characteristics were clarified through analyzing the groundwater level data.

In Chapter 6, a runoff calculation model of the sediment filled area was developed. Applicability of the model was validated by fit to the observed data of the groundwater level. In given year of 2006, effects of the check dam system were clarified through comparison of the numerical results between a control case of the original condition without a check dam and the present condition with a check dam system.

For the results of the check dam on runoff redistribution, there are two aspects listed as following:

(1) The surface runoff was significantly reduced to 40 % of the original condition

(2) The total water input was redistributed in the sediment deposited area. Redistribution ration to evapotranspiration and infiltration from the runoff was 49.3 %, 11.6 % respectively.

According to the analyzed results of the check dam system on runoff redistribution in this study combined with the related studies of the check dam system on reducing the soil erosion, the effects of the check dam system mainly manifests in the following areas.

(1) Increase the available water resources in every basin and increase rainfall probability within the range of Loess Plateau.

(2) Reduce soil erosion and sediment transportation

(3) Create the farmland and promote the agricultural production

Chapter 7 is the general summary of this study.

7.2 Innovations

1. Developed a numerical calculation model of the distributed-type basin for the surface runoff calculation of a representative basin in the northern Loess Plateau. Though the model

developed method is the conventional kinematic wave theory, however, towards the study on the surface runoff in Loess Plateau, the numerical calculation method which was developed by kinematic wave theory combined with hypothetical channel networks has not been applied before this study. Thus, the developed calculation model filled a gap of the researches on runoff calculation in Loess Plateau.

2. Established the index of annual water balance and index of monthly water income and expenditure for the northern Loess Plateau. The results of the annual water balance and monthly water income and expenditure are expected to contribute the sustainable utilization of the annual/monthly water resources in the northern Loess Plateau region.

3. Clarified the effects of the check dam system on the runoff redistribution by the method of runoff numerical calculation. The runoff model developed method can be applied to other check dam systems in the northern Loess Plateau.

7.3 Unresolved issues

1. Due to the complicated topography and some indistinct points of the ground conditions, the calculated results of the shallow groundwater by using the surface runoff calculation model is still roughness (in Chapter 4). Theoretically, the developed runoff calculation model also can be applied to the calculation of the groundwater. Thereupon, the more detailed field survey of the topography and ground condition must be carried out towards the accurate calculation of the surface runoff together with the groundwater.

2. Due to the data deficiency such as the annual rainfall and the groundwater level, the numerical simulation of the groundwater at the sediment filled area was only performed in a certain period in 2006. Also owing to data deficiency, the monthly groundwater flow was simply estimated by the interpolation method for the estimation of the monthly water income and expenditure. The data deficiency must influence the accuracy of the corresponding researched results to some extent. Therefore, accumulation of the useful hydrologic data and creation of the hydrological database for the study basin and for the northern Loess Plateau is necessary.

7.4 Postscript

In this study, the misconceptions or errors are unavoidable, if any, please to accord forgiveness and make a comment or criticism.

REFERENCES

[1]. Liu, J.G. and Diamond, J., 2005. China's environment in globalizing world. *Nature*, Vol. 435 (30). pp. 1179-1186.

[2]. Dregne, H.E., 2002. Land degradation in the drylands. *Arid Land Research and Management*, 16, pp. 99-132.

[3]. Yang, H., 2004. Land conservation campaign in China, integrated management, local participation and food supply option. *Geoforum*, 35, pp. 507-518.

[4]. Wang, X.H., Lu, C.H., Fang, J.F. and Shen, Y.C., 2007. Implications for development of grain-for-green policy based on cropland suitability evaluation in desertification-affected north China. *Land Use Policy*, 24, pp. 417-424.

[5]. Wang, T. and Wu, W., 1999. Land use and desertification in Northern China. *Journal of Natural Resources*, 14, pp. 355-368.

[6]. Wang, T., Zhu, Z.D. and Zhao, H.L., 2004. Study on desertification in China. *Journal of Desert Research*, 24, pp. 115-123.

[7]. Fan, S. and Zhou, L., 2001. Desertification in China: possible solutions, *Ambio*, 30(6), pp. 384-385.

[8]. Bo, W. and Long, J., 2002. Land change and desertification development in the Mu-Us Sand land, North China, *J. Arid. Environments*, Vol. 50. pp. 429-444.

[9]. Yang, W. and Shao, M.A, 2000. Study on the Soil Water in Loess Plateau. *Science Publisher Press*, Beijing, pp. 305. (In Chinese)

[10]. Kimura, R., Fan, J., Zhang, X.C., Takayama, N., Kamichika, M. and Matsuoka, N., 2005. Evapotranspiration over the Grassland Field in the Liudaogou Basin of the Loess Plateau, China. *Acta Oecologica*, 29, pp. 45-53.

[11]. Yao, Y.B., Wang, Y.R. and Li, Y.H., 2005. Climate warming and drying and its environmental effects in the Loess Plateau. *Resour Sci.*, 27(5), pp. 146-152. (in Chinese with English abstract)

[12]. Liu, X.Q., Zhao, J.B. and Yu, X.F., 2006. Study on the climatic warming-drying trend in the Loess Plateau and the countermeasures. *Arid Zone Res.*, 23(4), pp. 627-631. (in Chinese with English abstract)

[13]. Xin, Z.B, Xu, J.X. and Zheng, W., 2008. Spatiotemporal variations of vegetation cover on the Chinese Loess Plateau (1981-2006): Impacts of climate changes and human activities. *Science in China Series D: Earth Sciences*, 51 (1), 67-78.

[14]. Liu, L.Y., Li, X.Y., Shi, P.J., Gao, S.Y. Wang, J.H., (et. al), 2007. Wind erodibility of major soils in the farming-pastoral ecotone of China. *Journal of Arid Environments*, 68, pp. 611-623.

[15]. Mitchell, D.J., Fullen, M.A., Trueman, I.C. and Fearnehough, W., 1998. Sustainability of reclaimed desertified land in Ningxia, China. *Journal of Arid Environments*, 39, pp. 239-251.

[16]. Wang, X.H. and Fu, X.F., 2004. Sustainable management of alpine meadows on the Tibetan

Plateau, problems overlooked and suggestions for change. *Ambio*, 33(3), 168-170.

[17]. Feng, Z.M., Yang, Y.Z., Zhang, Y.Q., Zhang, P.T. and Li, Y.Q., 2005. Grain-for-green policy and its impacts on grain supply in West China. *Land Use Policy*, 22, 301-312.

[18]. Ginsberg, P., 2000. Man-made forestation in Israel: a source of social goods and services. *Society of American Foresters*, 98 (3), pp. 32–36.

[19]. Oscar, C., 2001. An analysis of externalities in agroforestry systems in the presence of land degradation. *Ecological Economics*, 39, pp. 131-143.

[20]. Thapa, R., 2003. Agroforestry can reverse land degradation in Nepal. *Appropriate Technology*, 30, pp. 40-41.

[21]. Priha, O., Lehto, T., Smolander, A., 1999. Mycorrhizae and C and N transformations in the rhizospheres of Pinus sylvestris, Picea abies and Betula pendula seedlings. *Plant and Soil*, 206, pp. 191-204.

[22]. Thomas, G. F., 2001. Man-made forestation in Uruguay: study of a changed landscape. *Journal of Forecasting*, 99, pp. 35-39.

[23]. Ivanko, J., 2001. Planting trees for the future. Environmental Magazine, 12, pp. 14.

[24]. Franco, D., Mannino, I., Zanetto, G., 2003. The impact of agroforestry networks on scenic beauty estimation. *Landscape and Urban Planning*, 62, pp. 119-138.

[25]. Kursten, E., 2000. Fuelwood production in agroforestry systems for sustainable land use and CO2-mitigation. *Ecological Engineering*, 16, pp. 69-72.

[26]. Cao, S., Chen, L., Liu, Z. and Wang, G., 2008. A new tree-planting technique to improve tree survival and growth on steep and arid land in the Loess Plateau of China. *Journal of Arid Environments*, 72, 1374-1382.

[27]. UNEP, 1997. World Atlas of Desertification. *Arnold*, London, pp. 1-182.

[28]. Wang, Q. and Takahashi, H., 1999. A land surface water deficit model for an arid and semiarid region: Impact of desertification on the water deficit status in the Loess Plateau, China. *Journal of Climate,* 12, 244-257.

[29]. Chen, H.S., Shao, M.A. and Li, Y. Y., 2008. Soil desiccation in the Loess Plateau of China. *Geoderma*, 143, pp. 91-100.

[30]. Kimura, R., Liu, Y., Takayama, X., Zhang, X.C., Kamichika, M. and Matsuoka, N., 2005. Heat and water balances of the bare soil surface and the potential distribution of vegetation in the Loess Plateau, China. *Journal of Arid Environments*, 63, pp. 439-457.

[31]. Xu, X.Z., Zhang, H.W. and Zhang, O.Y., 2004. Development of check-dam systems in gullies on the Loess Plateau, China. *Environmental Science & Policy*, 7, pp. 79-86.

[32]. Wang, L., Shao, M.A., Wang, Q.J. and Gale, W., 2006. Historical changes in the environment of the Chinese Loess Plateau. *Environmental Science & Policy*, 9, pp. 675-684.

[33]. Wang, Y.Q., Zhang, X.C., Cong, W. and Wei, Q.C., 2006. Spatial variability of soil moisture on slope-land under different land uses on the Loess Plateau. *Transactions of the CSAE*, 22(12), pp. 65-71. (in Chinese with English abstract)

[34]. Zhang, L.P., Zhang, D.R., Zhang, R.B. and Yang, Q.K., 2005. Research on Basic Ecological Landform Unit and Model of Soil Erosion Estimation and Predict in Small Watershed. *Journal of Soil and Water Conservation*, 19(1), pp. 101-104. (in Chinese with English abstract)

[35]. Fan, J. Shao, M.A. and Wang, Q.J. 2006. Soil Water Restoration of Alfalfa Land in the Wind-water Erosion Crisscross Region on the Loess Plateau. *Acta Agrestia Sinica*, Vol.13. (3). pp. 261-264. (in Chinese with English abstract)

[36]. Yamanaka, N., 2008. Desertification and its combating measures in Loess Plateau-China. *Kokon Shoin, Publishers, Co., Ltd. Tokyo,* pp. i-iii. (In Japanese)

[37]. Shi, H. and Shao, M.A., 2000. Soil and water loss from the Loess Plateau. *Journal of Arid Environments*, 45, pp. 9-20

[38]. Zheng, J.Y. 2004. Study on the Infiltration and Redistribution of Soil Water and the Spatial Variation of Soil Hydraulic Properties in Water-wind Erosion Crisscross. *Institute of Soil Science. CAS*, China, June S152.7, 631.43. pp. 1-10. (In Chinese)

[39]. Zheng, J.Y., Shao, M.A., Li, S.Q., Zhang, X.C. and Wen, Y.H., 2005. Variation of the hydraulic characteristics of the soil profile in water-wind erosion crisscross region. *Transactions of the CSAE*, 21(11), pp. 64-66. (In Chinese with English abstract)

[40]. Xiao, B., Zhao, Y.G. and Shao, M.A., 2007. Effect of biological soil crust on soil physicochemical properties in water-wind erosion crisscross region, northern Shaanxi Province, China. *Acta Ecologicsa. Sincia*, 27(11), pp. 4662-4670. (In Chinese with English abstract)

[41]. Jiang, N., Shao, M.A., Lei, T.W. and Zhang, X.C., 2005. Spatial Variability of Soil Infiltration Properties on Natural Slope in Liudaogou Catchment on Loess Plateau. Journal of Soil and Water Conservation, 19(1), ISSN:1009-2242(2005)01-0014-04. (In Chinese with English abstract)

[42]. Zhang, L.P, Ni, H.B. and Wu X.Y., 2005. Soil water erosion processes on sloping land with different material in the wind-water interaction zone in the Loess Plateau. *Research of Soil and Water Conversation*, 12 (5), 126-128. (In Chinese with English abstract)

[43]. Cheng, X.R., Huang, M.B. and Shao, M.A., 2007. Vertical Distribution of Representative Plantation's Fine Root in Wind-water Erosion Crisscross Region, Shenmu. *Acta Bot. Boreal.-Occident. Sin.*, 27(2), 321-327. (In Chinese with English abstract)

[44]. Fan, J. 2005. Study on the soil water dynamics and modeling in water-wind erosion crisscross region on the Loess Plateau, *Institute of Soil Science, CAS, China*, S152.7, UCD 631.43, pp. 30-45. (in Chinese)

[45]. Wang, H., Wang T.M., Yang, M.B et al., Quantitative monitoring of gully erosion in hilly-gully area of Loess Plateau based on aerial images. *Chinese Journal of Applied Ecology*, 19(1), 127-132, 2008. (In Chinese with English abstract).

[46]. Hinokidani, O., Huang, J.B., Yasuda, H., Yamamoto, S. and Zhang, X.C., 2006. Study on rainwater outflow of small basin in Loess Plateau. *Proceeding of the Eighth International Conference on Development on Drylands,* 294-299.

[47]. Gao, Z.L., and Mu, X.M., 2004. Spatio-Temporal Change of Land Use/ Coverage in Loess Wind-Water Erosion Crisscross Region. *Journal of Soil and Water Conservation*, Vol.18. pp. 147-150.(in Chinese with English abstract)

[48]. Lü, D.Q. and Pan, Y., 2008. Study on Soil Retention Characteristics of Different Position of Slope of Soil Under Different Land uses in Liudaogou Basin. *Chinese Agricultural Science Bulletin,* Vol. 24. pp. 279-282. (in Chinese with English abstract)

[49]. Li, S.Q.and Wei, X.R., 2008. Core University Program China-Japan Joint Open Seminar on Combating Desertification and Development in Inland China of Year 2008. *Published by Arid land Research Center, Tottori University, Japan.*

[50]. Li, M., Li, Z.B., Liu, P.L. and Yao, W.Y., 2005. Using Cesium-137 technique to study the characteristics of different aspect of soil erosion in the Wind-water Erosion Crisscross Region on Loess Plateau of China. *Applied Radiation and Isotopes*, 62, 109-113.

[51]. Wen, B. and Shao, M.A., 2006. Soil and water conservation information system for small watersheds based on component GIS technology. *Jisuji Gongcheng Computer Engineering*, 32(13), 243-245. (in Chinese)

[52]. Wei, X.R. and Shao, M.A., 2007. Distribution of Soil Properties as Affected by landforms in Small Watershed of Loessial Gully Region. *Journal of Natural Resources*, 22(6), 946-953. (in Chinese with English abstract)

[53]. Zhu, Y.J. and Shao, M.A., 2008. Variability and Pattern of surface moisture on a small-scale hillslope in Liudaogou catchment on the northern Loess Plateau of China. *Geoderma*, 147, 185-191.

[54]. Zhu, H., Shao, M.A. and Horton, R., 2008. Impact of Gully on Soil Moisture of Shrubland in Wind-Water Erosion Crisscross Region of the Loess Plateau. *Pedophere* 18(5), 674-680.

[55]. Zheng, J.Y., Shao, M.A. and Zhang, X.C., 2004. Spatial Variation of Surface Soil's Bulk Density and Saturated Hydraulic Conductivity on Slope in Loess Plateau. *Journal of Soil and Water Conservation*, 18(3), 53-56. (in Chinese with English abstract)

[56]. Hu, W., Shao, M.A. and Wang, Q.J., 2009. Temporal changes of soil hydraulic properties under different land uses. *Geoderma*, 10093, 1-12.

[57]. Kimura, R., 2007. Estimation of moisture availability over Liudaogou river basin of the Loess Plateau using new indices with surface temperature. *Journal of Arid Environments*, 70(2), 237-252

[58]. Fu, X.L., Shao, M.A. and Wei, X.R. (et. al), 2009. Effect of two perennials, fallow and millet on distribution of phosphorous in soil and biomass on slope loess land, China. *Catena*, 01384, No. of Pages 7.

[59]. Wen, B. and Shao, M.A., 2005. Design and realization of GIS model for hydrological cycle of a small watershed on the Loess Plateau. *Transactions of the CSAE*, 21(10), 36-40. (in Chinese with English abstract)

[60]. Huang, J.B., Hinokidani, O., Kajikawa, Y., Yasuda, H. and Zheng, J.Y., 2008. Analysis of annual

available water resources of a representative basin in upper Loess Plateau, *ICHE: Advances in Hydro-science and Engineering*, Vol. 3. pp. 129-130.

[61]. Hydraulic formulas collection. 1985. *Published by JSCE, (Japan Society of Civil Engineering)*, pp 11-13. (in Japanese)

[62]. Study on numerical analysis duties of sedimentation characteristics in front of the intake / Study on rational method of sediment flushing in front of the intake. 1999. *Japan Inst. of Systems Res.*, pp. 30-32. (in Japanese)

[63]. Jiang, N., Shao, M.A. and Lei, T.W., 2007. Soil water characteristics of different typical land use patterns in water-wind erosion interlaced region. *Journal of Beijing Forestry University*, 29(6), pp. 138-142. (in Chinese with English abstract)

[64]. Takasao, T., Shiiba, M. and Nakakita, E., 1985. Lumping of the Kinematic Wave Model. *Proceedings of the Japanese Conference on Hydraulics,* 29, 239-244. (in Japanese)

[65]. Tanaka, G. 2003. Stochastic Response Characteristics of Kinematic Wave Model. *Annual Journal of Hydraulic Engineering, JSCE,* 47, 229-234.

[66]. Suzuki, M., Momota, H., and Jinno, K., 1998. Statistical study for tank model identified by genetic algorithm. *Annual Journal of Hydraulic Engineering, JSCE,* 42, 115-120. (in Japanese)

[67]. Hatta, S., Fujita, M. and Yamanashi, M., 1997. Study on deep percolation based on the unsaturated flow theory and tank model. *Annual Journal of Hydraulic Engineering, JSCE,* 1997. 41, 25-30. (in Japanese)

[68]. Harada, M., 1999. Hydraulic analysis on stream-aquifer interaction by storage function models. *Journal of Hydraulic, Coastal and Environmental Engineering*, 628.II-48, 189-194. (in Japanese with English abstract)

[69]. Sonoyama, H., Hoshi, K. and Ide, Y., 2001. Generalization of storage routing function model with loss mechanisms. *Advances in River Engineering*, 7, 465-468. (in Japanese)

[70]. Paresh Deka and V. Chandramouli., 2005. Fuzzy Neural Network Model for Hydrologic Flow Routing. *Journal of Hydrologic Engineering, ASCE,* 10(4), 302-314.

[71]. Ao, T.Q., Ishidaira, H. and Takeuchi, K., 1999. Study on distributed runoff simulation model based on block type topmodel and Muskingum-Cunge method. *Annual Journal of Hydraulic Engineering, JSCE*, 43, 7-12. (in Japanese)

[72]. Oscar Luis, P.V. and Baltasar C.R., 1992. A distributed runoff model using irregular triangular facets. *Journal of Hydrology*, 134, 35-55.

[73]. Shen, C. Tachikawa, Y. and Takara, K., 2004. Rainfall-runoff simulation by using distributed instantaneous unit hydrograph derived from applying flow accumulation value of dam. *Annual Journal of Hydraulic Engineering, JSCE,* 48, 1-6.

[74]. Tomosugi, K. and Urata, H., 1993. Suggestion and investigation of a new method for flood runoff estimation in minor river basin. *Proceedings of Annual Conference of the Japan Society of Civil Engineers*, 48, 228-229. (in Japanese)

[75]. Shiiba, M. and Kanazawa, M., 2001. Study on river flow evaluation by semi-distributed runoff

model. *Proceedings of Annual Conference of the Japan Society of Civil Engineers*, 56, 494-495. (in Japanese)

[76]. Takasao, T., Takara, K. and Kusubashi, Y., 1985. Study on evaluation of probability process of flood runoff model. *Annuals of Disas. Prev. Res. Inst., Kyoto Univ.*, No. 28, B-2, pp. 221-235. (in Japanese)

[77]. Tanaka, G., Fujita, M. and Kudo, M., 1999. Comparison between the kinematic wave model and the storage routing function runoff model-frequency characteristic and stochastic characteristic. *Journal of Hydraulic, Coastal and Environmental Engineering* 614. Ⅱ-46, 21-36. (in Japanese)

[78]. Yamashita, M. and Ichikawa, A., 2005. A study on the improvement of the applicability of the distributed river simulation model. *Annual Journal of Hydraulic Engineering, JSCE*, 49, 181-186. (in Japanese with English Abstract)

[79]. Tang, Q.H., Oki, T. and Kanae, S., 2006. A distributed biosphere hydrological model (DBHM) for large river basin. *Annual Journal of Hydraulic Engineering, JSCE*, 50, 37-42.

[80]. Horiba, C., Mano, A. and Hayashi, S., 2001. Flood Runoff Analysis in the Upper Chang Jiang Bain. *Proceedings of the Symposium on Global Environment*, 9, 7-12. (in Japanese with English abstract)

[81]. Hashimoto, N., Fujita, A., Shiiba, M. And Tachikawa, Y., 2006. Development of dam inflow predication system based on distributed rainfall-runoff model. *Annual Journal of Hydraulic Engineering, JSCE,* 50, 289-294. (in Japanese with English abstract)

[82]. Huang, J.B., Hinokidani, O., Yasuda, H. and Kajikawa, Y., 2008. Study on characteristics of the s urface flow of the upstream region in Loess Plateau. *Annual Journal of Hydraulic Engineering, JSCE*, 52, 1-6.

[83]. Ichikawa, Y. 2001. Study on constitution and centralization of the runoff of the distributed type basin. *Doctoral thesis of Faculty of Engineering of Kyoto University, Japan,* pp. 11-23. (in Japanese)

[84]. Fujimura, K., Taira, Y. and Ando, Y., 2003. Storm water runoff analysis using GIS in the Kotta River basin. *Proceedings of Annual Conference of the Japan Society of Civil Engineers*, 58, 45-46. (in Japanese)

[85]. Kojiri, T. and Kobayashi, M. 2002. Spatial and temporal distribution of water quantity and quality with GIS-based runoff model. *Advances in River Engineering,* 8, 431-436. (in Japanese with English abstract)

[86]. Mihori, K. and Oka, Y. 2003. Applicability of the distributed model for natural basin using GIS. *Proceedings of Annual Conference of the Japan Society of Civil Engineers*, 58, 24-25. (in Japanese)

[87]. Nagami, M. and Sugiwura, Y., 1986. Numerical value mathematics geography practice with PC. *Kokon Shoin, Publisher, Co., Ltd. Tokyo.*(in Japanese)

[88]. Takasao, T., Kaoru, T. and Mizubuchi, S., 1988. Introduction of Hydrographic Topography Analysis by Computer. *Annuals of Disas. Prev. Res. Inst., Kyoto Univ.*, No. 31, B-2, pp. 325-340.

(in Japanese)

[89]. Tarboton D C., 1997. A new method for the determination of flow directions and upslope area in grid digital elevations models. *Water Resour. Res*, 33(2), 309-319.

[90]. Ao, T., Takeuchi, K. and Ishidaira, H., 2001. On the method of generating artificial stream networks of large river basins and its effect on runoff simulation. Annual *Annual Journal of Hydraulic Engineering, JSCE*, 45, 139-144. (in Japanese with English abstract)

[91]. Riku, S., Koike, T. and Hayakawa, N., 1989. A rainfall□runoff model using distributed data of radar rain and altitude. *Journal of Hydraulic, Coastal and Environmental Engineering* 411, II -12, 135-142. (in Japanese)

[92]. Takuma, T., Kaoru, T. and Mizubuchi, S., 1989. A basic study on hydrographic topography analysis by using numerical land information. *Annuals of Disas. Prev. Res. Inst., Kyoto Univ.*, No. 32, B-2, pp. 435-456. (in Japanese)

[93]. Iwasa, Y., 1998. Study on topographic survey & the flood stage plan & the river channel shape. *Results of Research Report*, pp. 3-13. (in Japanese)

[94]. Michiguchi, T., Fujita, M. and Enoki, K., 1990. Relationship between hypothetical channel network and threshold. *Proceedings of Annual Conference of the Japan Society of Civil Engineers*, 48(2), 142-143. (in Japanese)

[95]. Huang, J.B., Hinokidani, O., Kajikawa, Y. and Yasuda, H., 2008. Study on Numerical Simulation Technique of "Rainfall-Runoff" Process of a Distributed-type Basin. *Journal of Soil and Water Conservation*, 22(4), 52-55. (in Chinese with English abstract)

[96]. Takasao, T., Ikebuchi, S. and Shiiba, M., 1977. Study on flood analytical method of a river basin by considering structures of river channel network. *Annuals of Disas. Prev. Res. Inst., Kyoto Univ.*, 22, B-2, pp. 185-200. (in Japanese)

[97]. The Japan Society of Mechanical Engineers, 1988. Fundamentals of Computational Fluid Dynamics. *CORONA Publishing CO., LTD. Tokyo, Japan*, pp. 52-56.(in Japanese)

[98]. Japanese River Society, 1997. River erosion control technical criterion of MLIT (Ministry of Land, Infrastructure, Transport and Tourism, Japan), *Sankaido Publishing Co., Ltd,* pp. 85-87. (in Japanese)

[99]. Huang, M.B., Shao, M.A. and Li, Y.S., 2001. Comparison of a modified statistical-dynamic water balance model with the numerical model WAVES and field measurements. *Agricultural Water Management,* 48, 21-35.

[100]. Zhu, X.J., Wang, Z.G. and Xia, J., 2008. Basin level water balance analysis study based on distributed hydrological model--Case study in the Haihe River Basin. *Progress in Geography,* 27(4), 23-27. (in Chinese with English abstract).

[101]. Zhang, S.F., Jia, S.F., 2003. Water balance and water security study in the Haihe basin. *Journal of Natural Resources*, 18(6), 684-691. (in Chinese with English abstract)

[102]. Kamimera, H. and Lu, M.J., 2007. Water balance of the Kherlen River Basin, Eastern Mongolia. *Annual Journal of Hydraulic Engineering, JSCE,* 51, 397-402. (in Japanese with English

abstract)

[103]. Yu, W.D., 2008. Water balance and water resources sustainable development in Haihe River Basin. *Journal of China Hydrology,* 28(3), 79-82. (in China with English abstract)

[104]. Huang, J.B., Hinokidani, O. and Kajikawa, Y., 2007. A Basic Study on Water Income and Expenditure of Upstream Region in Loess Plateau. *Proceedings of The 3rd International Yellow River Forum*, Vol. (1). pp. 301-308.

[105]. Zheng, J.Y., Wang, L.M. and Shao, M.A. (et al), 2006. Gully impact on soil moisture in the gully bank. *Pedosphere*, 16(3), 339-344.

[106]. Ren, M.E. and Shi, T.L. 1986. Sediment discharge of the Yellow River China and its effect on the sedimentation of the Bohai and the Yellow Sea. *Con. Shelf Res.*, 6, 785-810.

[107]. Chen, L.D., Huang, Z.L. and Gong, J., 2007. The effect of land cover/vegetation on soil water dynamic in the hilly area of the Loess Plateau, China. *Catena*, 70, 200-208.

[108]. Chen, H. and Cai, Q.G. 2006. Impact of hillslope vegetation restoration on gully erosion induced sediment yield. *Science in China: Series D Earth Sciences,* 49(2), 176-192.

[109]. Huang, M.B. Gallichand, J. and Zhang, C.P. 2003. Runoff and sediment responses to conservation practices: Loess Plateau of China. *Journal of the American Water Resources Association,* 39(5), 1197-1204.

[110]. Xu, X.Z., Zhang, H.W. and Wang, G.Q., 2008. An experimental method to verify soil conservation by check dams on the Loess Plateau, China. *Environ Monit Assess*, DOI 10.1007/s 10661-008-0630-x.

[111]. Sun, J.Z. 1988. Environmental Geology in Loess Area of China. *Environ Geol Water Sci.*, 12(1), 49-61.

[112]. Krüger, S. and Rutschmann, P., 2006. Modeling 3D Supercritical Flow with Extended Shallow-water Approach. *Journal of Hydraulic Engineering, ASCE,* 10.1061, 0733-9429, 132, 9(916).

[113]. Saito, Y., Suzuki, A. and Itou, S., 2006. Development of Water Cycle Analysis Program (WCAP) Based on Quasi-3 dimensional Multilayer Groundwater model. *Journal of Hydraulic, Coastal and Environmental Engineering,* 810. II -74, 1-15. (in Japanese with English abstract)

[114]. F.ASCE, T.H.Y. and Kang, S.K., 2004. Finite Volume Model for Two-Dimensional Shallow Water Flow on Unstructured Grids. *Journal of Hydraulic Engineering, ASCE*, 10.1061, 0733-9429, 130:7 (678).

[115]. Nguyen, D.K., Shi, Y.E. and Wang, S.Y. (et al). 2006. 2D Shallow-Water Model Using Unstructured Finite-Volume Methods. *Journal of Hydraulic Engineering, ASCE*, 10.1061, 0733-9429, 132:3 (258).

[116]. Hunukumbura, P.B., Tachikawa, Y. and Ichikawa, Y. (et al), 2009. Extending a Storage-Discharge Relationship for Subsurface Flow Modeling in Dry Mild-Slope Basins. *Annual Journal of Hydraulic Engineering, JSCE,* 53, 25-30.

[117]. Kawano, Y., Yagi, S. and Yoshikini, H., 2005, Soil mechanics. *Gihodoshuppan*, pp. 1-20. (In

Japanese)

[118]. Allen, R.G., Pereira, L.S., Raes, D. and Smith, M., 1998. Crop Evapotranspiration: Guidelines for Computing Crop Water requirements. *FAO, Rome,* (300 pp).

[119]. Kimura, R., Bai, L., Fan, J.and Takayama, N. et al. 2007, Evapotranspiration estimation over the river basin of the Loess Plateau of China based on remote sensing. *Journal of Arid Environments,* 68, 53-65.

[120]. Kimura, R., 2007, Estimation of moisture availability over the Liudaogou river basin of the Loess Plateau using new indices with surface temperature. *Journal of Arid Environments*, 70, 237-252.

[121]. Dickinson, R.E., 1984, Modeling evapotranspiration for three-dimensional climate models. Climate process and climate sensitivity. In: *Geophy. Monogr. 29, Am. Geophys. Union*, pp. 58-72.

[122]. Jarvis, P.G., 1976, The interpretation of the variations in leaf water potential and stomatal conductance found in canopies in the field. *Phil. Trans. R. Soc. London Ser. B*, 273, 563-610.

[123]. Kimura, R., Takayama, N., Kamichika, M. and Matsuoka, N., 2004b, Soil water content and heat balance in the Loess Plateau. Determination of parameters in the three-layer soil model and experimental result of model calculation. *Journal of Agricultural Meteorology,* 60, 55-65 (in Japanese with English abstract)

[124]. Vereuijt, A.1982, Theory of Groundwater Flow (Second Edition). *Published by The Macmillan Press Ltd,* [M]. pp. 24-25.

[125]. Kamon, M., Hamada, S., Katsumi, T. and Inui, T., 2004, Experimental study on the Effect of the Pile Installation on the Hydraulic Barrier Performance of Landfill Bottom Clay Layer. *Annuals of Disas. Prev. Res. Inst., Kyoto Univ.,* No.43, B-21.

[126]. Matsushita, E., Yamamoto, T., Suzuki, M. and Sasanishi, T., 2004, Effect of PH on One-dimensional Consolidation Characteristics of Cohesive Soil. *Journal of Geotechnical Engineering*, Vol. 757, No. 3-66, pp. 57-72.

[127]. Li, G.Y., 2003, Yellow River management-Intellection and Practice. *Chinese WaterPower Press & Yellow River Water Conservancy Press,* pp. 3-40. (in Chinese)